Supporting Information for:

Cationic Polymerization and Insertion Chemistry in the Reactions of Vinyl Ethers with (α-diimine)PdMe$^+$ Species

Changle Chen, Shuji Luo and Richard F. Jordan*

Department of Chemistry, The University of Chicago

5735 South Ellis Avenue, Chicago, Illinois, 60637

E-mail: rfjordan@uchicago.edu

Contents

1. Materials and Methods

1.1 NMR characterization of some known compounds.

Data for (α-diimine)PdMeCl: ^{1}H NMR (CD_2Cl_2, 20 ^{o}C) δ 7.34-7.11 (m, 6H), 3.07 (sept, *J* = 7, 2H, C*H*Me$_2$), 3.01 (sept, *J* = 7, 2H, C*H*Me$_2$), 2.04 (s, 3H, N=C*Me*), 2.03 (s, 3H, N=C*Me*), 1.40 (d, *J* = 7, 6H, CH*Me$_2$*), 1.36 (d, *J* = 7, 6H, CH*Me$_2$*), 1.19 (d, *J* = 7, 6H, CH*Me$_2$*), 1.17 (d, *J* = 7, 6H, CH*Me$_2$*), 0.37 (s, 3H, Pd*Me*).

Data for [(α-diimine)PdMe(OEt$_2$)][SbF_6]: ^{1}H NMR (CD_3CN, 20 ^{o}C) δ 7.37-7.34 (m, 6H), 3.04 (sept, *J* = 7, 2H, C*H*Me$_2$), 2.99 (sept, *J* = 7, 2H, C*H*Me$_2$), 2.22 (s, 3H, N=C*Me*), 2.21 (s, 3H, N=C*Me*), 1.36 (d, *J* = 7, 6H, CH*Me$_2$*), 1.29 (d, *J* = 7, 6H, CH*Me$_2$*), 1.25 (d, *J* = 7, 6H, CH*Me$_2$*), 1.21 (d, *J* = 7, 6H, CH*Me$_2$*), 0.31 (s, 3H, Pd*Me*). ^{13}C{^{1}H} NMR (CD_3CN, 20 ^{o}C): δ 183.0 (N=*C*Me), 175.0 (N=*C*Me), 141.5, 141.3, 139.7, 138.9, 129.4, 128.6, 125.2, 124.9, 29.4, 29.1, 24.1, 23.8, 23.7, 23.2, 21.9, 20.3, 4.7 (Pd*Me*). ^{1}H NMR (CD_2Cl_2, -20 ^{o}C) δ 7.31-7.21 (m, 6H), 3.00 (sept, *J* = 7, 2H, C*H*Me$_2$), 2.93 (sept, *J* = 7, 2H, C*H*Me$_2$), 2.03 (b, 6H, N=C*Me*), 1.34 (d, *J* = 7, 6H, CH*Me$_2$*), 1.30 (d, *J* = 7, 6H, CH*Me$_2$*), 1.13 (d, *J* = 7, 12H, CH*Me$_2$*), 0.26 (s, 3H, Pd*Me*).

Data for (tmeda)Pd(OPh)$_2$: ^{1}H NMR (CD_2Cl_2, 20 ^{o}C) δ 7.12 (d, *J* = 8, 4H, H$_{ortho}$), 6.96 (t, *J* = 7, 4H, H$_{meta}$), 6.43 (t, *J* = 7, 2H, H$_{para}$), 2.58 (s, 12H, N*Me$_2$*), 2.55 (s, 4H, -C*H$_2$*-). ^{13}C{^{1}H} NMR (CD_2Cl_2, 20 ^{o}C) δ 168.3 (C$_{ipso}$), 127.9, 118.8, 113.7, 62.3 (-*C*H$_2$-), 50.6 (N*Me$_2$*).

Data for KOPh: ^{1}H NMR (THF-d_8, 20 ^{o}C) δ 6.81 (t, *J* = 8, 2H, H$_{meta}$), 6.28 (d, *J* = 8, 2H, H$_{ortho}$), 6.03 (t, *J* = 7, 1H, H$_{para}$).

Data for CH_2=CHO^{t}Bu: ^{1}H NMR (CD_2Cl_2, 20 ^{o}C) δ 6.48 (dd, *J* = 14, 6; 1H, H_{int}), 4.30 (d, *J* = 14, 1H, H_{trans}), 3.97 (d, *J* = 6, 1H, H_{cis}), 1.26 (s, 9H, OC*Me*$_3$). ^{13}C{^{1}H} NMR (CD_2Cl_2, 20 ^{o}C) δ 147.1 (CH_2=*C*H), 90.4 (*C*H_2=CH), 76.4 (O*C*Me$_3$), 28.3 (OC*Me*$_3$).

Data for CH_2=CHOEt: ^{1}H NMR data (CD_2Cl_2, 20 ^{o}C): δ 6.46 (dd, 1H, H_{int}), 4.15 (d, 1H, H_{trans}), 3.96 (d, 1H, H_{cis}), 3.73 (q, 2H, OC*H*$_2$CH$_3$), 1.16 (t, 1H, OCH$_2$C*H*$_3$). ^{13}C{1H} NMR (CD_2Cl_2, 20 ^{o}C): δ 152.4 (CH_2=*C*H), 86.5.4 (*C*H_2=CH), 64.2 (O*C*H$_2$CH$_3$), 14.9 (OCH$_2$*C*H$_3$).

Data for CH_2=CHOSiMe$_3$: ^{1}H NMR (CD_2Cl_2, 20 ^{o}C): δ6.41 (dd, J = 13, 6; 1H, H_{int}), 4.38 (d, J = 13, 1H, H_{trans}), 4.11 (d, J = 6, 1H, H_{cis}), 0.19 (s, 9H, OSi*Me*$_3$). ^{13}C{1H} NMR (CD_2Cl_2, 20 ^{o}C): δ 146.4 (CH_2=*C*H), 94.6 (*C*H_2=CH), -0.45 (OSi*Me*$_3$).

Data for CH_2=CHOSiMe$_2$Ph: ^{1}H NMR (CD_2Cl_2, 20 ^{o}C): δ 7.68 (d, *J* = 8, 6H, H_{ortho}), 7.48 (t, *J* = 7, 3H, H_{para}), 7.45 (t, *J* = 7, 6H, H_{meta}), 6.49 (dd, *J* = 14, 6; 1H, H_{int}), 4.72 (d, *J* = 14, 1H, H_{trans}), 4.21 (d, *J* = 6, 1H, H_{cis}) 0.53 (s, 6H, SiC*H*$_3$). ^{13}C NMR (CD_2Cl_2, 20 ^{o}C): δ 146.6 (=*C*H), 137.3 (C_{ipso}), 134.1, 130.6, 128.6, 95.5 (=*C*H_2), -1.4 (Si*C*H$_3$).

Data for CH_2=CHOSiMePh$_2$: ^{1}H NMR (CD_2Cl_2, 20 ^{o}C): δ 7.55 (d, *J* = 8, 6H, H_{ortho}), 7.37 (t, *J* = 7, 3H, H_{para}), 7.33 (t, *J* = 7, 6H, H_{meta}), 6.63 (dd, J = 14, 6 Hz, 1 H, =CH), 4.69 (dd, J = 14, 1 Hz, 1 H, =C*H*$_2$), 4,32 (dd, J = 6, 1 Hz, 1 H, =C*H*$_2$), 0.87 (s, 3 H, SiC*H*$_3$). ^{13}C NMR (CD_2Cl_2, 20 ^{o}C): δ 146.7 (=*C*H), 135.6 (C_{ipso}), 135.0, 130.9, 128.7, 96.0 (=*C*H_2), -2.6 (Si*C*H$_3$).

Data for CH_2=CHOSiPh$_3$: ^{1}H NMR (CD_2Cl_2) δ 7.67 (d, *J* = 8, 6H, H_{ortho}), 7.49 (t, *J* = 7, 3H, H_{para}), 7.43 (t, *J* = 7, 6H, H_{meta}), 6.65 (dd, *J* = 14, 6; 1H, H_{int}), 4.65 (d, *J* = 14, 1H, H_{trans}), 4.22 (d, *J* = 6, 1H, H_{cis}). ^{13}C NMR (CD_2Cl_2) δ 146.6 (=*C*H), 135.9, 133.5 (C_{ipso}), 131.0, 128.6, 96.1 (*C*H_2=). GC-MS: *m/z* = 302.

Data for CH_2=CHOPh: ^{1}H NMR (CD_2Cl_2): δ 7.34 (t, *J* = 7, 2H, H_{meta}), 7.08 (t, *J* = 7, 1H, H_{para}), 7.00 (d, *J* = 8, 2H, H_{ortho}), 6.67 (dd, *J* = 14, 6; 1H, H_{int}), 4.75 (d, *J* = 15, 1H, H_{trans}), 4.43 (d, *J* = 6, 1H, H_{cis}). GC-MS: *m/z* = 120.

1.2 Derivation of eq 7 of the manuscript and estimation of limits for $k_{\beta\text{-OR}}$ for 5c-f.

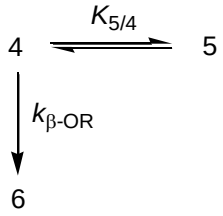

$K_{\mathbf{5/4}} = [\mathbf{5}]/[\mathbf{4}]$

$[\mathbf{5}] = K_{\mathbf{5/4}} \cdot [\mathbf{4}]$

$[\mathbf{4}] + [\mathbf{5}] = (K_{\mathbf{5/4}} + 1)[\mathbf{4}]$

$d([\mathbf{6}])/dt = k_{\beta\text{-OR,obs}} ([\mathbf{4}] + [\mathbf{5}])$

$\Rightarrow d([\mathbf{6}])/dt = k_{\beta\text{-OR,obs}} (K_{\mathbf{5/4}} + 1)[\mathbf{4}]$ (i)

$d([\mathbf{6}])/dt = k_{\beta\text{-OR}}[\mathbf{4}]$ (ii)

from eq i and eq ii $\Rightarrow k_{\beta\text{-OR,obs}} (K_{\mathbf{5/4}} + 1)[\mathbf{4}] = k_{\beta\text{-OR}}[\mathbf{4}]$

$\Rightarrow \quad k_{\beta\text{-OR}} = k_{\beta\text{-OR,obs}} (K_{\mathbf{5/4}} + 1)$ (7)

Estimation of limits for $k_{\beta\text{-OR}}$ for **5c-f** based on pre-equilibrium assumption:

since $K_{\mathbf{5c/4c}} > 19$, from eq 7

$\Rightarrow \quad k_{\beta\text{-OR}} > 20\ k_{\beta\text{-OR,obs}}$

1.3 Estimation of limits for $k_{\beta\text{-OR}}$ for 5c-f based on the steady state approximation for 4c-f.

$$d([\mathbf{4}])/dt = k_{\mathbf{5}\text{ to }\mathbf{4}}[\mathbf{5}] - k_{\mathbf{4}\text{ to }\mathbf{5}}[\mathbf{4}] - k_{\beta\text{-OR}}[\mathbf{4}] = 0$$

$$[\mathbf{4}] = k_{\mathbf{5}\text{ to }\mathbf{4}}[\mathbf{5}]/(k_{\mathbf{4}\text{ to }\mathbf{5}} + k_{\beta\text{-OR}}) \quad \text{(iii)}$$

$$d([\mathbf{6}])/dt = k_{\beta\text{-OR,obs}}[\mathbf{5}] \quad \text{(iv)}$$

$$d([\mathbf{6}])/dt = k_{\beta\text{-OR}}[\mathbf{4}] \quad \text{(v)}$$

from (iv) and (v): $k_{\beta\text{-OR,obs}}[\mathbf{5}] = k_{\beta\text{-OR}}[\mathbf{4}]$

$$==> [\mathbf{4}] = (k_{\beta\text{-OR,obs}}[\mathbf{5}])/k_{\beta\text{-OR}} \quad \text{(vi)}$$

from (iii) and (vi): $k_{\mathbf{5}\text{ to }\mathbf{4}}[\mathbf{5}]/(k_{\mathbf{4}\text{ to }\mathbf{5}} + k_{\beta\text{-OR}}) = (k_{\beta\text{-OR,obs}}[\mathbf{5}])/k_{\beta\text{-OR}}$

$$==> k_{\beta\text{-OR}} = k_{\beta\text{-OR,obs}}\, k_{\mathbf{4}\text{ to }\mathbf{5}} /(k_{\mathbf{5}\text{ to }\mathbf{4}} - k_{\beta\text{-OR,obs}})$$

$$k_{\beta\text{-OR}} > k_{\beta\text{-OR,obs}}\, k_{\mathbf{4}\text{ to }\mathbf{5}}/k_{\mathbf{5}\text{ to }\mathbf{4}}$$

$$k_{\beta\text{-OR}} > k_{\beta\text{-OR,obs}}\, K_{\mathbf{5/4}}$$

$$k_{\beta\text{-OR}} > 19\, k_{\beta\text{-OR,obs}} \quad (8)$$

1.4 Methods for kinetic studies. For all cases, the kinetics of both the decrease of the reactants and the increase of the products were measured, and found to be in good agreement.

The kinetics of the decrease of the reactants was analyzed according to the following equations:

$$Ln([A]/[A]_0) = kt$$

$$[A]/[A]_0 = I_{normalized}/I_{0,\ normalized}$$

$$I_{normalized} = I^*/I_{std}$$

$$I_{0,\ normalized} = I_0/I_{std}$$

I* is the intensity of the peak of interest, for example, the Pd*Me* resonance for insertion studies and the PdCMe_2 resonance for β-OR elimination studies. In some cases the integration of the OCH_2CH$_3$ resonance of OEt$_2$ was used as I_{std}. If peaks from other species overlapped

with the OCH_2CH$_3$ resonance we used the whole aromatic region as I_{std}. For the reaction of **1**[SbF_6] with **2f**, we analyzed the results by using both OCH_2CH$_3$ resonance from OEt_2 and the whole aromatic region as I_{std}, which gave the same results.

The kinetics of the increase of the products was analyzed according to the following equations:

$$Ln[([B]_\infty-[B])/([B]_\infty-[B]_0)] = kt$$

$$([B]_\infty-[B])/([B]_\infty-[B]_0) = (I_{\infty,\ normalized} - I^*)/(I_{\infty,\ normalized} - I_{0,\ normalized})$$

$$I_{normalized} = I^*/I_{std}$$

$$I_{0,\ normalized} = I_0/I_{std}$$

I* is the intensity of the peak of interest, for example, the PdCMe_2 and PdCH_2CH(OEt)Me resonances for insertion studies and the Pd(η^3-CH_2CHCH_2) resonance for β-OR elimination studies. Specifically, for the case of CH_2=CHOEt and CH_2=CHOPh, in which the β-OR elimination rate is comparable with the insertion rate, we used the sum of PdCMe_2, PdCH_2CH(OEt)Me and Pd(η^3-CH_2CHCH_2) resonances as the I* for insertion kinetics. Kinetic data and plots are shown in Sections 5, 6 and 7; representative NMR spectra from kinetic studies are shown in Section 10.

2. Cationic Polymerization of 2a,c and Characterization of Poly(vinyl ether).

2.1 Cationic polymerization of CH_2=CHO^{t}Bu (2a) by [Li(Et_2O)$_{2.8}$][B(C_6F_5)$_4$]. An NMR tube was charged with [Li(Et_2O)$_{2.8}$][B(C_6F_5)$_4$] (22.7 mg, 0.0254 mmol). CD_2Cl_2 (0.4 mL) was added by vacuum transfer at -196 °C. The tube was warmed to 20 °C and shaken. **2a** (1.25 mmol) was added by vacuum transfer at -196 °C. The tube was warmed to 20 °C, shaken vigorously, and monitored periodically by NMR. ^{1}H NMR spectra showed that **2a** was

quantitatively converted to polymer after 20 h. 2,6-di-tert-butylpyridine significantly retards the polymerization of **2a** by $[Li(Et_2O)_{2.8}][B(C_6F_5)_4]$.

2.2 Cationic polymerization of CH_2=CHO^{t}Bu (2a) by $[Ph_3C][B(C_6F_5)_4]$. An NMR tube was charged with $[Ph_3C][B(C_6F_5)_4]$ (24.5 mg, 0.0266 mmol). $CDCl_3$ (0.4 mL) was added by vacuum transfer at -196 °C. The tube was warmed to 20 °C and shaken. **2a** (1.25 mmol) was added by vacuum transfer at -196 °C. The tube was warmed to 20 °C, shaken vigorously, and monitored periodically by NMR. ^{1}H NMR spectra showed that **2a** was quantitatively converted to polymer after 20 h.

2.3 Polymerization of CH_2=CHOSiMe$_3$ (2c) by 1$[B(C_6F_5)_4]$. A Schlenk flask was charged with (α-diimine)PdMeCl (11.4 mg, 0.0203 mmol) and $[Li(Et_2O)_{2.8}][B(C_6F_5)_4]$ (17.6 mg, 0.0197 mmol). CH_2Cl_2 (1 mL) was added by syringe. The mixture was stirred vigorously at 20 ^{o}C for 10 min. A solution of **2c** (400 mg, 3.33 mmol) in CH_2Cl_2 (9 mL) was added by cannula. The mixture became dark within 10 min, indicating the formation of Pd^0. After 20 h, the volatiles were removed under vacuum, affording dark oil. NMR analysis showed that the oil contained poly(trimethylsilyl vinyl ether) (-$[CH_2CH(OSiMe_3)]_n$-), free α-diimine and other unidentified species. Approximately 7 % of **2c** was converted to polymer. 2,6-di-tert-butylpyridine does not significantly affect the polymerization of **2c** by **1**$[B(C_6F_5)_4]$.

2.4 Attempted polymerization of CH_2=CHOSiPh$_3$ by 1$[B(C_6F_5)_4]$. An NMR tube was charged with (α-diimine)PdMeCl (5.5 mg, 0.010 mmol), $[Li(Et_2O)_{2.8}][B(C_6F_5)_4]$ (8.3 mg, 0.0093 mmol) and CH_2=CHOSiPh$_3$ (176 mg, 0.582 mmol). CD_2Cl_2 (0.4 mL) was added

by vacuum transfer at -196 °C. The tube was warmed to 20 °C, shaken and monitored by ^{1}H NMR periodically. NMR spectra showed that no polymer had formed after 20 h.

2.5 Attempted polymerization of CH_2=CHOPh by 1[$B(C_6F_5)_4$]. An NMR tube was charged with (α-diimine)PdMeCl (8.4 mg, 0.015 mmol), [$Li(Et_2O)_{2.8}$][$B(C_6F_5)_4$] (13.4 mg, 0.0150 mmol) and CH_2=CHOPh (33 mg, 0.27 mmol). CD_2Cl_2 (0.4 mL) was added by vacuum transfer at -196 °C. The tube was warmed to 20 °C, shaken, and monitored by ^{1}H NMR periodically. NMR spectra showed that no polymer had formed after 20 h.

2.6 Cationic polymerization of CH_2=CHOSiMe_3 (2c) by [$Li(Et_2O)_{2.8}$][$B(C_6F_5)_4$]. A Schlenk flask was charged with [$Li(Et_2O)_{2.8}$][$B(C_6F_5)_4$] (17.8 mg, 0.0199 mmol). A solution of **2c** (320 mg, 2.67 mmol) in CH_2Cl_2 (10 mL) was added by cannula and the mixture was stirred vigorously at 20 °C. After 20 h, the volatiles were removed under vacuum. The nonvolatile oily residue was dried under vacuum to yield a white oil (120 mg), which was identified as poly(trimethylsilyl vinyl ether) (-[$CH_2CH(OSiMe_3)]_n$-) by NMR.

2.7 Cationic polymerization of CH_2=CHOSiMe_3 (2c) by [Ph_3C][$B(C_6F_5)_4$]. A flask was charged with [Ph_3C][$B(C_6F_5)_4$] (24.4 mg, 0.0265 mmol) and cooled to -196 °C. Chlorobenzene (1.2 mL) was added by vacuum transfer. The mixture was warmed to 23 °C. A Schlenk tube was charged with chlorobenzene or toluene (1.2 mL) and cooled to -196 °C. **2c** (1.50 mL, 1.17 g, 375 equiv) was added by vacuum transfer. The Schlenk tube was warmed to -40 °C with a dry ice/acetonitrile bath. The catalyst solution (at 23 °C) was transferred by cannula to the Schlenk tube. The mixture was stirred for 2 h at -40 °C and then quenched with methanol (1 mL) pre-cooled to -40 °C. Immediate gellation occurred upon the addition of

methanol. The mixture was transferred to a flask containing methanol (75 mL) and the mixture was stirred for 7.5 h. The white solid precipitate was collected by filtration, washed with methanol, dried under vacuum, and identified as poly(vinyl alcohol).[1] For reaction in chlorobenzene: yield 339 mg (76%), M_n 4000. For reaction in toluene: yield 429 mg (97 %), M_n 7000.

2.8 Key NMR data for -[$CH_2CH(OSiMe_3)]_n$-. ^{1}H NMR ($CDCl_3$): δ 9.72 (m, –$CH_2CH(OSiMe_3)CH_2C(=O)H$), 5.52 (-$CH_2CH(OSiMe_3)CH=CHCH_2$-), 5.42 (-$CH_2CH(OSiMe_3)CH=CHCH_2$-), 3.84 (br, -$CH_2CH(OSiMe_3)$-), 1.57 (br, -$CH_2CH(OSiMe_3)$-), 0.10 (br, -$CH_2CH(OSiMe_3)$-). **^{13}C{^{1}H} NMR** ($CDCl_3$): δ 70.8 (br, -$CH_2CH(OSiMe_3)$-), 69.4 (br, -$CH_2CH(OSiMe_3)$-), 65.7 (br, -$CH_2CH(OSiMe_3)$-), 65.4 (br, -$CH_2CH(OSiMe_3)$-), 46.6 (br, -$CH_2CH(OSiMe_3)$-), 1.0 (br, -$CH_2CH(OSiMe_3)$-).

3. Generation of [(α-diimine)PdMe(CH_2=CHOR)][SbF_6] (3b-g[SbF_6]) Complexes from 1[SbF_6].

The adducts [(α-diimine)PdMe(CH_2=CHOEt)][SbF_6] (**3b**[SbF_6]), [(α-diimine)PdMe(CH_2=CHOSiMe_3)][SbF_6] (**3c**[SbF_6]), [(α-diimine)PdMe(CH_2=CHOSiMe_2Ph)][SbF_6] **(3d**[SbF_6]**),** [(α-diimine)PdMe(CH_2=CHOSiMePh_2)][SbF_6] **(3e**[SbF_6]**),** [(α-diimine)PdMe(CH_2=CHOSiPh_3)][SbF_6] (**3f**[SbF_6]) and [(α-diimine)PdMe(CH_2=CHOPh)][SbF_6] (**3g**[SbF_6]) were generated using the procedure described for **3a**[SbF_6] on similar scales and with similar yields.

3.1 Generation of [(α-diimine)PdMe(CH_2=CHOEt)][SbF_6] (3b[SbF_6]). An NMR tube was charged with **1**[SbF_6] (13.0 mg, 0.0157 mmol) and CD_2Cl_2 (0.4 mL) was added by vacuum transfer at -196 °C. **2b** (0.0173 mmol) was added by vacuum transfer at -196 °C. The

tube was warmed to -78 °C, shaken to dissolve and thoroughly mix the components, and placed in an NMR probe that had been pre-cooled to -20 °C. NMR spectra at -60 °C showed that **3b**[SbF_6] (95 %) had formed. **^{1}H NMR** (CD_2Cl_2, -20 °C): δ 7.37-7.32 (m, 6H), 6.76 (dd, *J* = 13, 4; 1H, H_{int}), 4.04 (dq, J = 17, 8, 2H, OC*H*$_2$CH$_3$), 3.26 (d, *J* = 13, 1H, H_{trans}), 3.11 (d, *J* = 4, 1H, H_{cis}), 3.00 (sept, *J* = 7, 1H, C*H*Me$_2$), 2.85 (sept, *J* = 7, 1H, C*H*Me$_2$), 2.81 (sept, *J* = 7, 1H, C*H*Me$_2$), 2.73 (sept, *J* = 7, 1H, C*H*Me$_2$), 2.33 (s, 3H, N=C*Me*), 2.25 (s, 3H, N=C*Me*), 1.41 (d, *J* = 7, 3H, CH*Me$_2$*), 1.37 (d, *J* = 7, 3H, CH*Me$_2$*), 1.32 (d, *J* = 7, 3H, CH*Me$_2$*), 1.29 (d, *J* = 7, 3H, CH*Me$_2$*), 1.28 (d, *J* = 7, 3H, CH*Me$_2$*), 1.19 (t, *J* = 7, 3H, OCH$_2$C*H*$_3$), 1.15 (d, *J* = 7, 3H, CH*Me$_2$*), 1.13 (d, *J* = 7, 3H, CH*Me$_2$*), 1.08 (free Et_2O and CH*Me$_2$*), 0.18 (s, 3H, Pd*Me*). **^{13}C{^{1}H} NMR** (CD_2Cl_2, -20 °C): δ 179.8 (N=*C*Me), 175.7 (N=*C*Me), 148.4 (CH$_2$=*C*HOEt), 139.8, 139.4, 138.3, 138.2, 138.1, 137.4, 128.65, 128.60, 125.2, 125.0, 124.7, 124.5, 71.8 (O*C*H$_2$CH$_3$), 56.7 (*C*H$_2$=CHOEt), 29.3, 29.2, 29.0, 28.9, 24.6 (2C), 23.9, 23.8, 23.5, 23.4, 23.3, 23.0, 22.0, 21.7, 15.4 (OCH$_2$*C*H$_3$), 14.9 (Pd*Me*).

3.2 [(α-diimine)PdMe(CH$_2$=CHOSiMe$_3$)][SbF$_6$] (3c[SbF$_6$]). ^{1}H NMR (CD_2Cl_2, -60 °C): δ 7.38-7.25 (m, 6H), 6.91 (dd, *J* = 12, 4; 1H, H_{int}), 3.36 (d, *J* = 12, 1H, H_{trans}), 3.14 (d, *J* = 4, 1H, H_{cis}), 2.87-2.78 (m, 4H, C*H*Me$_2$), 2.32 (s, 3H, N=C*Me*), 2.24 (s, 3H, N=C*Me*), 1.36 (d, *J* = 7, 3H, CH*Me$_2$*), 1.33 (d, *J* = 7, 3H, CH*Me$_2$*), 1.28 (d, *J* = 7, 3H, CH*Me$_2$*), 1.23 (d, *J* = 7, 3H, CH*Me$_2$*), 1.18 (d, *J* = 7, 3H, CH*Me$_2$*), 1.15 (d, *J* = 7, 3H, CH*Me$_2$*), 1.12 (d, *J* = 7, 3H, CH*Me$_2$*), 1.06 (d, *J* = 7, 3H, CH*Me$_2$*), 0.25 (s, 9H, OSi*Me$_3$*), 0.15 (s, Pd*Me*). **^{13}C{^{1}H} NMR** (CD_2Cl_2, -60 °C): δ 179.8 (N=*C*Me), 175.4 (N=*C*Me), 143.1 (CH$_2$=*C*HOSiMe$_3$), 139.2, 138.7, 138.0, 137.7, 137.5, 137.0, 128.1 (2C), 124.6, 124.5, 124.1, 124.0, 60.6 (*C*H$_2$=CHOSiMe$_3$), 28.70, 28.68,

28.31, 28.27, 24.3, 24.0, 23.8, 23.6, 23.4, 23.3, 22.7, 22.6, 21.5, 21.4, 15.6 (Pd*Me*), -1.0 (OSi*Me*$_3$).

3.3 [(α-diimine)PdMe(CH$_2$=CHOSiMe$_2$Ph)][SbF$_6$] (3d[SbF$_6$]). ^{1}H NMR (CD_2Cl_2, -60 °C): δ 6.83 (dd, *J* = 12, 3; 1H, H_{int}), 3.50 (d, *J* = 12, 1H, H_{trans}), 3.18 (d, *J* = 3, 1H, H_{cis}), 2.91 (m, 1H, C*H*Me$_2$), 2.83 (m, 1H, C*H*Me$_2$), 2.78 (m, 1H, C*H*Me$_2$), 2.56 (m, 1H, C*H*Me$_2$), 2.34 (s, 3H, N=C*Me*), 2.22 (s, 3H, N=C*Me*), 1.29 (m, 6H, CH*Me*$_2$), 1.23 (m, 6H, CH*Me*$_2$), 1.12 (d, *J* = 7, 3H, CH*Me*$_2$), 1.03 (m, 6H, CH*Me*$_2$), 0.91 (d, *J* = 7, 3H, CH*Me*$_2$), 0.53 (s, 3H, SiC*H*$_3$), 0.44 (s, 3H, SiC*H*$_3$), 0.20 (s, 3H, Pd*Me*); the α-diimine and free and coordinated CH$_2$=CHOSiMePh$_2$ aromatic resonances overlap and are not listed. Key ^{13}C NMR (CD_2Cl_2, -60 ^{o}C) data: δ180.2 (N=*C*Me), 175.6 (N=*C*Me), 142.6 (CH$_2$=*C*HOSiMePh$_2$), 139.2 (Ar, C_{ipso}), 138.5 (Ar, C_{ipso}), 138.1 (Ar, C_o), 138.0 (Ar, C_o), 137.4 (Ar, C_o), 137.1 (Ar, C_o), 124.6 (Ar, C_m), 124.4 (Ar, C_m), 124.2 (Ar, C_m), 124.0 (Ar, C_m), 61.6 (*C*H$_2$=CHOSiMePh$_2$), 28.8 (*C*HMe$_2$), 28.7 (*C*HMe$_2$), 28.3 (*C*HMe$_2$, 2C), 24.2 (CH*Me*$_2$), 23.9 (CH*Me*$_2$), 23.8 (CH*Me*$_2$), 23.6 (CH*Me*$_2$), 23.4 (CH*Me*$_2$), 23.3 (CH*Me*$_2$), 22.9 (CH*Me*$_2$), 22.6 (CH*Me*$_2$), 21.5 (N=C*Me*), 21.4 (N=C*Me*), 9.0 (Pd*Me*), -2.0 (Si*Me*), -2.3 (Si*Me*).

3.4 [(α-diimine)PdMe(CH$_2$=CHOSiMePh$_2$)][SbF$_6$] (3e[SbF$_6$]). ^{1}H NMR (CD_2Cl_2, -60 °C): δ 6.89 (dd, *J* = 12, 3; 1H, H_{int}), 3.67 (d, *J* = 12, 1H, H_{trans}), 3.18 (d, *J* = 3, 1H, H_{cis}), 3.03-2.30 (m, 4H, C*H*Me$_2$), 2.37 (s, 3H, N=C*Me*), 2.22 (s, 3H, N=C*Me*), 1.28-1.21 (m, 12H, CH*Me*$_2$), 1.17 (d, *J* = 7, 3H, CH*Me*$_2$), 1.12 (d, *J* = 7, 3H, CH*Me*$_2$), 1.02 (d, *J* = 7, 3H, CH*Me*$_2$), 0.97 (d, *J* = 7, 3H, CH*Me*$_2$), 0.70 (s, 3H, SiC*H*$_3$), 0.26 (s, 3H, Pd*Me*); the α-diimine and free and coordinated CH$_2$=CHOSiMePh$_2$ aromatic resonances overlap and are not listed. Key ^{13}C NMR (CD_2Cl_2, -60 ^{o}C) data: δ 180.5 (N=*C*Me), 175.7 (N=*C*Me), 141.8 (CH$_2$=*C*HOSiMePh$_2$), 139.2

(Ar, C_{ipso}), 138.4 (Ar, C_{ipso}), 138.2 (Ar, C_o), 138.0 (Ar, C_o), 137.1 (Ar, C_o), 137.0 (Ar, C_o), 124.6 (Ar, C_m), 124.3 (Ar, C_m), 124.2 (Ar, C_m), 124.0 (Ar, C_m), 62.5 (CH_2=CHOSiMePh_2), 28.9 (*C*HMe_2), 28.8 (*C*HMe_2), 28.4 (*C*HMe_2, 2C), 24.1 (CH*Me*$_2$), 24.0 (CH*Me*$_2$), 23.8 (CH*Me*$_2$), 23.7 (CH*Me*$_2$), 23.3 (CH*Me*$_2$), 23.1 (CH*Me*$_2$), 22.7 (CH*Me*$_2$), 22.5 (CH*Me*$_2$), 21.5 (N=C*Me*), 21.4 (N=C*Me*), 8.9 (Pd*Me*), -1.1 (Si*Me*Ph_2).

3.5 [(α-diimine)PdMe(CH_2=CHOSiPh_3)][SbF_6] (3f[SbF_6]). ^{1}H NMR (CD_2Cl_2, -60 °C) δ 7.12 (dd, *J* = 12, 4; 1H, H_{int}), 3.78 (d, *J* = 12, 1H, H_{trans}), 3.22 (d, *J* = 4, 1H, H_{cis}), 2.97-2.65 (m, 4H, C*H*Me_2), 2.37 (s, 3H, N=C*Me*), 2.22 (s, 3H, N=C*Me*), 1.29 (d, *J* = 7, 3H, CH*Me*$_2$), 1.25 (d, *J* = 7, 6H, CH*Me*$_2$), 1.11 (d, *J* = 7, 3H, CH*Me*$_2$), 1.05 (d, *J* = 7, 3H, CH*Me*$_2$), 0.91 (d, *J* = 7, 3H, CH*Me*$_2$), 0.84 (d, *J* = 7, 3H, CH*Me*$_2$), 0.34 (d, *J* = 7, 3H, CH*Me*$_2$), 0.23 (s, 3H, Pd*Me*); the α-diimine and free and coordinated CH_2=CHOSiPh_3 aromatic resonances overlap and are not listed. Key ^{13}C NMR (CD_2Cl_2, -60 °C) data: δ 180.7 (N=*C*Me), 175.9 (N=*C*Me), 141.8 (CH_2=*C*HOSiPh_3), 139.2 (Ar, C_{ipso}), 138.6 (Ar, C_{ipso}), 138.2 (Ar, C_o), 138.0 (Ar, C_o), 137.6 (Ar, C_o), 137.0 (Ar, C_o), 124.6 (Ar, C_m), 124.3 (Ar, C_m), 124.2 (Ar, C_m), 124.0 (Ar, C_m), 62.8 (*C*H_2=CHOSiPh_3), 28.9 (*C*HMe_2), 28.8 (*C*HMe_2), 28.6 (*C*HMe_2), 28.4 (*C*HMe_2), 24.0 (CH*Me*$_2$), 23.9 (CH*Me*$_2$), 23.7 (CH*Me*$_2$), 23.3 (CH*Me*$_2$), 23.2 (CH*Me*$_2$), 22.7 (CH*Me*$_2$), 22.4 (CH*Me*$_2$), 22.3 (CH*Me*$_2$), 21.5 (N=C*Me*), 21.4 (N=C*Me*), 9.0 (Pd*Me*).

3.6 [(α-diimine)PdMe(CH_2=CHOPh)][SbF_6] (3g[SbF_6]). ^{1}H NMR (CD_2Cl_2, -20 °C)[2] δ 7.51 (t, *J* = 8, 2H, H_{meta}), 7.39-7.27 (m, 9H), 7.00 (dd, *J* = 12, 4; 1H, H_{int}), 3.77 (d, *J* = 12, 1H, H_{trans}), 3.35 (d, *J* = 4, 1H, H_{cis}), 2.99 (m, 2H, C*H*Me_2), 2.88 (m, 1H, C*H*Me_2), 2.82 (m, 1H, C*H*Me_2), 2.41 (s, 3H, N=C*Me*), 2.35 (s, 3H, N=C*Me*), 1.35 (d, *J* = 7, 3H, CH*Me*$_2$), 1.24 (d, *J* = 7, 3H, CH*Me*$_2$), 1.22 (d, *J* = 7, 3H, CH*Me*$_2$), 1.20 (d, *J* = 7, 3H, CH*Me*$_2$), 1.18 (d, *J* = 7, 3H,

CH*Me*$_2$), 1.10 (d, *J* = 7, 3H, CH*Me*$_2$), 1.08 (d, *J* = 7, 3H, CH*Me*$_2$), 0.94 (d, *J* = 7, 3H, CH*Me*$_2$), 0.26 (s, 3H, Pd*Me*).

3.7 [(2,6-^{i}Pr$_2$-C$_6$H$_3$)N=CAnCAn=N(2,6-^{i}Pr$_2$-C$_6$H$_3$)][SbF$_6$] (3h[SbF$_6$]). A NMR tube was charged with [(2,6-^{i}Pr$_2$-C$_6$H$_3$)N=CAnCAn=N(2,6-^{i}Pr$_2$-C$_6$H$_3$)]PdMeCl (19.2 mg, 29.0 μmol), AgSbF$_6$ (10 mg, 29.1 μmol) and CH$_2$=CHOSiPh$_3$ (8.8 mg, 29.1 μmol), and CD_2Cl_2 (0.4 mL) was added by vacuum transfer at –78 °C. The tube was shaken to dissolve and thoroughly mix the components, and placed in an NMR probe that had been pre-cooled to -60 °C. NMR spectra at -60 °C showed that **3h**[SbF$_6$] (95 %) had formed. **^{1}H NMR** (CD_2Cl_2, -60 °C): δ 8.24 (δ, *J* = 8, 1H, An: H$_p$), 8.19 (δ, *J* = 8, 1H, An: H$_{p'}$), 7.65-7.33 (m, 23 H, An: H$_m$, H$_{m'}$, 6 H$_{aryl}$, 15 H$_{aryl}$ from SiPh$_3$), 7.32 (dd, *J* = 12, 4; 1H, H$_{int}$), 6.49 (δ, *J* = 7, 1H, An: H$_o$), 6.39 (δ, *J* = 7, 1H, An: H$_{o'}$), 4.00 (d, *J* = 12, 1H, H$_{trans}$), 3.59 (d, *J* = 4, 1H, H$_{cis}$), 3.29 (m, 1H, C*H*Me$_2$), 3.01 (m, 2H, C*H*Me$_2$), 2.50 (m, 1H, C*H*Me$_2$), 1.29 (d, *J* = 7, 3H, CH*Me*$_2$), 1.27 (br, 3H, CH*Me*$_2$), 1.06 (br, 3H, CH*Me*$_2$), 0.97 (d, *J* = 7, 3H, CH*Me*$_2$), 0.81 (d, *J* = 7, 3H, CH*Me*$_2$), 0.70 (d, 6H, CH*Me*$_2$), 0.51 (s, 3H, Pd*Me*), 0.48 (br, 3H, CH*Me*$_2$). Key ^{13}C NMR (CD_2Cl_2, -60 ^{o}C) data: δ 175.4 (N=*C*Me), 171.2 (N=*C*Me), 141.7 (CH$_2$=*C*HOSiPh$_3$), 145.7, 139.0, 138.8, 138.5, 138.0, 137.3, 137.2, 135.2, 133.6, 132.7, 131.5, 130.9, 129.5, 129.2, 129.1, 128.9, 128.5, 128.2, 126.6, 126.1, 125.2, 125.0, 124.9, 124.8, 124.7 and 124.6 (An 4 quaternary C, C$_o$, C$_o$', C$_m$, C$_m$', C$_p$, C$_p$'; Ar, Ar' C$_{ipso}$, C$_{ipso}$', C$_o$, C$_o$', C$_o$", C$_o$"', C$_m$, C$_m$', C$_m$", C$_m$"', C$_p$, C$_p$'; SiPh C$_{ipso}$, C$_o$, C$_m$, C$_p$,) , 62.2 (*C*H$_2$=CHOSiPh$_3$), 29.4 (*C*HMe$_2$), 29.2 (*C*HMe$_2$), 29.0 (*C*HMe$_2$), 28.9 (*C*HMe$_2$), 24.7 (CH*Me*$_2$), 24.5 (CH*Me*$_2$), 23.8 (CH*Me*$_2$), 23.4 (CH*Me*$_2$), 23.3 (CH*Me*$_2$), 23.0 (CH*Me*$_2$), 22.8 (CH*Me*$_2$), 22.4 (CH*Me*$_2$), 13.4 (Pd*Me*).

3.8 [{(4-Me-C_6H_5)N=CMeCMe=N(4-Me-C_6H_5)}PdMe(CH_2=CHOSiPh_3)][SbF_6] (3i).

A NMR tube was charged with (α-diimine-Me)PdMeCl (19.2 mg, 29.0 μmol), $AgSbF_6$ (10 mg, 29.1 μmol) and CH_2=CHOSiPh_3 (8.8 mg, 29.1 μmol), and CD_2Cl_2 (0.4 mL) was added by vacuum transfer at –78 °C. The tube was shaken to dissolve and thoroughly mix the components. NMR spectra at -70 °C showed that two rotamers of **3i** (95 %) had formed. **^{1}H NMR** (CD_2Cl_2, -70 °C) δ 7.59 (t, J = 7 Hz, 12H, C_m, Si-Ph), 7.55 (d, J = 7 Hz, 12H, C_o, Si-Ph), 7.44 (t, J = 7 Hz, 6H, C_p, Si-Ph), 7.35 (d, J = 4 Hz, 1H, Ar), 7.32 (d, J = 4 Hz, 1H, Ar), 7.26 (b, 1H, Ar), 7.25 (d, 2H, Ar), 7.17 (d, J = 4 Hz, 1H, Ar), 6.94 (d, J = 4 Hz, 1H, Ar), 6.92 (d, J = 4 Hz, 1H, Ar), 6.90 (d, 1H, H_{int}), 6.78 (d, J = 4 Hz, 1H, Ar), 6.76 (d, J = 4 Hz, 1H, Ar), 6.74 (d, J = 4 Hz, 1H, Ar), 6.67 (d, J = 4 Hz, 1H, Ar), 6.65 (d, J = 4 Hz, 1H, Ar), 6.64 (d, J = 4 Hz, 1H, Ar), 6.34 (d, 1H, H_{int}), 6.05 (d, J = 4 Hz, 1H, Ar), 5.62 (d, J = 4 Hz, 1H, Ar), 3.78 (d, *J* = 12, 1H, H_{trans}), 3.56 (b, 2H, H_{cis}), 3.49 (d, *J* = 12, 1H, H_{trans}), 2.37, 2.34, 2.32, 2.25, 2.24, 2.16, 2.04, 1.91, 0.17 (s, 3H, Pd-Me), -0.18 (s, 3H, Pd-Me).

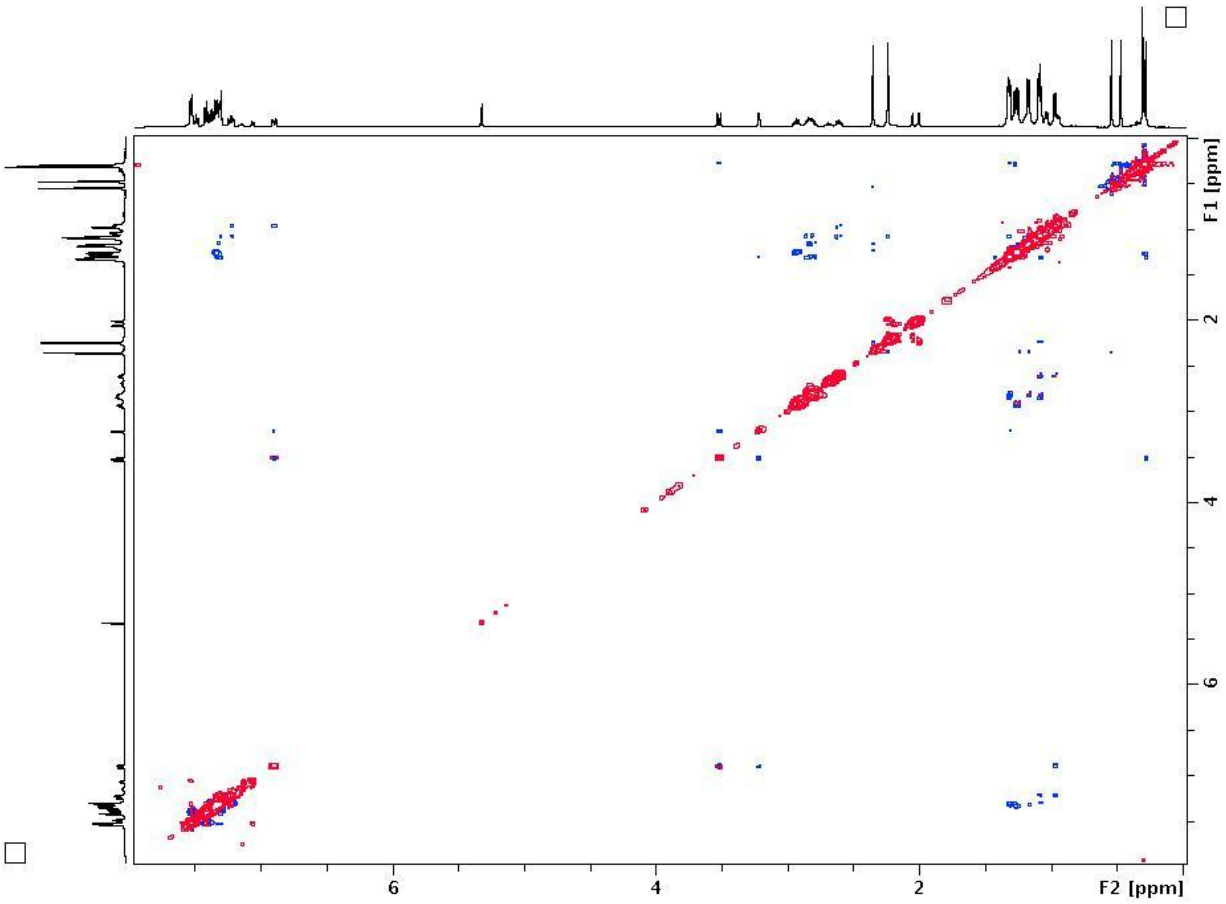

Figure 3.1. NOSEY NMR of **3d**[SbF_6] (CD_2Cl_2, -20 °C): expansion of the δ 8.0-0.0;8.0-0.0 region.

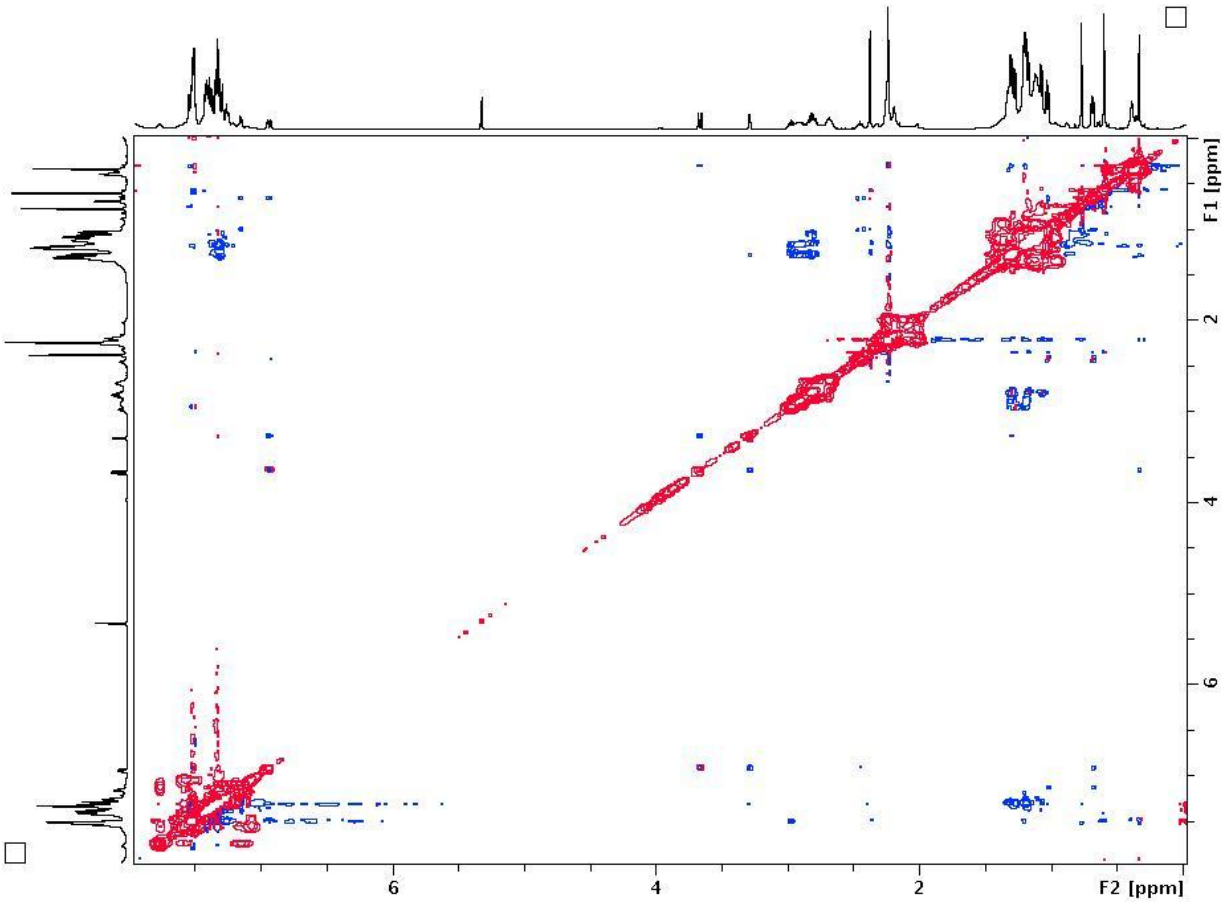

Figure 3.2. NOSEY NMR of **3e**[SbF_6] (CD_2Cl_2, -20 °C): expansion of the δ 8.0-0.0;8.0-0.0 region.

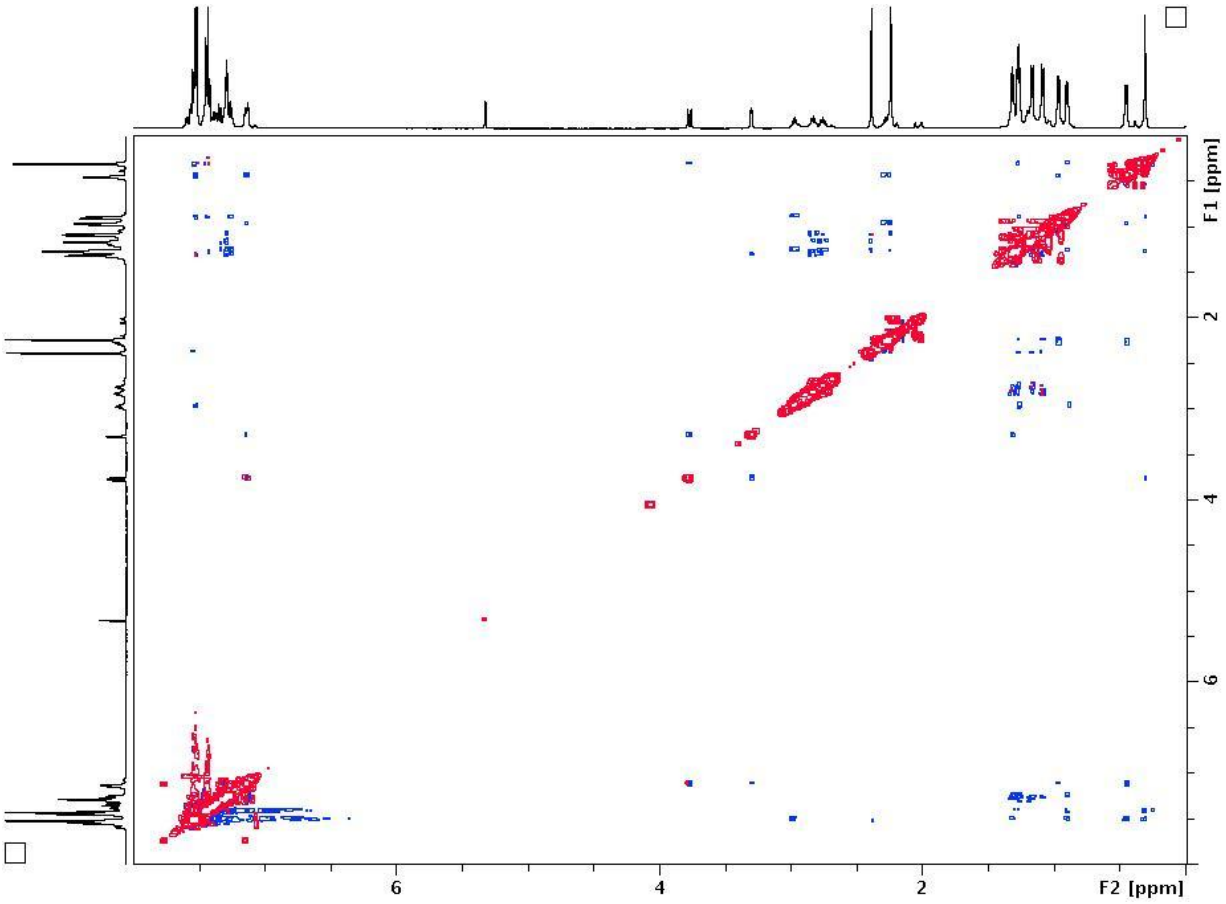

Figure 3.3. NOSEY NMR of **3f**[SbF_6] (CD_2Cl_2, -20 °C): expansion of the δ 8.0-0.0;8.0-0.0 region.

4. Competitive Binding Studies.

4.1 Competitive binding of 2d-g and 2c to 1[SbF_6] at -20 °C (eq 5). The procedure for **2d** is described here; an identical procedure was used for **2e**-**g**. An NMR tube was charged with **1**[SbF_6] (15.0 mg, 0.0179 mmol) and **2d** (31.0 mg, 0.258 mmol). CD_2Cl_2 (0.4 mL) and **2c** (0.034 mmol) were added by vacuum transfer at -196 °C. The tube was warmed to -78 °C, shaken and placed in an NMR probe that had been pre-cooled to -20 °C. The reaction was monitored periodically by ^{1}H NMR at -20 °C until after 30 min, when the reaction quotient $Q_{2e/2c} = [\mathbf{3d}][\mathbf{2c}][\mathbf{3c}]^{-1}[\mathbf{2d}]^{-1}$ reached a constant value. Additional **2d** (0.14 mmol) was added by

vacuum transfer to change the **2c**/**2d** ratio, and the tube was monitored by ^{1}H NMR at -20 ^{o}C until $Q_{\mathbf{2d/2c}}$ again reached a constant value. The process was repeated one more time and the average $K_{\mathbf{2d/2c}}$ value is reported in Table 2 of the text.

4.2 Competitive binding of ethylene and CH_2=CHOR (2a-c, 2g) to 1[$B(C_6F_5)_4$] at -60 ^{o}C (eq 4). The procedure for **2a** is described here; an identical procedure was used for **2b**, **2c**, **2f**, **2g**. An NMR tube was charged with (α-diimine)PdMeCl (11.2 mg, 0.0199 mmol) and $[Li(Et_2O)_{2.8}][B(C_6F_5)_4]$ (17.5 mg, 0.0196 mmol). CD_2Cl_2 (0.4 mL) was added by vacuum transfer at -196 °C. The tube was warmed to 20 ^{o}C and shaken. Ethylene (0.062 mmol) and **2a** (0.040 mmol) were added by vacuum transfer at -196 °C. The tube was warmed to -78 °C, shaken, and placed in an NMR probe that had been pre-cooled to -60 °C. The reaction was monitored periodically by ^{1}H NMR at -60 °C until after 1 h, when the reaction quotient $Q_{\mathbf{2a}/\text{ethylene}} = [\mathbf{3a}][CH_2{=}CH_2][(\alpha\text{-diimine})PdMe(CH_2{=}CH_2)^+]^{-1}[\mathbf{2a}]^{-1}$ reached a constant value. Additional **2a** (0.062 mmol) was added by vacuum transfer to change the ethylene/**2a** ratio, and the tube was monitored by ^{1}H NMR at -60 ^{o}C until $Q_{\mathbf{2a}/\text{ethylene}}$ reached a constant value again.

5. Reaction of CH_2=CHO^{t}Bu (2a) with 1[$B(C_6F_5)_4$].

5.1 Kinetics of insertion of 3a[$B(C_6F_5)_4$]. The first-order rate constant for the consumption of **3a**[$B(C_6F_5)_4$], $k_{\text{insert, }\mathbf{3a}}$, was measured by the disappearance of the Pd*Me* ^{1}H NMR resonance and the increase of the $PdCH_2CHMe$ resonance of **4a**[$B(C_6F_5)_4$] plus the $PdCMe_2$ resonance of **5a**[$B(C_6F_5)_4$], both at 0 °C and at 20 °C.

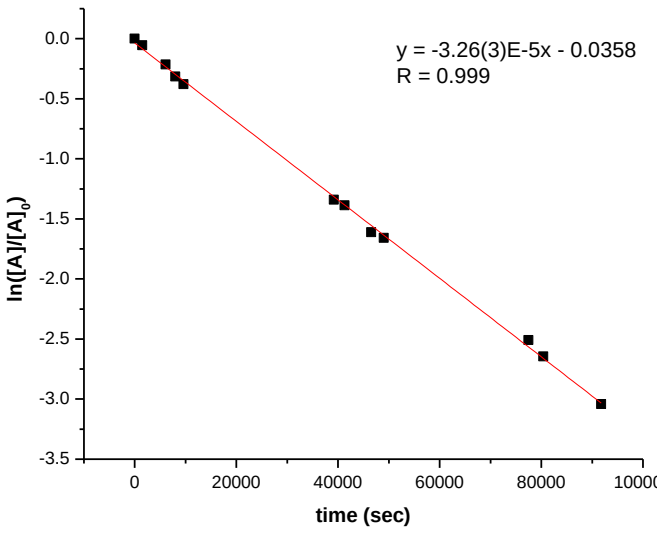

$[A]/[A]_0$	$\ln([A]/[A]_0)$	Time(s)
1	0	0
0.947231	-0.05421	1500
0.807385	-0.21395	6060
0.730323	-0.31427	7980
0.685211	-0.37803	9600
0.262019	-1.33934	39180
0.249934	-1.38656	41280
0.199764	-1.61062	46560
0.190482	-1.6582	49020
0.081449	-2.50777	77460
0.070989	-2.64523	80400
0.047803	-3.04066	91800

Figure 5.1. First-order consumption of **3a**[$B(C_6F_5)_4$] at 0 °C.

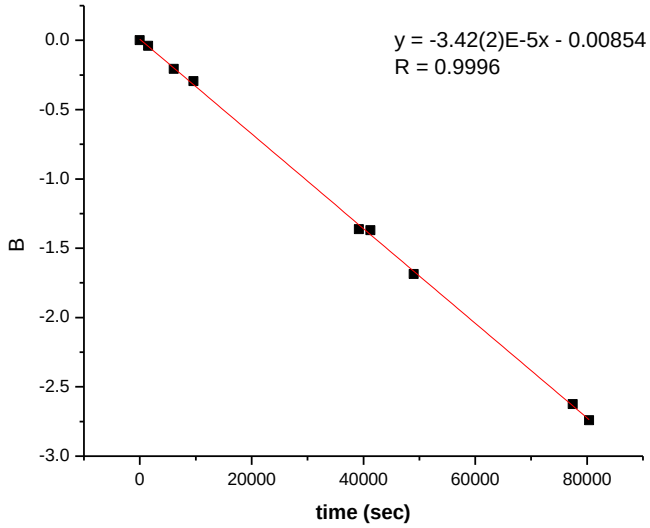

$[B]_\infty-[B]/[B]_\infty-[B]_0$	$\ln[([B]_\infty-[B])/([B]_\infty-[B]_0)]$	Time(s)
1	0	0
0.9609	-0.03988	1500
0.8141	-0.20567	6060
0.7441	-0.29558	9600
0.256	-1.36258	39180
0.2541	-1.37003	41280
0.1851	-1.68686	49020
0.0724	-2.62555	77460
0.0645	-2.74109	80400

Figure 5.2. First-order consumption of **3a**[$B(C_6F_5)_4$] at 0 °C based on the increase of the sum of **4a**[$B(C_6F_5)_4$] + **5a**[$B(C_6F_5)_4$]. B = $\ln[([B]_\infty-[B])/([B]_\infty-[B]_0)]$.

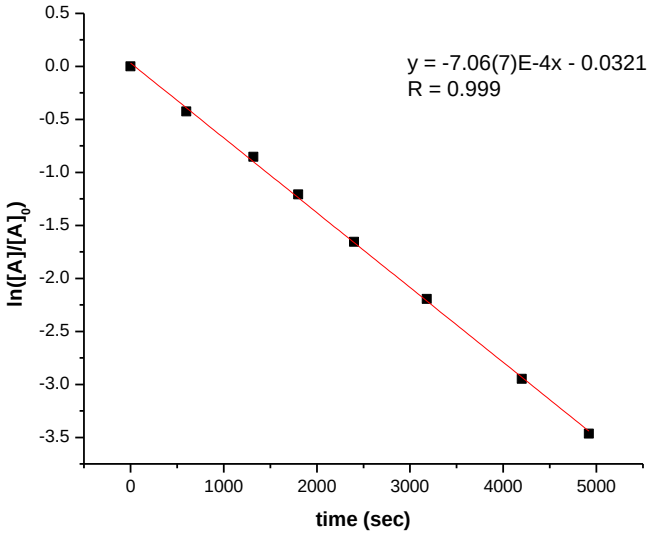

$[A]/[A]_0$	$\ln([A]/[A]_0)$	Time(s)
1	0	0
0.6538	-0.42495	600
0.4262	-0.85285	1320
0.2985	-1.20899	1800
0.1911	-1.65496	2400
0.1115	-2.19373	3180
0.0525	-2.94694	4200
0.0313	-3.46414	4920

Figure 5.3. First-order consumption of **3a**[$B(C_6F_5)_4$] at 20 °C.

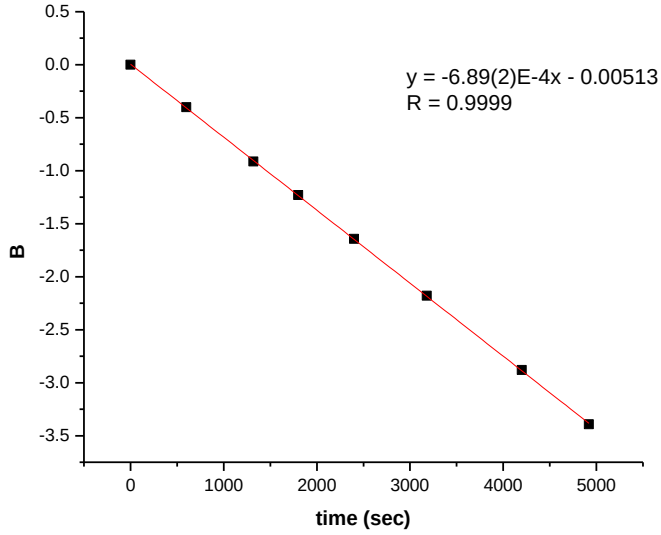

$[B]_\infty-[B]/[B]_\infty-[B]_0$	$\ln([([B]_\infty-[B])/([B]_\infty-[B]_0)]$	Time(s)
1	0	0
0.6694	-0.40137	600
0.4007	-0.91454	1320
0.2921	-1.23066	1800
0.1932	-1.64403	2400
0.113	-2.18037	3180
0.0561	-2.88062	4200
0.0336	-3.39323	4920

Figure 5.4. First-order consumption of **3a**[$B(C_6F_5)_4$] at 20 °C based on the increase of the sum of **4a**[$B(C_6F_5)_4$] + **5a**[$B(C_6F_5)_4$]. $B = \ln[([B]_\infty-[B])/([B]_\infty-[B]_0)]$.

5.2 Kinetics of the β-O^{t}Bu elimination of 5a[B(C$_6$F$_5$)$_4$] and 4a[B(C$_6$F$_5$)$_4$]. The first-order rate constant for consumption of the total of **4a**[B(C$_6$F$_5$)$_4$] and **5a**[B(C$_6$F$_5$)$_4$], $k_{\beta\text{-OtBu, obs}}$, was measured by the disappearance of the PdCH$_2$C*H*Me resonance of **4a**[B(C$_6$F$_5$)$_4$] and the PdC*Me*$_2$ resonance of **5a**[B(C$_6$F$_5$)$_4$] and the increase of the H_{int} resonance of **6**[B(C$_6$F$_5$)$_4$] at 20 °C.

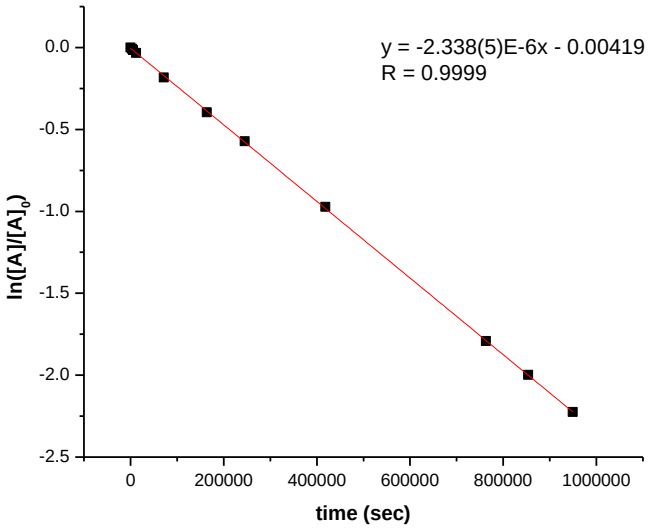

[A]/[A]$_0$	ln([A]/[A]$_0$)	Time(s)
1	0	0
0.99176	-0.00827	3300
0.984	-0.01613	5640
0.9674	-0.03314	12180
0.8327	-0.18308	71460
0.67372	-0.39494	163920
0.5641	-0.57252	245340
0.37786	-0.97323	418380
0.16663	-1.79198	762780
0.1355	-1.99878	853980
0.108	-2.22562	949260

Figure 5.5. First-order consumption of the sum of **4a**[B(C$_6$F$_5$)$_4$] + **5a**[B(C$_6$F$_5$)$_4$] at 20 °C.

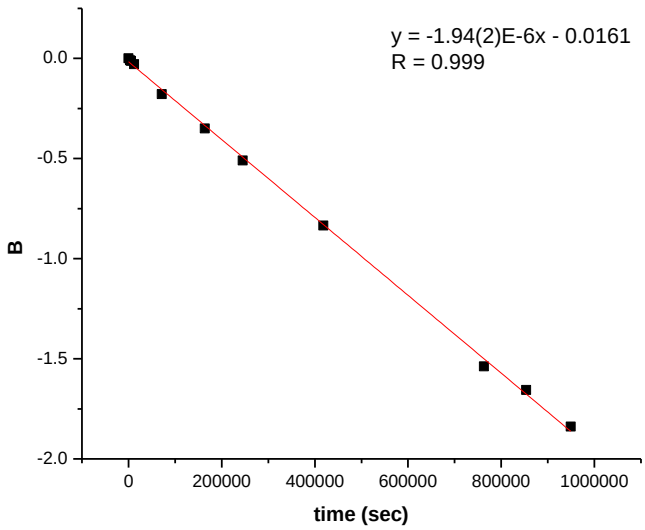

$[B]_\infty$-[B]/ $[B]_\infty$-$[B]_0$	ln[($[B]_\infty$-[B])/ ($[B]_\infty$-$[B]_0$)]	Time(s)
1	0	0
0.9907	-0.00934	3300
0.9881	-0.01197	5640
0.9719	-0.0285	12180
0.8364	-0.17865	71460
0.7044	-0.35041	163920
0.6006	-0.50983	245340
0.4339	-0.83494	418380
0.2147	-1.53851	762780
0.191	-1.65548	853980
0.159	-1.83885	949260

Figure 5.6. First-order consumption of the sum of **4a**[$B(C_6F_5)_4$] + **5a**[$B(C_6F_5)_4$] at 20 °C based on the increase of **6**[$B(C_6F_5)_4$]. B = ln[($[B]_\infty$-[B])/($[B]_\infty$-$[B]_0$)].

6. Reaction of 1[$B(C_6F_5)_4$] with 2b-g.

6.1 Reaction of 1[$B(C_6F_5)_4$] with CH_2=CHOEt (2b). An NMR tube was charged with (α-diimine)PdMeCl (14.0 mg, 0.0249 mmol) and [$Li(Et_2O)_{2.8}$][$B(C_6F_5)_4$] (22.0 mg, 0.0246 mmol) and CH_2Cl_2 (0.4 mL) were added by vacuum transfer at -196 °C. The tube was warmed to 20 °C, shaken vigorously. After 20min, **2b** (0.0325 mmol) were added by vacuum transfer at -196 °C. The tube was kept at 0 °C for 10 min. All the volatiles were evacuated and CD_2Cl_2 (0.4 mL) was added by vacuum transfer at -196 °C. The tube was warmed to 20 °C, shaken vigorously and monitored periodically by NMR. NMR analysis showed that after 10 min, a mixture of [{(α-diimine)PdMe}$_2$(μ-Cl)]$^+$ (8 %), [(α-diimine)PdMe(CH_2=CHOEt)][$B(C_6F_5)_4$] (**3b**[$B(C_6F_5)_4$], 27 %), [(α-diimine)Pd{$CH_2CH(OEt)Me$}][$B(C_6F_5)_4$] (**4b**[$B(C_6F_5)_4$], 18 %), [(α-diimine)Pd{$CMe_2(OEt)$}][$B(C_6F_5)_4$] (**5b**[$B(C_6F_5)_4$], 35 %), **6**[$B(C_6F_5)_4$] (12 %) and C_2H_5OH (12 %) was present. After 1 h, **6** and C_2H_5OH[3] had formed quantitatively. The

α-diimine and OEt ^{1}H NMR resonances of **3b**[$B(C_6F_5)_4$], **4b**[$B(C_6F_5)_4$] and **5b**[$B(C_6F_5)_4$] overlap. Therefore only key NMR data are listed. **Key Data for 4b**[$B(C_6F_5)_4$]**: ^{1}H NMR** (CD_2Cl_2, 0 °C) δ 4.86 (sextet, *J* = 7, $PdCH_2CH$(OEt)Me), 3.41 (q, J = 7, 2H, OCH_2CH_3), 2.20 (s, 3H, N=C*Me*), 2.16 (s, 3H, N=C*Me*), 0.59 (t, J = 7, 3H,OCH_2CH_3), 0.37 (t, *J* = 7, $PdCHH'CH$(OEt)Me). The $PdCHH'CH$(OEt)Me and $PdCH_2CH$(OEt)*Me* resonances are obscured by the α-diimine resonances. **Key Data for 5b**[$B(C_6F_5)_4$]**: ^{1}H NMR** (CD_2Cl_2, 0 °C) δ3.56 (q, J = 7, 2H, OCH_2CH_3), 2.92 (septa, J = 7, 1H, $CHMe_2$), 2.23 (s, 3H, N=C*Me*), 2.19 (s, 3H, N=C*Me*), 1.41 (d, J = 7, 6H, $CHMe_2$), 1.39 (d, J = 7, 6H, $CHMe_2$), 1.29 (d, J = 7, 6H, $CHMe_2$), 1.16 (d, J = 7, 6H, $CHMe_2$), 0.60 (s, $PdCMe_2$(OEt)) 0.55 (t, *J* = 7, $PdCMe_2(OCH_2CH_3)$). The first-order rate constant for the consumption of **3b**[$B(C_6F_5)_4$] measured by the disappearance of the Pd*Me* ^{1}H NMR resonance is $k_{\text{insert, }\mathbf{3c}} = 8.01(6) \times 10^{-5}$ s^{-1} at 0 °C and $k_{\text{insert, }\mathbf{3c}} = \sim\ 2.0 \times 10^{-3}$ s^{-1} at 20 °C (ca. 83% consumption after 15 min). The first-order rate constant for consumption of the total of **4b**[$B(C_6F_5)_4$] and **5b**[$B(C_6F_5)_4$] measured by the disappearance of the $PdCH_2CH$Me resonance of **4b**[$B(C_6F_5)_4$] and the $PdCMe_2$ resonance of **5b**[$B(C_6F_5)_4$], or by the appearance of the H_{int} resonance of **6**[$B(C_6F_5)_4$] is $k_{\beta\text{-OEt, obs}} = 9.12(1) \times 10^{-4}$ s^{-1} at 20 °C.

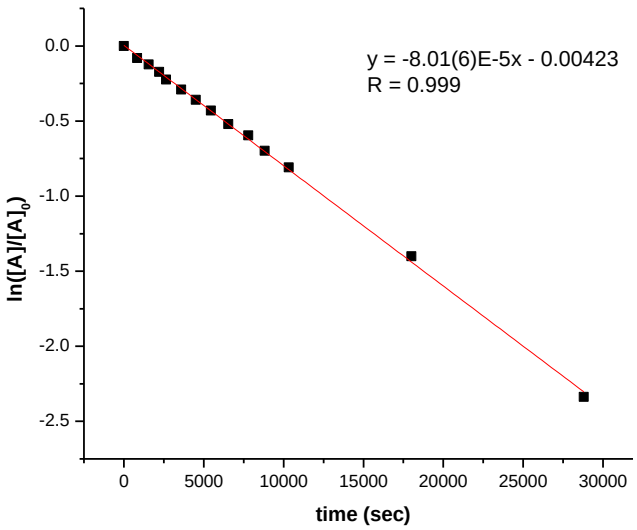

$[A]/[A]_0$	$\ln([A]/[A]_0)$	Time(s)
1	0	0
0.9229	-0.08023	840
0.8844	-0.12285	1560
0.8405	-0.17376	2220
0.799	-0.22439	2640
0.7473	-0.29129	3600
0.6988	-0.35839	4500
0.6507	-0.42971	5460
0.5941	-0.52071	6540
0.5512	-0.59566	7800
0.4971	-0.69896	8820
0.4454	-0.80878	10320
0.2463	-1.4012	18000
0.117	-2.14558	23400
0.0966	-2.33718	28800

Figure 6.1. First-order consumption of **3b**[$B(C_6F_5)_4$] at 0 °C.

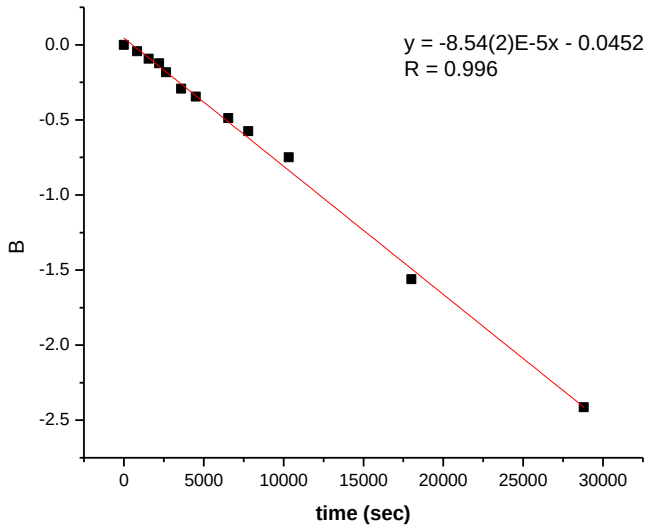

$[B]_\infty-[B]/[B]_\infty-[B]_0$	$\ln([([B]_\infty-[B])/([B]_\infty-[B]_0)]$	Time(s)
1	0	0
0.9578	-0.04312	840
0.9111	-0.0931	1560
0.8841	-0.12319	2220
0.8319	-0.18404	2640
0.7465	-0.29236	3600
0.7086	-0.34446	4500
0.6139	-0.48792	6540
0.5626	-0.57519	7800
0.4724	-0.74993	10320
0.21	-1.56065	18000
0.0894	-2.41463	28800

Figure 6.2. First-order consumption of **3b**[$B(C_6F_5)_4$] at 0 °C based on the increase of the sum of **4b**[$B(C_6F_5)_4$] + **5b**[$B(C_6F_5)_4$] + **6**[$B(C_6F_5)_4$]. $B = \ln([([B]_\infty-[B])/([B]_\infty-[B]_0)]$.

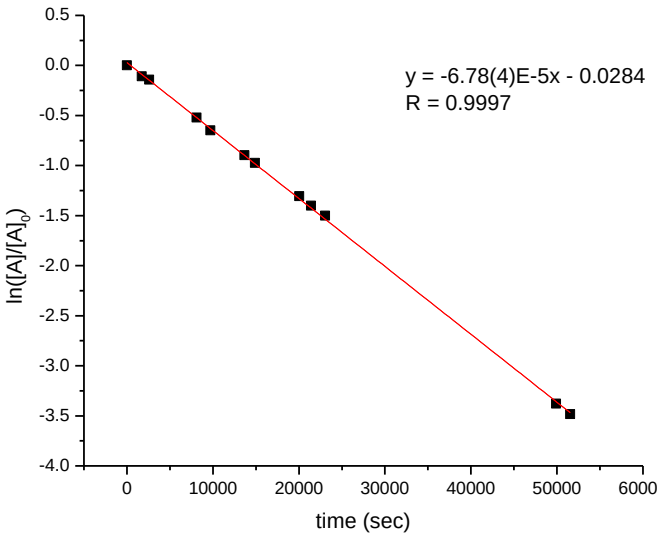

$[A]/[A]_0$	$\ln([A]/[A]_0)$	Time(s)
1	0	0
0.9028	-0.10225	1740
0.822	-0.19601	2580
0.5428	-0.61101	8100
0.5105	-0.67236	9720
0.4097	-0.89233	13680
0.335	-1.09362	14880
0.2309	-1.46577	20040
0.2088	-1.56638	21420
0.1889	-1.66654	23040
0.0341	-3.37846	49920
0.0307	-3.48349	51540

Figure 6.3. First-order consumption of the sum of **4b**[$B(C_6F_5)_4$] + **5b**[$B(C_6F_5)_4$] at 0 °C.

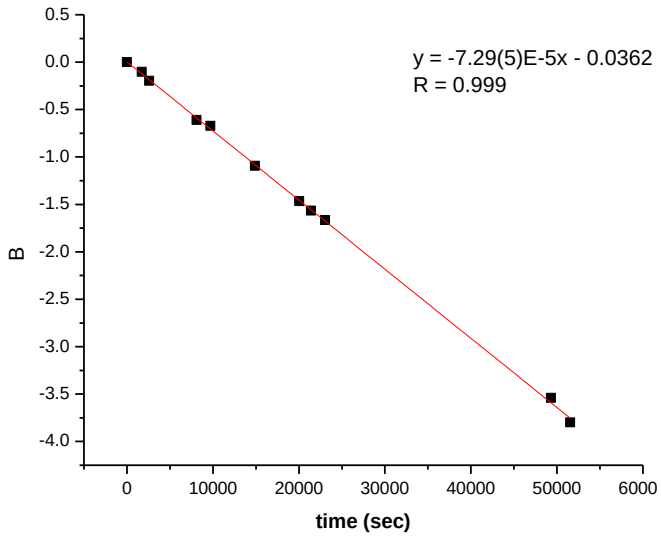

$[B]_\infty-[B]/[B]_\infty-[B]_0$	$\ln([([B]_\infty-[B])/([B]_\infty-[B]_0)]$	Time(s)
1	0	0
0.8979	-0.1077	1740
0.8675	-0.14214	2580
0.5945	-0.52003	8100
0.5228	-0.64856	9720
0.4077	-0.89722	13680
0.378	-0.97286	14880
0.2708	-1.30637	20040
0.2462	-1.40161	21420
0.223	-1.50058	23040
0.029	-3.54046	49920
0.0224	-3.79869	51540

Figure 6.4. First-order consumption of the sum of **4b**[$B(C_6F_5)_4$] + **5b**[$B(C_6F_5)_4$] at 0 °C based on increase of **6**[$B(C_6F_5)_4$]. $B = \ln([([B]_\infty-[B])/([B]_\infty-[B]_0)]$.

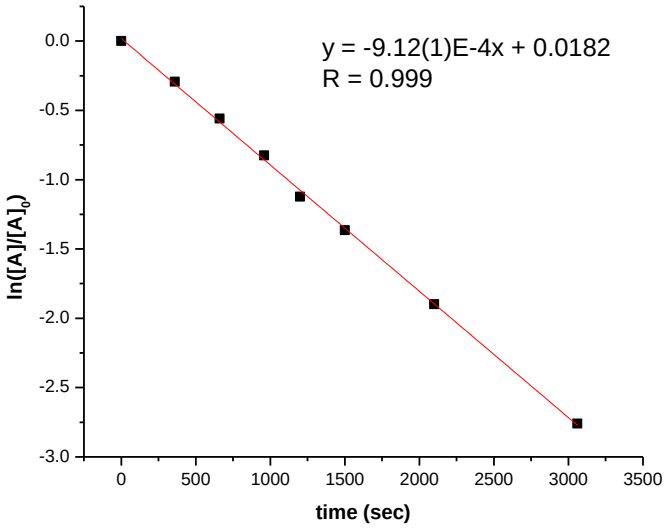

$[A]/[A]_0$	$\ln([A]/[A]_0)$	Time(s)
1	0	0
0.746441	-0.29244	360
0.571525	-0.55945	660
0.437966	-0.82561	960
0.325537	-1.12228	1200
0.255254	-1.3655	1500
0.149718	-1.899	2100

Figure 6.5. First-order consumption of the sum of **4b**[$B(C_6F_5)_4$] + **5b**[$B(C_6F_5)_4$] at 20 °C.

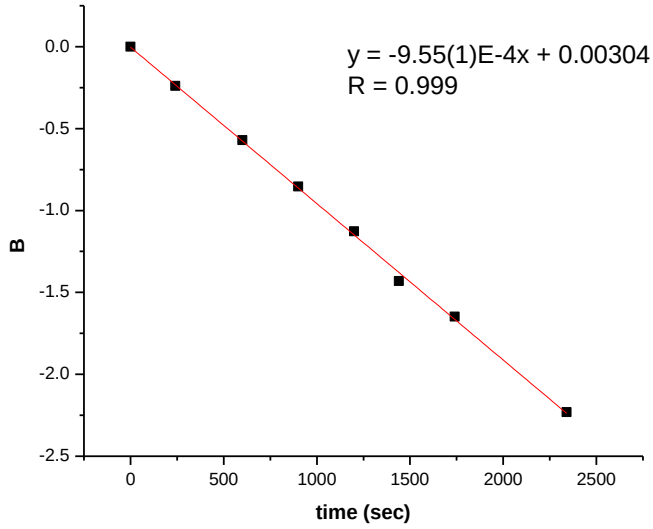

$[B]_\infty-[B]/[B]_\infty-[B]_0$	$\ln([([B]_\infty-[B])/([B]_\infty-[B]_0)]$	Time(s)
1	0	0
0.7875	-0.23889	240
0.5652	-0.57058	600
0.4255	-0.85449	900
0.3239	-1.12732	1200
0.239	-1.43129	1440
0.1749	-1.74354	1740
0.1074	-2.2312	2340

Figure 6.6. First-order consumption of the sum of **4b**[$B(C_6F_5)_4$] + **5b**[$B(C_6F_5)_4$] at 20 °C based on increase of **6**[$B(C_6F_5)_4$]. B = $\ln([([B]_\infty-[B])/([B]_\infty-[B]_0)]$.

6.2 Reaction of 1[B(C_6F_5)$_4$] with CH_2=CHOSiMe_3 (2c). An NMR tube was charged with (α-diimine)PdMeCl (14.0 mg, 0.0249 mmol) and [Li(Et_2O)$_{2.8}$][B(C_6F_5)$_4$] (22.0 mg, 0.0246 mmol) and CD_2Cl_2 (0.4 mL) were added by vacuum transfer at -196 °C. The tube was warmed to 20 °C, shaken vigorously. After 20min, **2c** (0.0225 mmol) were added by vacuum transfer at -196 °C. The tube was warmed to 20 °C, shaken vigorously and monitored periodically by NMR. NMR analysis showed that after 10 min, [(α-diimine)Pd{CMe_2(OSiMe_3)}][B(C_6F_5)$_4$] (**5c**[B(C_6F_5)$_4$]) had formed quantitatively. **^{1}H NMR** (CD_2Cl_2): δ 7.35 (s, 3H), 7.31 (s, 3H), 3.05 (sept, *J* = 7, 2H, C*H*Me_2), 2.95 (sept, *J* = 7, 2H, C*H*Me_2), 2.22 (s, 3H, N=C*Me*), 2.17 (s, 3H, N=C*Me*), 1.44 (d, *J* = 7, 6H, CH*Me*$_2$), 1.40 (d, *J* = 7, 6H, CH*Me*$_2$), 1.27 (d, *J* = 7, 6H, CH*Me*$_2$), 1.16 (d, *J* = 7, 6H, CH*Me*$_2$), 0.54 (s, 6H, PdC*Me*$_2$(OSiMe_3)), -0.07 (s, 9H, OSi*Me*$_3$); the aromatic reagion is simpler than expected due to accidental degeneracies. **^{13}C{^{1}H} NMR** (CD_2Cl_2, -60 °C): δ 174.2 (N=*C*Me), 170.7 (N=*C*Me), 143.2, 142.6, 136.5, 135.9, 127.6, 127.2, 124.1, 123.8, 84.5 (Pd*C*Me_2(OSiMe_3)), 28.7, 28.4, 25.4, 23.4, 23.2, 22.4, 22.2, 20.9, 18.9, -0.3 (OSi*Me*$_3$). **ESI-MS**: (α-diimine)Pd{CMe_2(OSiMe_3)}$^+$ calcd. *m/z* = 641.3, found 641.2. **5c**[B(C_6F_5)$_4$] converts to Me_3SiOH and **6**[B(C_6F_5)$_4$].[4] Me_3SiOH was slowly converted to Me_3SiOSiMe_3 in CD_2Cl_2 at RT over 1 week.

The first-order rate constant for consumption of **5c**[B(C_6F_5)$_4$] measured by the disappearance of the PdC*Me*$_2$ resonance is $k_{\beta\text{-OSiMe3, obs}}$ = 3.22(2) × 10^{-5} s^{-1} at 20 °C. Since $K_{\mathbf{5c/4c}}$ > 20, the actual β-OSiMe_3 elimination rate constant $k_{\beta\text{-OSiMe3}} = k_{\beta\text{-OSiMe3, obs}}$ ($K_{\mathbf{5c/4c}}$ + 1) > 7.35 × 10^{-4} s^{-1}.

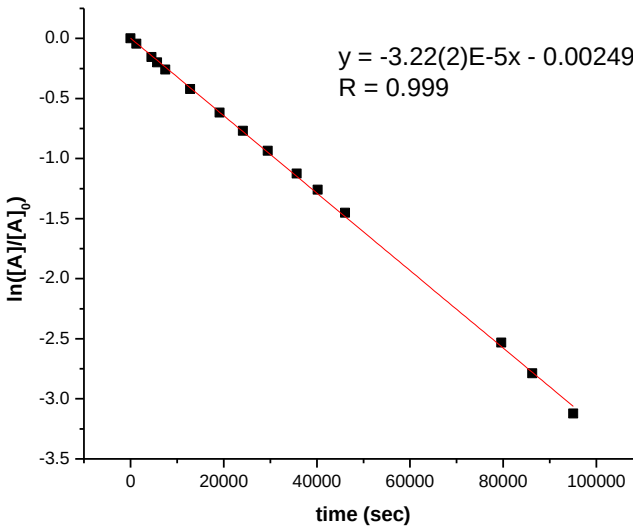

$[A]/[A]_0$	$\ln([A]/[A]_0)$	Time(s)
1	0	0
0.956075	-0.04492	1260
0.855535	-0.15603	4500
0.818662	-0.20008	5700
0.771719	-0.25914	7500
0.655878	-0.42178	12840
0.539722	-0.6167	19140
0.462979	-0.77007	24120
0.392663	-0.9348	29460
0.324426	-1.1257	35700
0.283986	-1.25883	40200
0.234038	-1.45227	46080
0.079466	-2.53242	79620
0.061597	-2.78714	86280
0.044065	-3.12208	95040

Figure 6.7. First-order consumption of **5c**[$B(C_6F_5)_4$] at 20 °C.

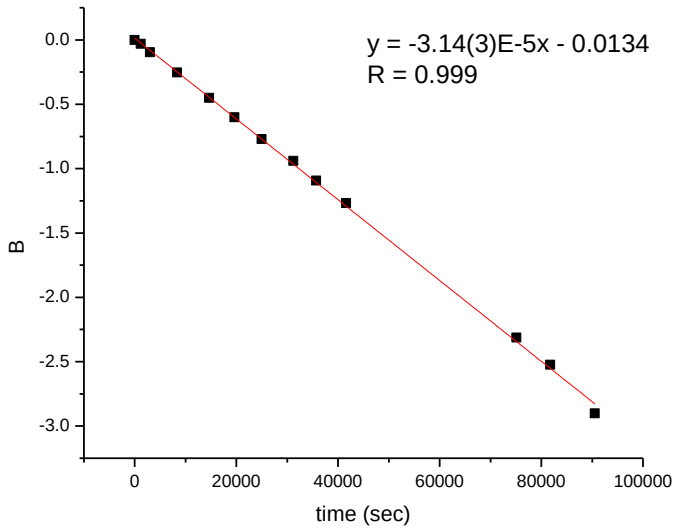

$[B]_\infty$-[B]/ $[B]_\infty$-$[B]_0$	$\ln([[B]_\infty$-[B])/ $([B]_\infty$-$[B]_0)]$	Time(s)
1	0	0
0.968942	-0.03155	1200
0.908864	-0.09556	3000
0.775626	-0.25409	8340
0.637261	-0.45058	14640
0.547685	-0.60205	19620
0.462589	-0.77092	24960
0.390599	-0.94007	31200
0.33499	-1.09365	35700
0.281142	-1.2689	41580
0.098926	-2.31339	75120
0.080237	-2.52277	81780
0.054918	-2.90192	90540

Figure 6.8. First-order consumption of **5c**[$B(C_6F_5)_4$] at 20 °C based on the increase of **6**[$B(C_6F_5)_4$]. B = $\ln[([B]_\infty$-[B])/($[B]_\infty$-$[B]_0)]$.

6.3 Reaction of 5c[B(C_6F_5)$_4$] with MeCN. An NMR tube containing a CD_2Cl_2 solution of **5c**[B(C_6F_5)$_4$] (0.020 mmol) was frozen at -196 °C and MeCN (0.040 mmol) was added by vacuum transfer. The tube was warmed to -78 °C, agitated to mix the components, placed in an NMR probe that had been pre-cooled to -40 °C, and monitored by NMR. ^{1}H NMR spectra showed that after 10 min, 36 % of **5c**[B(C_6F_5)$_4$] had been converted to **[4c-MeCN]**[B(C_6F_5)$_4$]. Therefore the tube was warmed to 0 ^{o}C for 10 min to facilitate the reaction of **5c**[B(C_6F_5)$_4$] with MeCN. The tube was cooled to -40 ^{o}C and ^{1}H NMR spectra were recorded and showed that 90 % of **5c**[B(C_6F_5)$_4$] had been converted to **[4c-MeCN]**[B(C_6F_5)$_4$]. This species decomposes within a few minutes at 20 ^{o}C. **Key NMR data for [4c-MeCN]**[B(C_6F_5)$_4$]**: ^{1}H NMR** (CD_2Cl_2, -40 °C) δ 7.38-7.24 (m, 6H), 3.49 (m, 1H, PdCH_2C*H*Me(OSiMe_3)), 2.90 (m, 2H, C*H*Me_2), 2.81 (m, 2H, C*H*Me_2), 2.22 (s, 3H, N=C*Me*), 2.21 (s, 3H, N=C*Me*), 1.70 (s, 3H, *Me*CN), 1.44 (m, 1H, PdC*H*H'CHMe(OSiMe_3)), 1.32 (d, *J* = 7, 12H, CH*Me$_2$*), 1.25 (m, 1H, PdCH*H'*CHMe(OSiMe_3)), 1.17 (d, *J* = 7, 3H, CH*Me$_2$*), 1.16 (d, *J* = 7, 3H, CH*Me$_2$*), 1.12 (3H, CH*Me$_2$*), 1.10 (3H, CH*Me$_2$*, partially obscured by Et_2O resonance), 0.93 (d, *J* = 6, 3H, PdCH_2CH*Me*(OSiMe_3)), -0.13 (s, 9H, OSi*Me$_3$*). Key ^{1}H-^{1}H **COSY** correlations δ/δ: (CD_2Cl_2, -40 °C) 3.49 (PdCH_2C*H*Me(OSiMe_3))/1.44 (PdC*H*H'CHMe(OSiMe_3)); 3.49 (PdCH_2C*H*Me(OSiMe_3))/1.25 (PdCH*H'*CHMe(OSiMe_3)); 3.49 (PdCH_2C*H*Me(OSiMe_3))/0.93 (PdCH_2CH*Me*(OSiMe_3)); 1.44 (PdC*H*H'CHMe(OSiMe_3))/1.25 (PdCH*H'*CHMe(OSiMe_3)). **^{13}C{^{1}H} NMR** (CD_2Cl_2, -60 °C): δ 179.7 (N=*C*Me), 172.1 (N=*C*Me), 139.4, 139.1, 138.2, 138.0, 137.2, 137.1, 128.6, 127.8, 124.4, 124.3, 123.9, 123.8, 121.6, 68.9 (PdCH_2*C*HMe(OSiMe_3)), 37.9 (Pd*C*H_2CHMe(OSiMe_3)), 28.7, 28.5, 25.6, 23.6, 23.4, 23.4, 23.1, 23.0, 22.9, 22.8, 22.7, 22.5, 22.3, 22.0, 19.9, 2.2 (*Me*CN), -0.4 (OSi*Me$_3$*).

6.4 Reaction of 1[$B(C_6F_5)_4$] with CH_2=CHOSiMe_2Ph (2d).

An NMR tube was charged with (α-diimine)PdMeCl (14.0 mg, 0.0249 mmol) and [$Li(Et_2O)_{2.8}$][$B(C_6F_5)_4$] (22.0 mg, 0.0246 mmol) and CD_2Cl_2 (0.4 mL) were added by vacuum transfer at -196 °C. The tube was warmed to 20 °C, shaken vigorously. After 20min, **2d** (0.0224 mmol) were added by syringe at -196 °C under nitrogen. The tube was warmed to 20 °C, shaken vigorously and monitored periodically by NMR. NMR spectrum showed that **5d**[$B(C_6F_5)_4$] was generated cleanly after 10min at RT. **5d**[$B(C_6F_5)_4$] converts to $PhMe_2SiOH$ and 6[$B(C_6F_5)_4$].[5] $PhMe_2SiOH$ was slowly converted to $PhMe_2SiOSiMe_2Ph$ in CD_2Cl_2 at RT over 1 week.

The first-order rate constant for consumption of of **5d** measured by the disappearance of the PdCMe_2 resonance is $k_{\beta\text{-OSiMe2Ph, obs}} = 5.06(2) \times 10^{-5}$ s^{-1} at 20 °C. The actual first-order rate constant $k_{\beta\text{-OSiPh3}} = k_{\beta\text{-OSiPh3, obs}}(K_{\mathbf{5d/4d}} + 1) > 1.8 \times 10^{-3}$ s^{-1} ($K_{\mathbf{5d/4d}} > 20$).

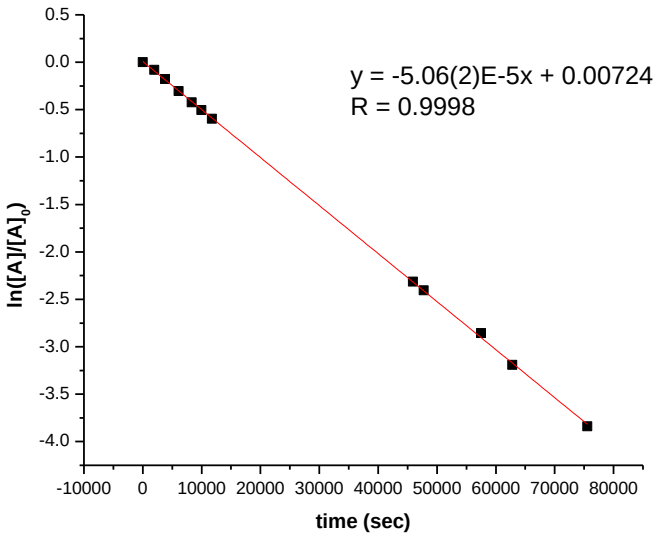

$[A]/[A]_0$	$\ln([A]/[A]_0)$	Time(s)
1	0	0
0.92138	-0.08188	1980
0.83677	-0.17821	3780
0.7379	-0.30395	6120
0.65545	-0.42243	8340
0.60408	-0.50405	9960
0.55127	-0.59553	11760
0.09892	-2.31344	45900
0.09021	-2.40561	47760
0.05748	-2.85632	57480
0.04112	-3.19126	62820
0.0215	-3.8397	75540

Figure 6.9. First-order consumption of **5d**[$B(C_6F_5)_4$] at 20 °C.

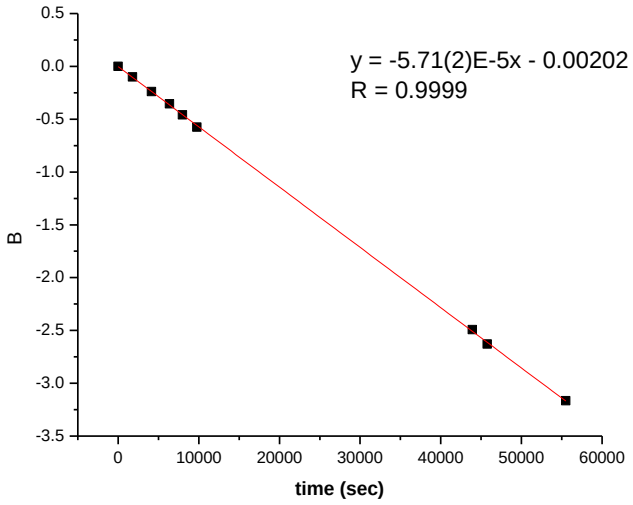

$[B]_\infty$-[B]/ $[B]_\infty$-$[B]_0$	ln[($[B]_\infty$-[B])/ ($[B]_\infty$-$[B]_0$)]	Time(s)
0.88374	-0.12359	1980
0.7999	-0.22327	3780
0.6952	-0.36356	6120
0.61925	-0.47925	8340
0.5582	-0.58304	9960
0.4973	-0.69856	11760
0.073	-2.6173	45900
0.0638	-2.752	47760
0.03724	-3.29037	57480

Figure 6.10. First-order consumption of **5d**[$B(C_6F_5)_4$] at 20 °C based on the increase of **6**[$B(C_6F_5)_4$]. B = ln[($[B]_\infty$-[B])/($[B]_\infty$-$[B]_0$)].

6.5 Reaction of 1[$B(C_6F_5)_4$] with CH_2=CHOSiMePh_2 (2e).

An NMR tube was charged with (α-diimine)PdMeCl (14.0 mg, 0.0249 mmol) and [$Li(Et_2O)_{2.8}$][$B(C_6F_5)_4$] (22.0 mg, 0.0246 mmol) and CD_2Cl_2 (0.4 mL) were added by vacuum transfer at -196 °C. The tube was warmed to 20 °C, shaken vigorously. After 20min, **2e** (0.0242 mmol) were added by syringe at -196 °C under nitrogen. The tube was warmed to 20 °C, shaken vigorously and monitored periodically by NMR. NMR spectrum showed that **5e**[$B(C_6F_5)_4$] was generated cleanly after 10min at RT. **5e**[$B(C_6F_5)_4$] converts to Ph_2MeSiOH and 6[$B(C_6F_5)_4$].[6] Ph_2MeSiOH does not react to generate Ph_2MeSiOSiMePh_2 in CD_2Cl_2 at RT over 2 weeks.

The first-order rate constant for consumption of of **5e** measured by the disappearance of the PdC*Me*$_2$ resonance is $k_{\beta\text{-OSiMePh2, obs}} = 1.34(1) \times 10^{-4}$ s^{-1} at 20 °C. The actual first-order rate constant $k_{\beta\text{-OSiPh3}} = k_{\beta\text{-OSiPh3, obs}}(K_{\mathbf{5d/4d}} + 1) > 1.8 \times 10^{-3}$ s^{-1} ($K_{\mathbf{5d/4d}} > 20$).

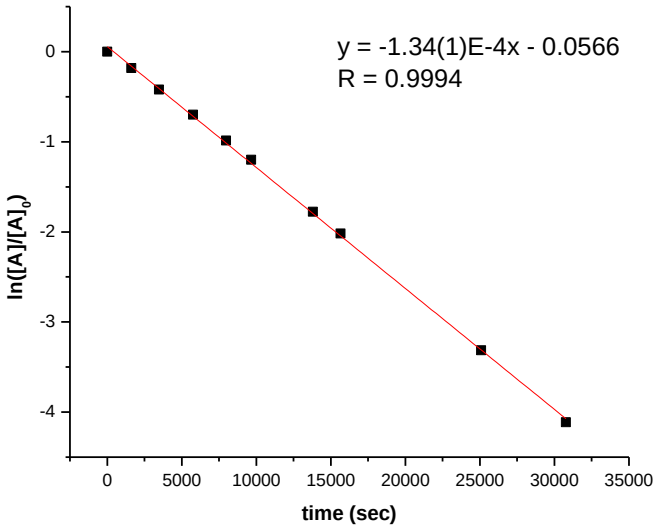

$[A]/[A]_0$	$\ln([A]/[A]_0)$	Time(s)
1	0	0
0.8342	-0.18128	1620
0.65629	-0.42115	3480
0.49737	-0.69842	5760
0.37262	-0.9872	7980
0.30166	-1.19845	9660
0.16894	-1.77821	13800
0.1328	-2.01891	15660
0.03638	-3.31374	25080
0.01634	-4.11414	30780

Figure 6.11. First-order consumption of **5e**[$B(C_6F_5)_4$] at 20 °C.

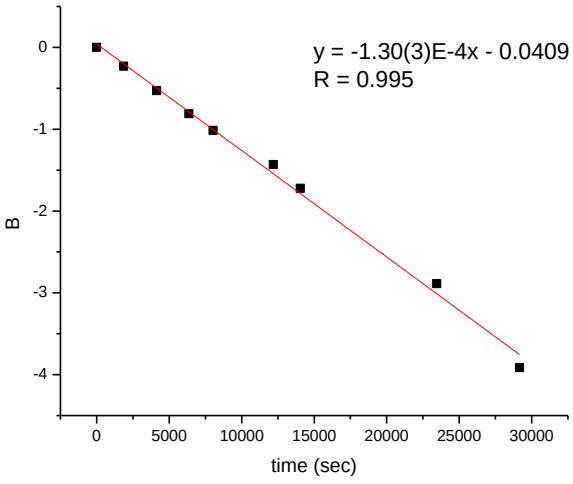

$[B]_\infty-[B]/[B]_\infty-[B]_0$	$\ln[([B]_\infty-[B])/([B]_\infty-[B]_0)]$	Time(s)
1	0	0
0.795203	-0.22916	1860
0.588524	-0.53014	4140
0.444502	-0.8108	6360
0.362202	-1.01555	8040
0.238376	-1.4339	12180
0.178475	-1.72331	14040
0.055683	-2.88809	23460
0.019926	-3.91572	29160

Figure 6.12. First-order consumption of **5e**[$B(C_6F_5)_4$] at 20 °C based on the increase of **6**[$B(C_6F_5)_4$]. $B = \ln[([B]_\infty-[B])/([B]_\infty-[B]_0)]$.

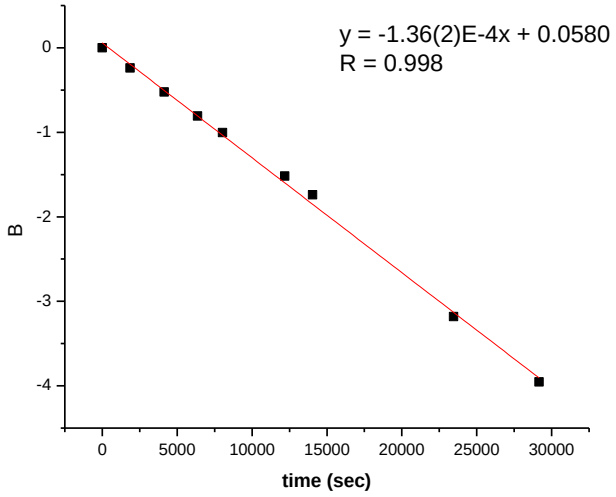

$[B]_\infty$-[B]/ $[B]_\infty$-$[B]_0$	ln[($[B]_\infty$-[B])/ ($[B]_\infty$-$[B]_0$)]	Time(s)
1	0	0
0.788471	-0.23766	1860
0.592499	-0.52341	4140
0.44561	-0.80831	6360
0.366257	-1.00442	8040
0.219006	-1.51865	12180
0.17535	-1.74097	14040
0.041486	-3.1824	23460
0.019175	-3.95414	29160

Figure 6.13. First-order consumption of **5e**[$B(C_6F_5)_4$] at 20 °C based on the increase of $Ph_2MeSiOH$. B = ln[($[B]_\infty$-[B])/($[B]_\infty$-$[B]_0$)].

6.6 Reaction of 1[$B(C_6F_5)_4$] with CH_2=CHOSiPh_3 (2f). An NMR tube was charged with (α-diimine)PdMeCl (14.0 mg, 0.0249 mmol) and [$Li(Et_2O)_{2.8}$][$B(C_6F_5)_4$] (22.0 mg, 0.0246 mmol) and CD_2Cl_2 (0.4 mL) were added by vacuum transfer at -196 °C. The tube was warmed to 20 °C, shaken vigorously. After 20min, **2f** (0.0232 mmol) were added by syringe at -196 °C under nitrogen. The tube was warmed to 20 °C, shaken vigorously and monitored periodically by NMR. NMR analysis showed that after 10 min at 20 °C, [{(α-diimine)PdMe}$_2$(μ-Cl)]$^+$ (14 %), free **2f** (17 %), [(α-diimine)Pd{CMe_2($OSiPh_3$)}][$B(C_6F_5)_4$] (**5f**, 64 %) and **6** (2 %) were present. After 20 min the free **2f** was completely consumed, and a mixture of [{(α-diimine)PdMe}$_2$(μ-Cl)]$^+$ (6 %), **5f** (65 %) and **6** (11 %) was present. The resonances of the elimination product Ph_3SiOH overlaped with other resonances. But Ph_3SiOH was isolated by hexanes wash after the elimination, and it does not react to generate $Ph_3SiOSiPh_3$ in CD_2Cl_2 at room temperature over

2 weeks.[7] **ESI-MS**: (α-diimine)Pd{$CMe_2(OSiPh_3)$}$^+$ calcd. *m/z* = 827.4, found 827.2. **Key NMR Data for 5d: ^{1}H NMR** (CD_2Cl_2)[8] δ 7.45 (d, *J* = 8, H_{ortho} of OSi*Ph*$_3$), 7.31 (m, OSi*Ph*$_3$), 7.28 (m, OSi*Ph*$_3$), 3.06 (m, 2H, C*H*Me_2), 2.96 (m, 2H, C*H*Me_2), 2.25 (s, 3H, N=C*Me*), 2.11 (s, 3H, N=C*Me*), 1.35 (d, *J* = 7, 6H, CH*Me*$_2$), 1.19 (d, *J* = 7, 6H, CH*Me*$_2$), 1.16 (d, *J* = 7, 6H, CH*Me*$_2$), 1.13 (d, *J* = 7, 6H, CH*Me*$_2$), 0.30 (s, 6H, PdC*Me*$_2$($OSiPh_3$)). **^{13}C{^{1}H} NMR** (CD_2Cl_2, -40 °C): δ 175.0 (N=*C*Me), 172.1 (N=*C*Me), 142.9, 142.4, 137.1, 136.6, 134.8, 131.4, 128.3, 127.9, 127.7, 124.4, 124.1, 87.2 (Pd*C*Me_2($OSiPh_3$)), 28.9, 28.6, 26.1, 23.8, 23.5, 22.9, 22.7, 21.6, 19.6. The C_{ipso} signal of OSi*Ph*$_3$ was obscured.

The first-order rate constant for consumption of of **5f** measured by the disappearance of the PdC*Me*$_2$ resonance is $k_{\beta\text{-OSiPh3, obs}}$ = 1.071(5) × 10^{-4} s^{-1} at 20 °C. The actual first-order rate constant $k_{\beta\text{-OSiPh3}} = k_{\beta\text{-OSiPh3, obs}}(K_{\mathbf{5f/4f}} + 1) > 1.8 \times 10^{-3}$ s^{-1} ($K_{\mathbf{5f/4f}} > 20$).

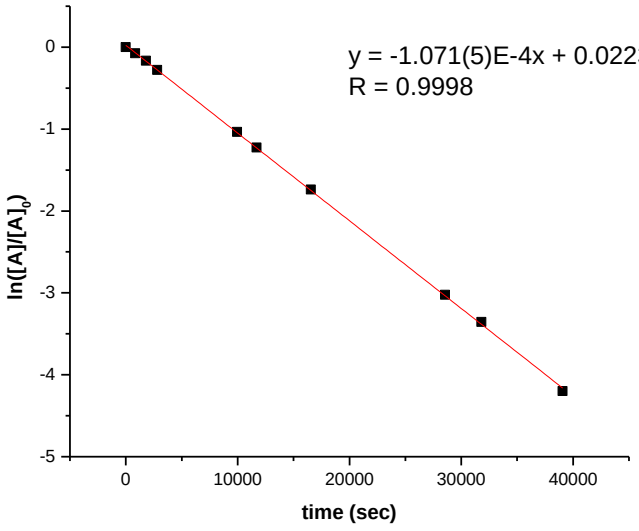

[A]/[A]$_0$	ln([A]/[A]$_0$)	Time(s)
1	0	0
0.92615	-0.07672	840
0.8465	-0.16665	1800
0.7569	-0.27852	2820
0.35546	-1.03434	9960
0.2939	-1.22452	11700
0.1755	-1.74012	16560
0.04858	-3.02454	28560
0.0349	-3.35527	31800
0.01498	-4.20104	39060

Figure 6.14. First-order consumption of **5f**[$B(C_6F_5)_4$] at 20 °C.

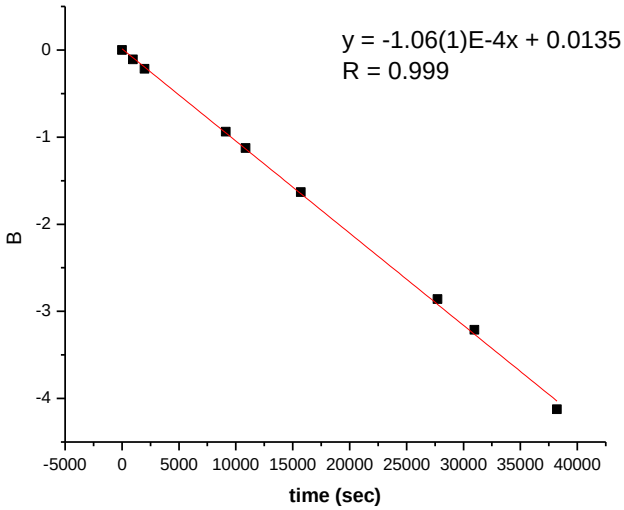

$[B]_\infty$-[B]/ $[B]_\infty$-$[B]_0$	ln[($[B]_\infty$-[B])/ ($[B]_\infty$-$[B]_0$)]	Time(s)
1	0	0
0.897074	-0.10862	960
0.805922	-0.21577	1980
0.390957	-0.93916	9120
0.324306	-1.12607	10860
0.195446	-1.63247	15720
0.057317	-2.85915	27720
0.040258	-3.21245	30960
0.016151	-4.12576	38220

Figure 6.15. First-order consumption of **5f**[$B(C_6F_5)_4$] at 20 °C based on the increase of **6**[$B(C_6F_5)_4$]. B = ln[($[B]_\infty$-[B])/($[B]_\infty$-$[B]_0$)].

6.7 Reaction of 5f[$B(C_6F_5)_4$] with MeCN. An NMR tube containing a CD_2Cl_2 solution of **5f**[$B(C_6F_5)_4$] (0.020 mmol) was frozen at -196 °C and MeCN (0.030 mmol) was added by vacuum transfer. The tube was warmed to -78 °C, agitated to mix the components, placed in an NMR probe that had been pre-cooled to -60 °C, and monitored by NMR. ^{1}H NMR spectra showed that after 5 min, complex **5f**[$B(C_6F_5)_4$] had been converted cleanly to **[4f-MeCN]**[$B(C_6F_5)_4$]. **^{1}H NMR** (CD_2Cl_2, -60 °C): δ 7.58 (t, *J* = 8, 3H, H_{para} of $OSiPh_3$), 7.43 (d, *J* = 7, 6H, H_{ortho} of $OSiPh_3$), 3.66 (q, *J* = 6, 1H, $PdCH_2CHMe(OSiPh_3)$), 2.92 (sept, *J* = 7, 1H, $CHMe_2$), 2.75 (m, 3H, $CHMe_2$), 2.23 (s, 3H, N=C*Me*), 2.21 (s, 3H, N=C*Me*), 1.99 (br s, *Me*CN), 1.40 (m, 1H, $PdCHH'CHMe(OSiPh_3)$), 1.31 (d, *J* = 7, 3H, $CHMe_2$), 1.23 (d, *J* = 7, 3H, $CHMe_2$), 1.15 (d, *J* = 7, 3H, $CHMe_2$), 1.14 (d, *J* = 7, 3H, $CHMe_2$), 1.12 (d, 6H, $CHMe_2$, partially obscured by Et_2O resonance), 1.05 (d, *J* = 6, 3H, $CHMe_2$), 1.04 (d, *J* = 6, 3H, $CHMe_2$), 0.99 (d, *J* = 6, 3H, $PdCH_2CHMe(OSiPh_3)$), 0.83 (m, 1H, $PdCHH'CHMe(OSiPh_3)$). **^{13}C{^{1}H} NMR**

(CD_2Cl_2, -60 °C): δ 179.6 (N=*C*Me), 172.3 (N=*C*Me), 139.2, 139.1, 138.2, 137.8, 137.1, 137.0, 135.0, 134.6, 134.3, 129.8, 127.9, 127.7, 127.5, 124.4, 124.3, 123.9, 123.7, 121.0 (CH_3CN), 71.5 ($PdCH_2CHMe(OSiPh_3)$), 38.9 ($PdCH_2CHMe(OSiPh_3)$), 28.8, 28.7, 28.6, 28.5, 25.1, 23.6, 23.3, 23.12, 23.08, 23.0, 22.8 (2C), 22.6, 22.0, 19.9, 1.1 (*Me*CN).

6.8 Reaction of 1[$B(C_6F_5)_4$] with CH_2=CHOPh (2g). An NMR tube was charged with (α-diimine)PdMeCl (11.1 mg, 0.0198 mmol) and $[Li(Et_2O)_{2.8}][B(C_6F_5)_4]$ (18.4 mg, 0.0206 mmol). CD_2Cl_2 (0.4 mL) and **2g** (0.021 mmol) were added by vacuum transfer at -196 °C. The tube was warmed to 20 °C, shaken vigorously, and monitored periodically by NMR. NMR analysis showed that after 10 min, **6** and phenol had formed quantitatively.

7. Reaction of 1[SbF_6] with 2a-g.

7.1 Reaction of 1[SbF_6] with CH_2=CHO^{t}Bu (2a). An NMR tube was charged with **1**[SbF_6] (14.9 mg, 0.0178 mmol) and **2a** (0.0325 mmol). CD_2Cl_2 was added by vacuum transfer at -196 ^oC. ^1H NMR spectrum at -60 ^oC confirmed the formation of **3a**[SbF_6]. The tube was kept at 0 °C for 10 min. All the volatiles were evacuated and CD_2Cl_2 (0.4 mL) was added by vacuum transfer at -196 °C. The tube was warmed to 0 ^oC and monitored by ^1H NMR periodically. Complex **3a**[SbF_6] was converted to **4a**[SbF_6] and **5a**[SbF_6]. The NMR resonances of **4a**[SbF_6] and **5a**[SbF_6] is very similar to **4a**[$B(C_6F_5)_4$] and **5a**[$B(C_6F_5)_4$]. The first-order rate constant for the consumption of **3a**[SbF_6] measured by the disappearance of the Pd*Me* ^1H NMR resonance is $k_{\text{insert, 3c}}$ = 3.29(2) × 10^{-5} s^{-1} at 0 °C. After **3a**[SbF_6] is fully consumed, the tube was warmed to 20 ^oC and monitored by ^1H NMR periodically. NMR analysis showed a mixture of **4a**[SbF_6] (66%), **5a**[SbF_6] (22%) and **6**[SbF_6] (12%) was present after 5min. The first-order rate constant for the consumption of **3a**[SbF_6] measured by the

disappearance of the Pd*Me* ^{1}H NMR resonance is $k_{\text{insert, 3c}}$ = 3.29 (2) × 10^{-5} s^{-1} at 0 °C and $k_{\text{insert, 3c}}$ = 6.33 (5) × 10^{-4} s^{-1} at 20 °C. The first-order rate constant for consumption of the total of **4a**[SbF_6] and **5a**[SbF_6] measured by the disappearance of the PdCH_2CHMe resonance of **4a**[SbF_6] and the PdCMe_2 resonance of **5a**[SbF_6] is $k_{\beta\text{-OtBu, obs}}$ = 1.50(2) × 10^{-5} s^{-1} at 20 °C.

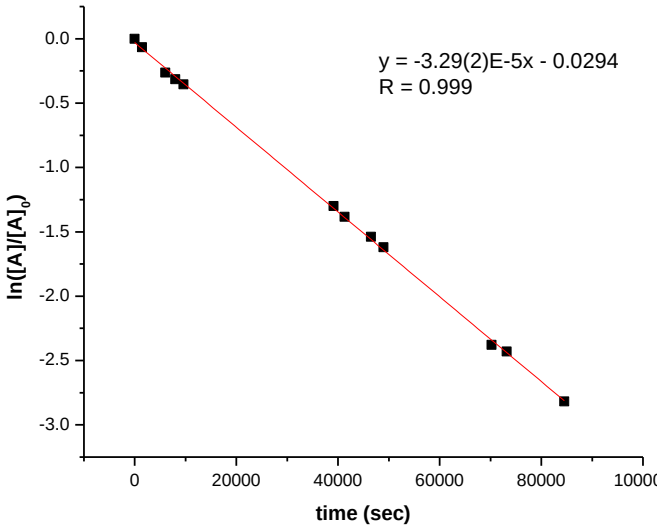

[A]/[A]$_0$	ln([A]/[A]$_0$)	Time(s)
1	0	0
0.934971	-0.06724	1440
0.768362	-0.26349	6000
0.729062	-0.316	7980
0.700928	-0.35535	9600
0.272626	-1.29965	39120
0.250891	-1.38274	41280
0.214482	-1.53953	46500
0.197932	-1.61983	48960
0.092722	-2.37815	70200
0.088021	-2.43017	73200
0.059733	-2.81787	84540

Figure 7.1. First-order consumption of **3a**[SbF_6] at 0 °C.

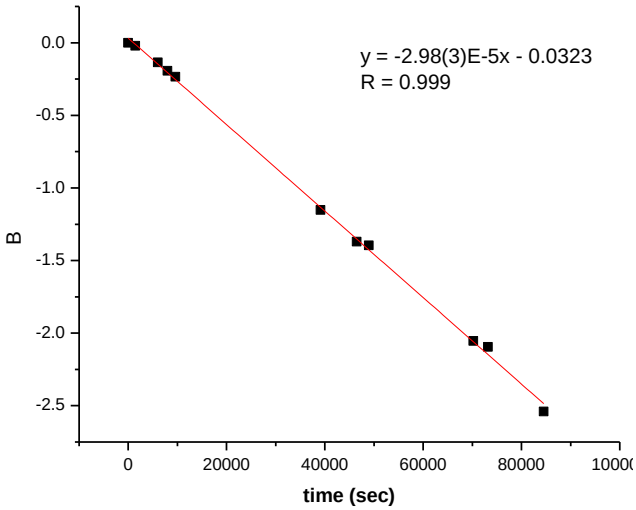

$[B]_\infty$-[B]/ $[B]_\infty$-$[B]_0$	ln[($[B]_\infty$-[B])/ ($[B]_\infty$-$[B]_0$)]	Time(s)
1	0	0
0.97916	-0.02106	1440
0.8729	-0.13593	6000
0.8248	-0.19261	7980
0.7917	-0.23357	9600
0.3161	-1.1517	39120
0.2542	-1.36963	46500
0.2477	-1.39554	48960
0.1283	-2.05338	70200
0.1231	-2.09476	73200
0.0788	-2.54084	84540

Figure 7.2. First-order consumption of **3a**[SbF_6] at 0 °C based on increase of the sum of **4a**[SbF_6] + **5a**[SbF_6]. B = ln[($[B]_\infty$-[B])/($[B]_\infty$-$[B]_0$)].

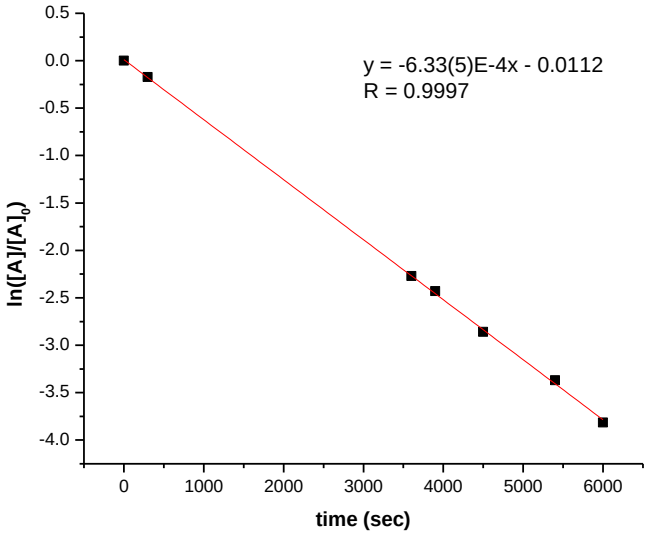

$[A]/[A]_0$	ln($[A]/[A]_0$)	Time(s)
1	0	0
0.84141	-0.17268	300
0.1032	-2.27109	3600
0.0881	-2.42928	3900
0.05727	-2.85998	4500
0.03436	-3.37086	5400
0.02203	-3.81535	6000

Figure 7.3. First-order consumption of **3a**[SbF_6] at 20 °C.

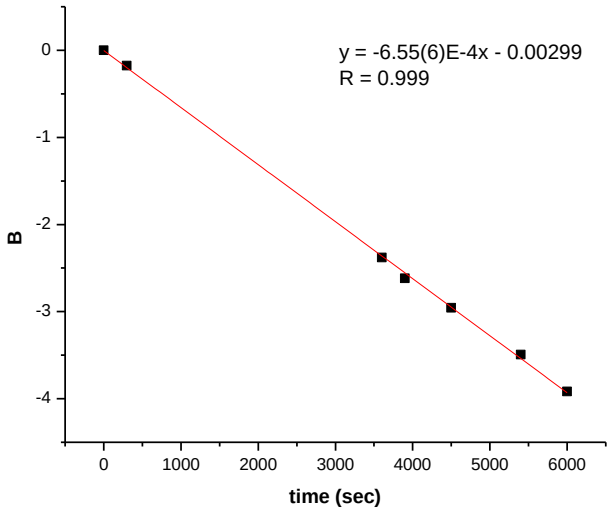

$[B]_\infty-[B]/[B]_\infty-[B]_0$	$\ln[([B]_\infty-[B])/([B]_\infty-[B]_0)]$	Time(s)
1	0	0
0.8393	-0.17519	300
0.0927	-2.37839	3600
0.073	-2.6173	3900
0.052	-2.95651	4500
0.0304	-3.49331	5400
0.0199	-3.91704	6000

Figure 7.4. First-order consumption of **3a**[SbF_6] at 20 °C based on the increase of the sum of **4a**[SbF_6] + **5a**[SbF_6] + **6**[SbF_6]. B = $\ln[([B]_\infty-[B])/([B]_\infty-[B]_0)]$.

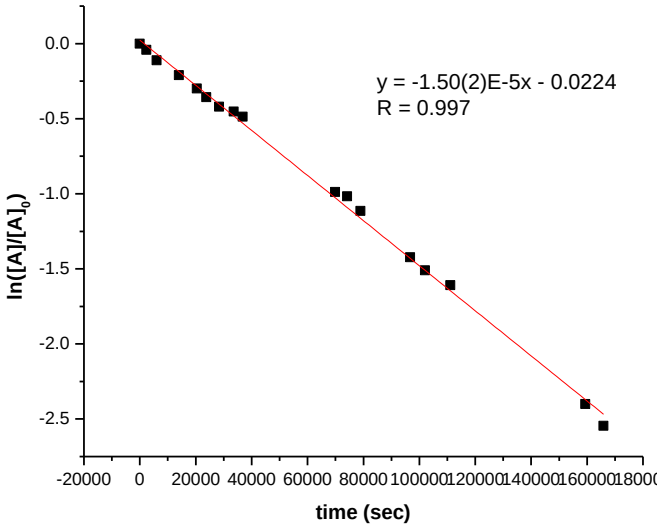

$[A]/[A]_0$	$\ln([A]/[A]_0)$	Time(s)
1	0	0
0.95849	-0.0424	2400
0.8945	-0.11149	6060
0.8105	-0.2101	13980
0.741	-0.29975	20400
0.6992	-0.35782	23820
0.65734	-0.41955	28380
0.6361	-0.4524	33600
0.6145	-0.48695	36780
0.3723	-0.98806	69900
0.3616	-1.01722	74220
0.3279	-1.11505	78960
0.241	-1.42296	96720
0.221	-1.50959	102060
0.2	-1.60944	111060
0.0907	-2.4002	159420
0.07851	-2.54453	165900

Figure7.5. First-order consumption of the sum of **4a**[SbF_6] + **5a**[SbF_6] at 20 °C.

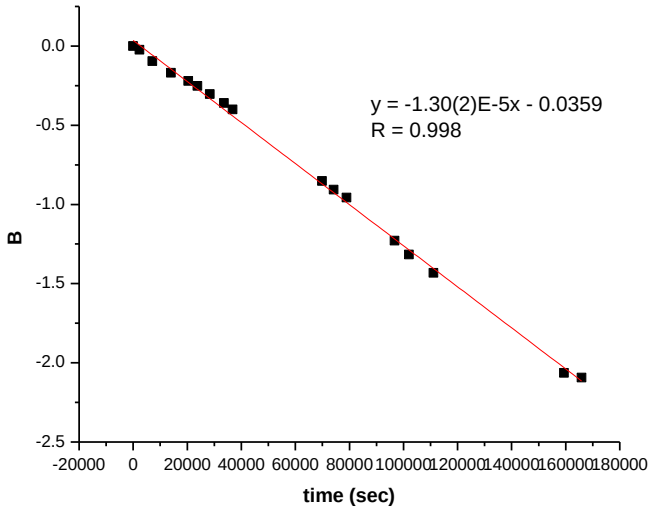

$[B]_\infty$-[B]/ $[B]_\infty$-$[B]_0$	ln[($[B]_\infty$-[B])/ ($[B]_\infty$-$[B]_0$)]	Time(s)
1	0	0
0.97674	-0.02353	2400
0.909	-0.09541	7140
0.844	-0.1696	13980
0.8019	-0.22077	20400
0.7769	-0.25244	23820
0.7386	-0.303	28380
0.6976	-0.36011	33600
0.6698	-0.40078	36780
0.4266	-0.85191	69900
0.404	-0.90634	74220
0.38385	-0.9575	78960
0.2925	-1.22929	96720
0.2682	-1.31602	102060
0.2388	-1.43213	111060
0.127	-2.06357	159420
0.1232	-2.09395	165900

Figure 7.6. First-order consumption of the sum of **4a**[SbF_6] + **5a**[SbF_6] at 20 °C based on increase of **6**[SbF_6]. B = ln[($[B]_\infty$-[B])/($[B]_\infty$-$[B]_0$)].

7.2 Reaction of 1[SbF_6] with CH_2=CHOEt (2b). An NMR tube was charged with **1**[SbF_6] (14.9 mg, 0.0178 mmol) and **2b** (0.0325 mmol). CD_2Cl_2 was added by vacuum transfer at -196 ^oC. A ^1H NMR spectrum at -60 ^oC confirmed the formation of **3b**[SbF_6]. The tube was kept at 0 °C for 10 min. All the volatiles were evacuated and CD_2Cl_2 (0.4 mL) was added by vacuum transfer at -196 °C. The tube was warmed to 0 ^oC and monitored by ^1H NMR periodically. Complex **3b**[SbF_6] was converted to **4b**[SbF_6] and **5b**[SbF_6]. The NMR resonances of **4b**[SbF_6] and **5b**[SbF_6] is very similar to **4b**[$B(C_6F_5)_4$] and **5b**[$B(C_6F_5)_4$]. The first-order rate constant for the consumption of **3b**[SbF_6] measured by the disappearance of the Pd*Me* ^1H NMR resonance is $k_{\text{insert, 3c}}$ = 8.41(6) × 10^{-5} s^{-1} at 0 °C. After **3b**[SbF_6] is fully consumed, the tube was warmed to 20 ^oC and monitored by ^1H NMR periodically. NMR analysis showed a mixture of **4b**[SbF_6] (13%), **5b**[SbF_6] (27%) and **6**[SbF_6] (60%) was present

after 5min. The first-order rate constant for consumption of the total of **4a**[SbF_6] and **5a**[SbF_6] measured by the disappearance of the $PdCH_2CHMe$ resonance of **4b**[SbF_6] and the $PdCMe_2$ resonance of **5b**[SbF_6] is $k_{\beta\text{-OtBu, obs}}$ = 1.200(8) × 10^{-3} s^{-1} at 20 °C. The first-order rate constant for the consumption of **3b**[SbF_6] estimated by the disappearance of the $PdMe$ ^{1}H NMR resonance is $k_{\text{insert, }\mathbf{3c}}$ = ~ 2.7 × 10^{-3} s^{-1} at 20 °C (ca. 56% consumption after 5min).

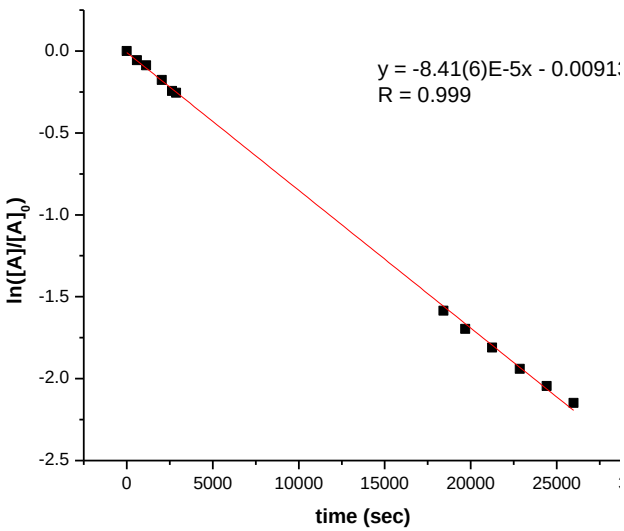

[A]/[A]$_0$	ln([A]/[A]$_0$)	Time(s)
1	0	0
0.9452	-0.05636	600
0.9156	-0.08818	1140
0.8376	-0.17721	2040
0.784	-0.24335	2640
0.7755	-0.25425	2880
0.205	-1.58475	18420
0.1834	-1.69609	19680
0.1635	-1.81094	21240
0.1437	-1.94003	22860
0.1294	-2.04485	24420
0.1167	-2.14815	25980

Figure 7.7. First-order consumption of **3b**[SbF_6] at 0 °C.

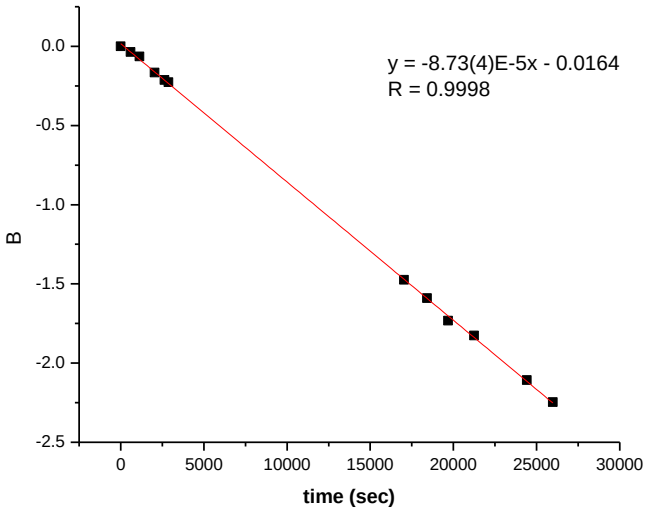

$[B]_\infty-[B]/[B]_\infty-[B]_0$	$\ln([([B]_\infty-[B])/([B]_\infty-[B]_0)]$	Time(s)
1	0	0
0.9649	-0.03573	600
0.9374	-0.06465	1140
0.8471	-0.16594	2040
0.8085	-0.21257	2640
0.7965	-0.22753	2880
0.2154	-1.53526	17040
0.2039	-1.59013	18420
0.177	-1.73161	19680
0.161	-1.82635	21240
0.1215	-2.10784	24420
0.1058	-2.2462	25980

Figure 7.8. First-order consumption of **3b**[SbF_6] at 0 °C based on increase of the sum of **4b**[SbF_6] + **5b**[SbF_6] + **6**[SbF_6]. B = $\ln[([B]_\infty-[B])/([B]_\infty-[B]_0)]$.

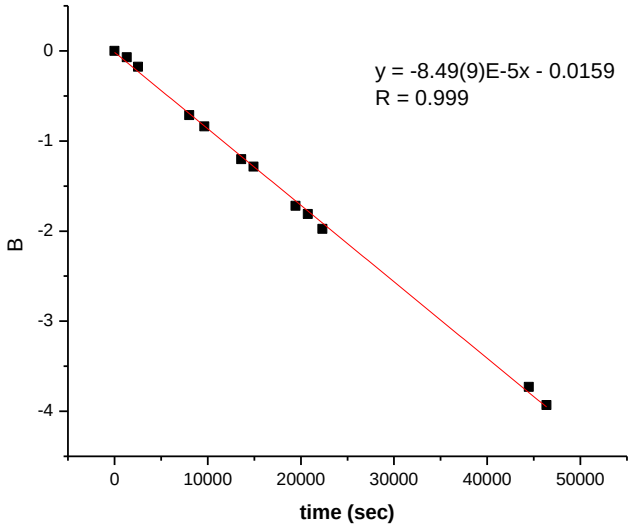

$[A]/[A]_0$	$\ln([A]/[A]_0)$	Time(s)
1	0	0
0.9299	-0.07268	1320
0.8378	-0.17698	2520
0.4896	-0.71417	8040
0.4322	-0.83887	9660
0.3006	-1.20197	13620
0.2767	-1.28482	14940
0.1789	-1.72093	19440
0.1633	-1.81217	20760
0.1385	-1.97688	22320
0.0215	-3.8397	44460
0.0196	-3.93223	46380

Figure 7.9. First-order consumption of the sum of **4b**[SbF_6] + **5b**[SbF_6] at 0 °C. B = $\ln[([B]_\infty-[B])/([B]_\infty-[B]_0)]$.

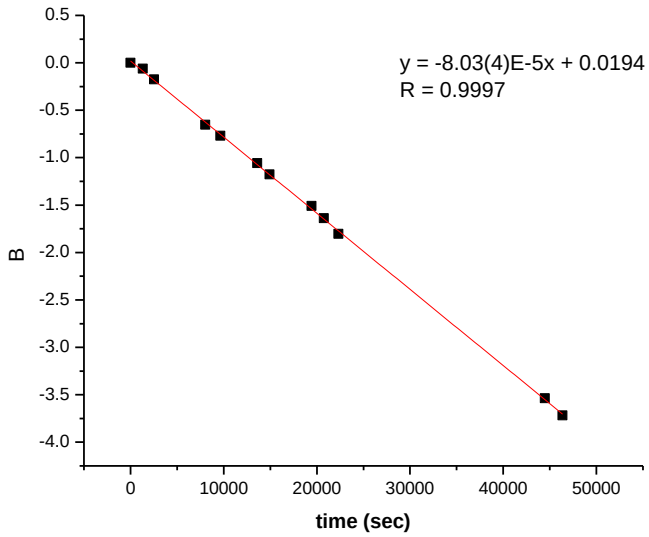

$[B]_\infty$-[B]/ $[B]_\infty$-$[B]_0$	ln[($[B]_\infty$-[B])/ ($[B]_\infty$-$[B]_0$)]	Time(s)
1	0	0
0.9397	-0.06219	1320
0.84	-0.17435	2520
0.5204	-0.65316	8040
0.4636	-0.76873	9660
0.3469	-1.05872	13620
0.3079	-1.17798	14940
0.2212	-1.50869	19440
0.1943	-1.63835	20760
0.1648	-1.80302	22320
0.0291	-3.53702	44460
0.0243	-3.71728	46380

Figure 7.10. First-order consumption of the sum of **4b**[SbF_6] + **5b**[SbF_6] at 0 °C based on increase of **6**[SbF_6]. B = ln[($[B]_\infty$-[B])/($[B]_\infty$-$[B]_0$)].

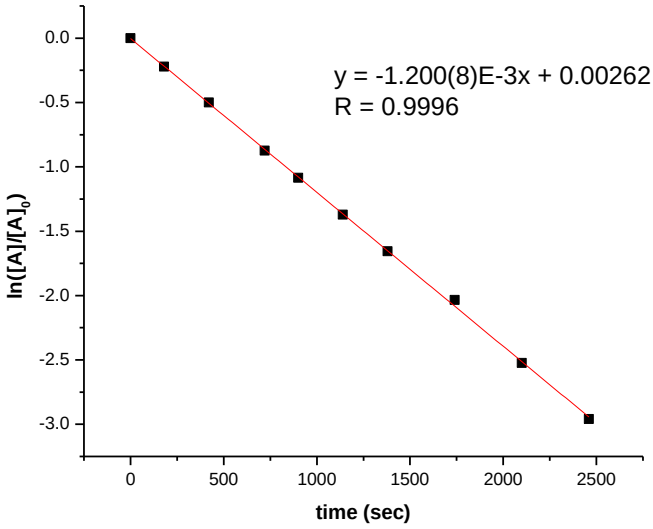

$[A]/[A]_0$	ln($[A]/[A]_0$)	Time(s)
1	0	0
0.802	-0.22065	180
0.6065	-0.50005	420
0.4172	-0.87419	720
0.3376	-1.08589	900
0.2536	-1.372	1140
0.191	-1.65548	1380
0.1308	-2.03409	1740
0.0802	-2.52323	2100
0.0518	-2.96037	2460

Figure 7.11. First-order consumption of the sum of **4b**[SbF_6] + **5b**[SbF_6] at 20 °C.

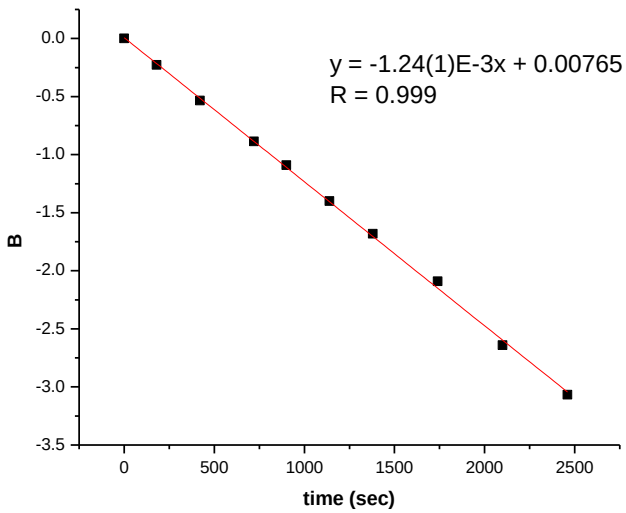

$[B]_\infty$-[B]/ $[B]_\infty$-$[B]_0$	ln[($[B]_\infty$-[B])/ ($[B]_\infty$-$[B]_0$)]	Time(s)
1	0	0
0.7967	-0.22728	180
0.5863	-0.53392	420
0.4124	-0.88576	720
0.3356	-1.09184	900
0.2467	-1.39958	1140
0.186	-1.68201	1380
0.1236	-2.0907	1740
0.0713	-2.64086	2100
0.04655	-3.06723	2460

Figure 7.12. First-order consumption of the sum of **4b**[SbF_6] + **5b**[SbF_6] at 20 °C based on increase of **6**[SbF_6]. B = ln[($[B]_\infty$-[B])/($[B]_\infty$-$[B]_0$)].

7.3 Simulation of the concentration data for the reaction of 1[SbF_6] with 2b.

The first-order rate constant for the consumption of **3b**[SbF_6] measured by the disappearance of the Pd*Me* ^{1}H NMR resonance is $k_{\text{insert, }\mathbf{3b}}$ = 8.41(6) × 10^{-5} s^{-1} at 0 °C. The first-order rate constant for consumption of the total of **4b**[SbF_6] and **5b**[SbF_6] measured by the disappearance of the $PdCH_2CHMe$ resonance of **4b**[SbF_6] and the $PdCMe_2$ resonance of **5b**[SbF_6] is $k_{\beta\text{-OtBu, obs}}$ = 2.65(3) × 10^{-5} s^{-1} at 0 °C. By using these two rate constants, simulation[9] was performed to demonstrate the change in concentrations of **3b**[SbF_6], **4b**[SbF_6], **5b**[SbF_6] and **6**[SbF_6] over time. The simulated data agree very well with the experimental data. Similarly, the comparison between the simulated data and the experimental data was carried out for the $B(C_6F_5)_4$ anion, which also shows good agreement.

Based on the simulation results, it is concluded that the rate constants determined from the experimental data are very reliable. The comparison of the $k_{\text{insert, }\mathbf{3b}}$ between SbF_6 anion

and $B(C_6F_5)_4$ anion both at 0 °C and at 20 °C showed that the anion only has minimal affect on the insertion rate (Table 2, 3). The similar comparison of the $k_{\text{insert, }\mathbf{3a}}$ gave the same conclusion.

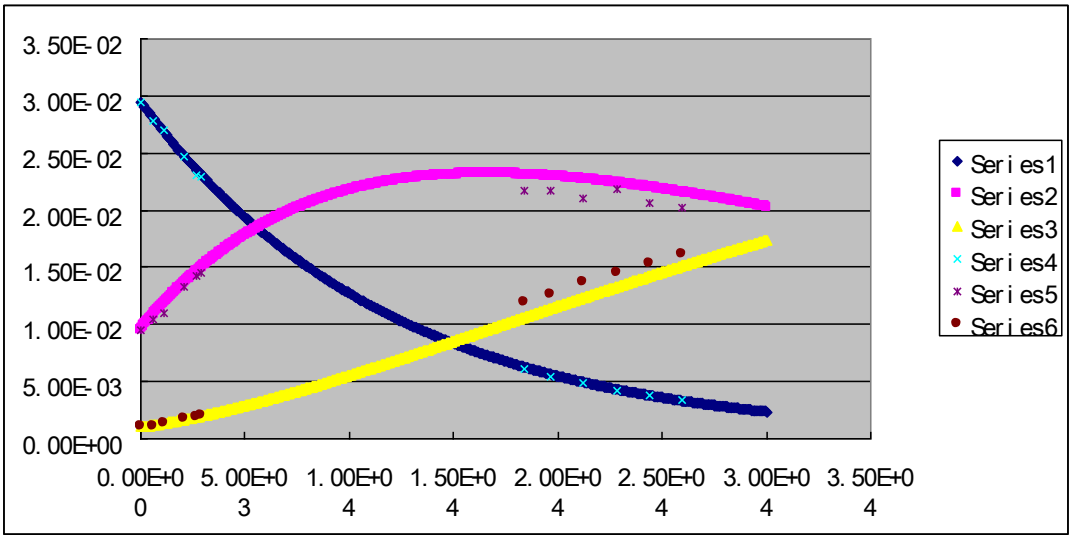

Figure 7.13. The experimental and simulated concentration vs time plot for SbF_6 anion. Series 1-3 are the simulated concentration of **3b**, **4b**+**5b** and **6** over time, by using $k_{insert,3}$ = 8.41 $\times 10^{-5}$ s^{-1}, and $k_{\beta\text{-OR, obs}}$ = 2.65 $\times$ 10^{-5} s^{-1}. Series 4-6 are the experimental concentration of **3b**, **4b**+**5b** and **6** over time.

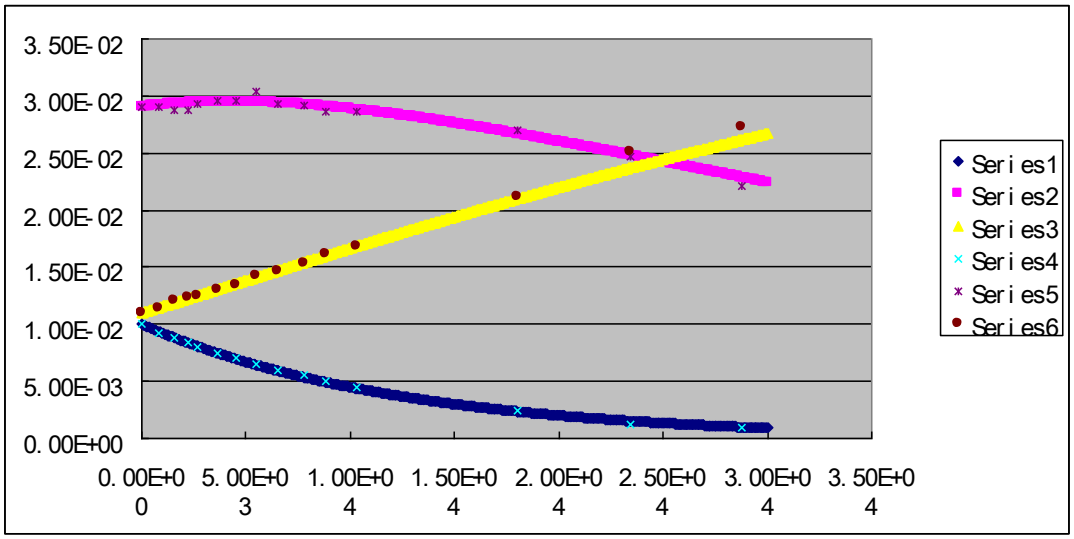

Figure 7.14. The experimental and simulated concentration vs time plot for $B(C_6F_5)_4$ anion. Series 1-3 are the simulated concentration of **3b**, **4b**+**5b** and **6** over time, by using $k_{insert,3}$ = 8.01 $\times 10^{-5}$ s^{-1}, and $k_{\beta\text{-OR, obs}}$ = 1.94 $\times$ 10^{-5} s^{-1}. Series 4-6 are the experimental concentration of **3b**, **4b**+**5b** and **6** over time.

7.4 Reaction of 1[SbF_6] with CH_2=CHOSiMe_3 (2c). An NMR tube was charged with **1**[SbF_6] (14.9 mg, 0.0178 mmol) and **2c** (0.027 mmol). CD_2Cl_2 was added by vacuum transfer at -196 ^oC. A ^1H NMR spectrum at -60 ^oC confirmed the formation of **3c**[SbF_6]. The tube was warmed to 0 ^oC and monitored by ^1H NMR periodically. Complex **3c**[SbF_6] was converted to **5c**[SbF_6]. The NMR resonances of **5c**[SbF_6] is very similar to **5c**[$B(C_6F_5)_4$]. The first-order rate constant for the consumption of **3c**[SbF_6] measured by the disappearance of the Pd*Me* ^1H NMR resonance is $k_{\text{insert, 3c}}$ = 1.645(7) $\times$ 10^{-4} s^{-1} at 0 °C. After **3c**[SbF_6] is fully consumed, the tube was warmed to 20 ^oC and monitored by ^1H NMR periodically. Complex **5c**[SbF_6] was converted to **6**[SbF_6]. The first-order rate constant for consumption of **5c**[SbF_6] measured by the disappearance of the PdC*Me*$_2$ resonance is $k_{\beta\text{-OSiMe3, obs}}$ = 1.11(2) $\times$ 10^{-4} s^{-1} at 20 °C.

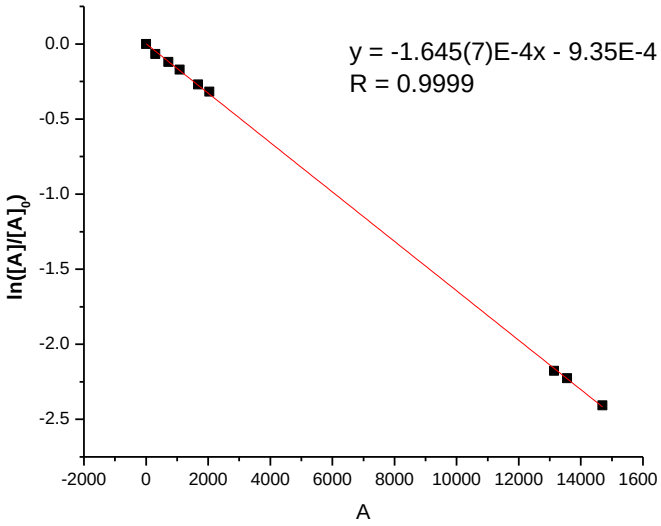

$[A]/[A_0]$	$\ln([A]/[A_0])$	Time(s)
1	0	0
0.935	-0.06721	300
0.8871	-0.1198	720
0.8427	-0.17114	1080
0.7626	-0.27102	1680
0.7274	-0.31828	2040
0.1134	-2.17683	13140
0.108	-2.22562	13560
0.09	-2.40795	14700

Figure 7.15. First-order consumption of **3c**[SbF_6] at 0 °C.

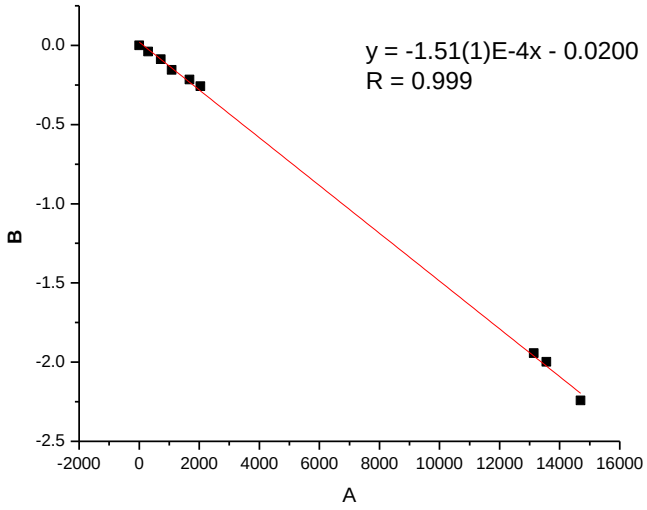

$[B]_\infty-[B]/[B]_\infty-[B]_0$	$\ln([[B]_\infty-[B])/([B]_\infty-[B]_0)]$	Time(s)
1	0	0
0.9608	-0.03999	300
0.9158	-0.08796	720
0.857	-0.15432	1080
0.8059	-0.2158	1680
0.7722	-0.25851	2040
0.1433	-1.94281	13140
0.1355	-1.99878	13560
0.1062	-2.24243	14700

Figure 7.16. First-order consumption of **3c**[SbF_6] at 0 °C based on increase of **4c**[SbF_6]. B = $\ln([[B]_\infty-[B])/([B]_\infty-[B]_0)]$.

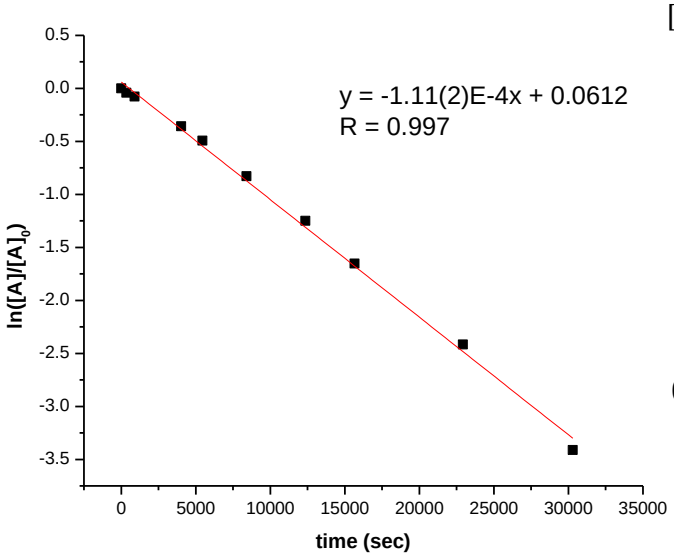

$[A]/[A]_0$	$\ln([A]/[A]_0)$	Time(s)
1	0	0
0.9605	-0.0403	360
0.925	-0.07796	900
0.6987	-0.35853	4020
0.6115	-0.49184	5460
0.4364	-0.8292	8400
0.2866	-1.24967	12360
0.1915	-1.65287	15660
0.08926	-2.4162	22920
0.033	-3.41125	30300

Figure 7.17. First-order consumption of **5c**[SbF_6] at 20 °C.

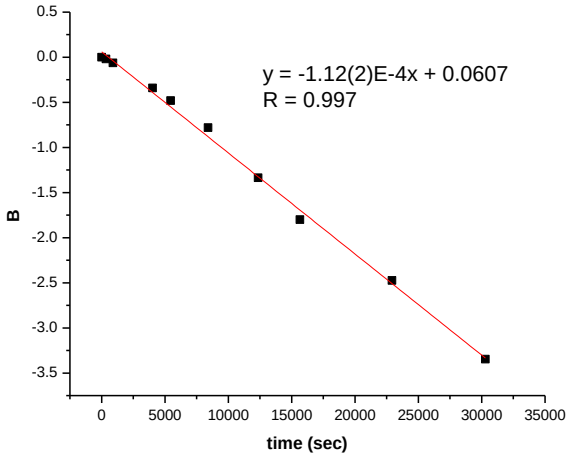

$[B]_\infty$-[B]/ $[B]_\infty$-$[B]_0$	$\ln([([B]_\infty$-[B])/ $([B]_\infty$-$[B]_0)]$	Time(s)
1	0	0
0.9796	-0.02061	360
0.9394	-0.06251	900
0.7112	-0.3408	4020
0.6183	-0.48078	5460
0.4583	-0.78023	8400
0.2629	-1.33598	12360
0.1651	-1.8012	15660
0.0842	-2.47456	22920
0.0352	-3.34671	30300

Figure 7.18. First-order consumption of **5c**[SbF_6] at 20 °C based on increase of **6**[SbF_6]. B = $\ln([([B]_\infty$-[B])/$([B]_\infty$-$[B]_0)]$.

7.5 Reaction of 1[SbF_6] with CH_2=CHOSiMe_2Ph (2d). A NMR tube was charged with (α-diimine)PdMeCl (16.3 mg, 29.0 μmol), $AgSbF_6$ (10 mg, 29.1 μmol) and CH_2=CHOSiMe_2Ph (5.2 mg, 29.2 μmol), and CD_2Cl_2 (0.4 mL) was added by vacuum transfer

at –78 °C. The tube was shaken to dissolve and thoroughly mix the components. A ^{1}H NMR spectrum at -60 ^{o}C confirmed the formation of **3d**[SbF_6]. The tube was warmed to 0 ^{o}C and monitored by ^{1}H NMR periodically. Complex **3d**[SbF_6] was converted to **5d**[SbF_6]. Key NMR Data for **5d**[SbF_6]: ^{1}H NMR (CD_2Cl_2) δ 3.05 (m, 4H, C*H*Me_2), 2.26 (s, 3H, N=C*Me*), 2.21 (s, 3H, N=C*Me*), 1.46 (d, *J* = 7, 6H, CH*Me*$_2$), 1.38 (d, *J* = 7, 6H, CH*Me*$_2$), 1.30 (d, *J* = 7, 6H, CH*Me*$_2$), 1.18 (d, *J* = 7, 6H, CH*Me*$_2$), 0.38 (s, 6H, PdC*Me*$_2$(OSiMe_2Ph)), 0.19(s, 6H, Si*Me*$_2$). The first-order rate constant for the consumption of **3d**[SbF_6] measured by the disappearance of the Pd*Me* ^{1}H NMR resonance is $k_{\text{insert, 3d}} = 3.18(5) \times 10^{-4}$ s^{-1} at 0 °C. After **3d**[SbF_6] is fully consumed, the tube was warmed to 20 ^{o}C and monitored by ^{1}H NMR periodically. Complex **5d**[SbF_6] was converted to **6**[SbF_6]. The first-order rate constant for consumption of **5d**[SbF_6] measured by the disappearance of the PdC*Me*$_2$ resonance is $k_{\text{β-OSiMe2Ph, obs}} = 1.56(3) \times 10^{-4}$ s^{-1} at 20 °C.

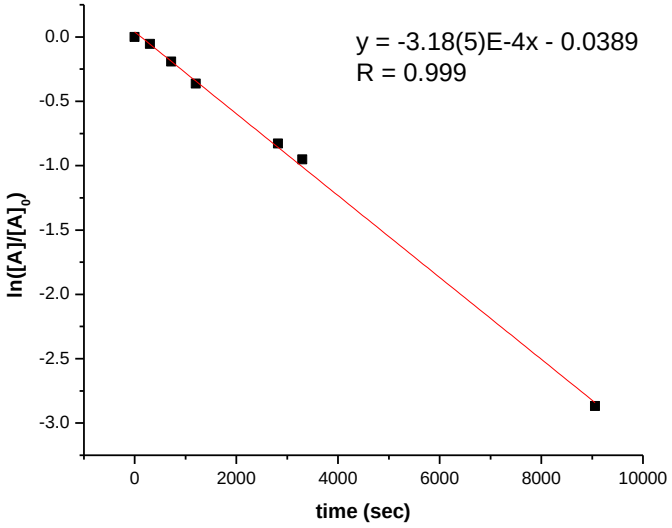

[A]/[A]$_0$	ln([A]/[A]$_0$)	Time(s)
1	0	0
0.9461	-0.05541	300
0.8253	-0.19201	720
0.6955	-0.36312	1200
0.4371	-0.82759	2820
0.3858	-0.95244	3300
0.05676	-2.86892	9060

Figure 7.19. First-order consumption of **3d**[SbF_6] at 0 °C.

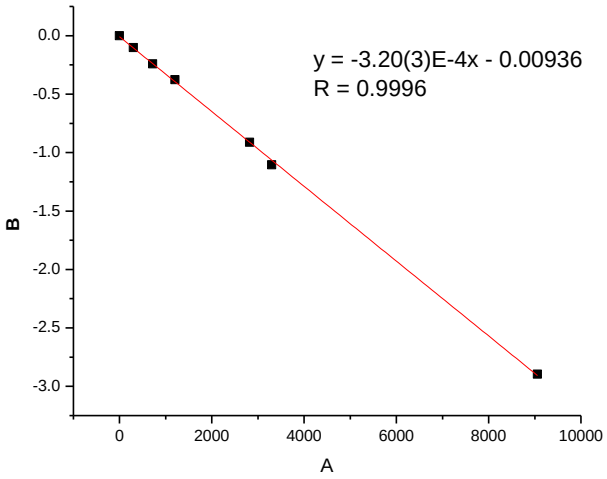

$[B]_\infty-[B]/[B]_\infty-[B]_0$	$\ln([[B]_\infty-[B])/([B]_\infty-[B]_0)]$	Time(s)
1	0	0
0.90365	-0.10131	300
0.785	-0.24207	720
0.6857	-0.37732	1200
0.4019	-0.91155	2820
0.3315	-1.10413	3300
0.05527	-2.89553	9060

Figure 7.20. First-order consumption of **3d**[SbF_6] at 0 °C based on increase of **4d**[SbF_6]. B = $\ln([[B]_\infty-[B])/([B]_\infty-[B]_0)]$.

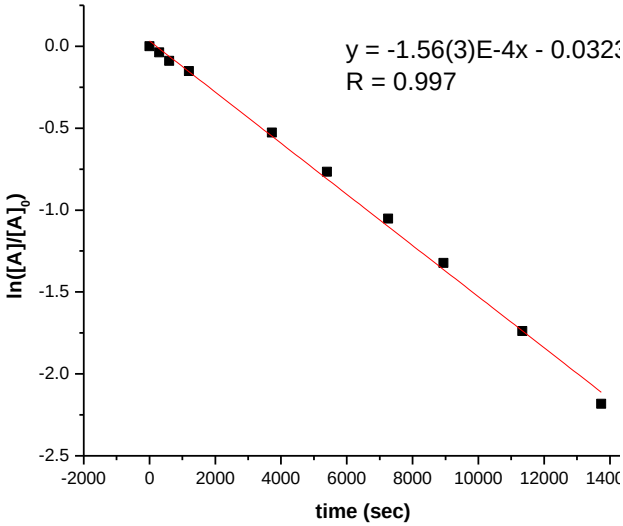

$[A]/[A]_0$	$\ln([A]/[A]_0)$	Time(s)
1	0	0
0.9627	-0.03801	300
0.9153	-0.0885	600
0.859	-0.15199	1200
0.5908	-0.52628	3720
0.4645	-0.76679	5400
0.3491	-1.0524	7260
0.2662	-1.32351	8940
0.1757	-1.73898	11340
0.1127	-2.18303	13740

Figure 7.21. First-order consumption of **5d**[SbF_6] at 20 °C.

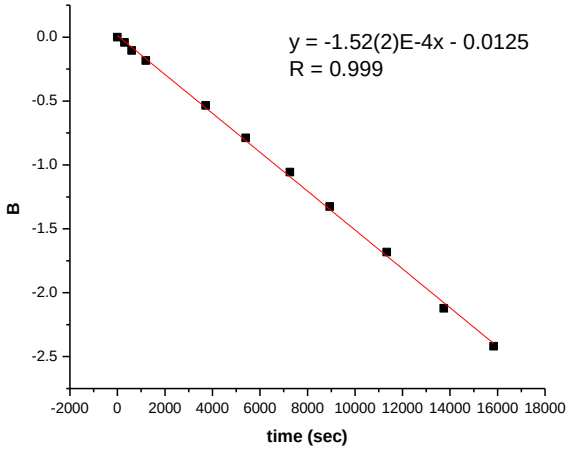

$[B]_\infty$-[B]/ $[B]_\infty$-$[B]_0$	ln[($[B]_\infty$-[B])/ ($[B]_\infty$-$[B]_0$)]	Time(s)
1	0	0
0.9589	-0.04197	300
0.9	-0.10536	600
0.8323	-0.18356	1200
0.5857	-0.53495	3720
0.4543	-0.789	5400
0.3477	-1.05642	7260
0.2657	-1.32539	8940
0.1859	-1.68255	11340
0.1198	-2.12193	13740
0.089	-2.41912	15840

Figure 7.22. First-order consumption of **5d**[SbF_6] at 20 °C based on the increase of **6**[SbF_6]. B = ln[($[B]_\infty$-[B])/($[B]_\infty$-$[B]_0$)].

7.6 Reaction of 1[SbF_6] with CH_2=CHOSiMePh_2 (2e). A NMR tube was charged with (α-diimine)PdMeCl (16.3 mg, 29.0 μmol), $AgSbF_6$ (10 mg, 29.1 μmol) and CH_2=CHOSiMePh_2 (6.9 mg, 29.1 μmol), and CD_2Cl_2 (0.4 mL) was added by vacuum transfer at –78 °C. The tube was shaken to dissolve and thoroughly mix the components. A ^{1}H NMR spectrum at -60 ^{o}C confirmed the formation of **3e**[SbF_6]. The tube was warmed to 0 ^{o}C and monitored by ^{1}H NMR periodically. Complex **3e**[SbF_6] was converted to **5e**[SbF_6]. Key NMR Data for **5e**[SbF_6]: ^{1}H NMR (CD_2Cl_2) δ 3.06 (m, 4H, C*H*Me_2), 2.25 (s, 3H, N=C*Me*), 2.18 (s, 3H, N=C*Me*), 1.37 (d, *J* = 7, 6H, CH*Me*$_2$), 1.30 (d, *J* = 7, 6H, CH*Me*$_2$), 1.25 (d, *J* = 7, 6H, CH*Me*$_2$), 1.16 (d, *J* = 7, 6H, CH*Me*$_2$), 0.57 (s, 3H, Si*Me*), 0.34 (s, 6H, PdC*Me*$_2$(OSiMePh_2)). The first-order rate constant for the consumption of **3e**[SbF_6] measured by the disappearance of the Pd*Me* ^{1}H NMR resonance is $k_{\text{insert, 3d}}$ = 5.22(7) × 10^{-4} s^{-1} at 0 °C. After **3e**[SbF_6] is fully consumed, the tube was warmed to 20 ^{o}C and monitored by ^{1}H NMR periodically. Complex

5e[SbF_6] was converted to **6**[SbF_6]**.** The first-order rate constant for consumption of **5e**[SbF_6] measured by the disappearance of the PdC*Me*$_2$ resonance is $k_{\beta\text{-OSiMePh2, obs}} = 2.46(4) \times 10^{-4}$ s^{-1} at 20 °C.

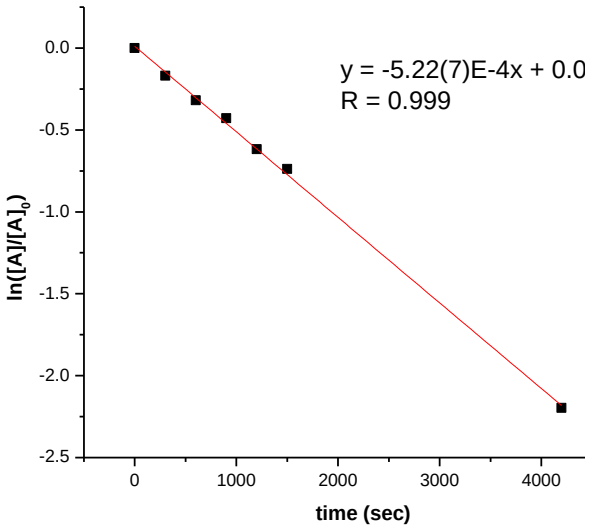

$[A]/[A]_0$	$\ln([A]/[A]_0)$	Time(s)
1	0	0
0.84457	-0.1689	300
0.72727	-0.3185	600
0.65103	-0.4292	900
0.53959	-0.6169	1200
0.478	-0.7381	1500
0.1111	-2.1973	4200

Figure 7.23. First-order consumption of **3e**[SbF_6] at 0 °C.

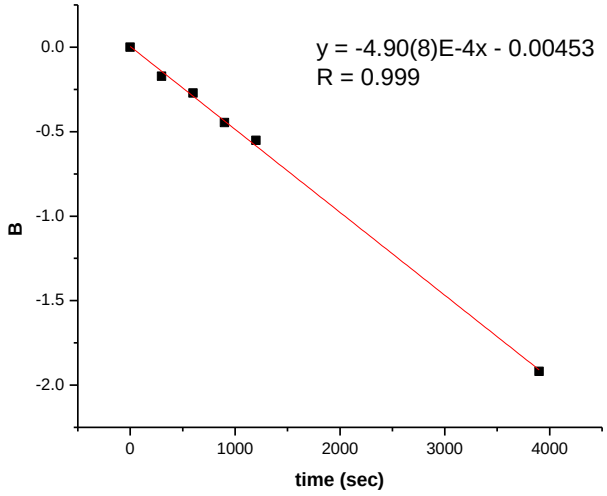

$[B]_\infty-[B]/[B]_\infty-[B]_0$	$\ln[([B]_\infty-[B])/([B]_\infty-[B]_0)]$	Time(s)
1	0	0
0.842221	-0.17171	300
0.76187	-0.27198	600
0.639883	-0.44647	900
0.576333	-0.55107	1200
0.146822	-1.91853	3900

Figure 7.24. First-order consumption of **3e**[SbF_6] at 0 °C based on increase of **4e**. B = $\ln[([B]_\infty-[B])/([B]_\infty-[B]_0)]$.

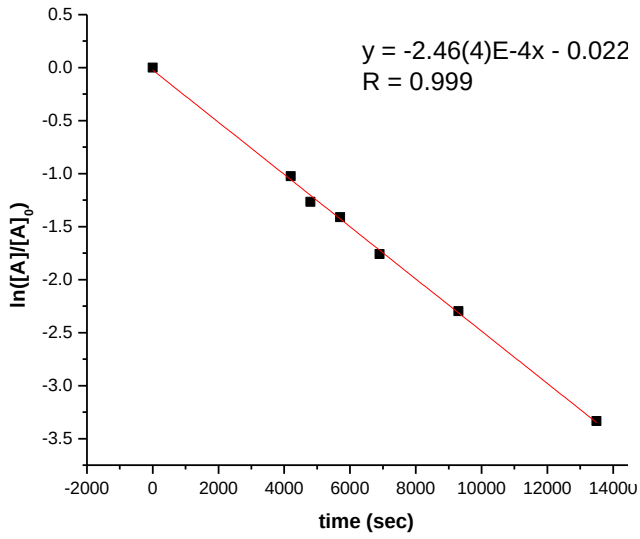

$[A]/[A]_0$	$\ln([A]/[A]_0)$	Time(s)
1	0	0
0.358538	-1.02572	4200
0.28163	-1.26716	4800
0.243731	-1.41169	5700
0.172331	-1.75834	6900
0.10053	-2.2973	9300
0.0356	-3.33541	13500

Figure 7.25. First-order consumption of **5e**[SbF_6] at 20 °C.

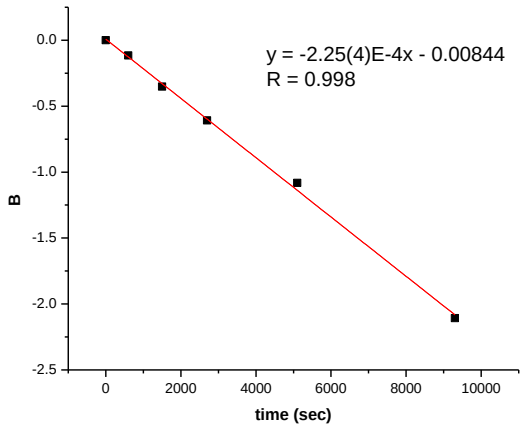

$[B]_\infty$-[B]/ $[B]_\infty$-$[B]_0$	ln[($[B]_\infty$-[B])/ ($[B]_\infty$-$[B]_0$)]	Time(s)
1	0	0
0.89039	-0.1161	600
0.702817	-0.35266	1500
0.544577	-0.60775	2700
0.338865	-1.08215	5100
0.121575	-2.10723	9300

Figure 7.26. First-order consumption of **5e**[SbF_6] at 20 °C based on the increase of **6**[SbF_6]. B = ln[($[B]_\infty$-[B])/($[B]_\infty$-$[B]_0$)].

7.7 Reaction of 1[SbF_6] with CH_2=CHOSiPh_3 (2f). A NMR tube was charged with (α-diimine)PdMeCl (16.3 mg, 29.0 μmol), $AgSbF_6$ (10 mg, 29.1 μmol) and CH_2=CHOSiPh_3 (8.8 mg, 29.1 μmol), and CD_2Cl_2 (0.4 mL) was added by vacuum transfer at –78 °C. The tube was shaken to dissolve and thoroughly mix the components. A ^{1}H NMR spectrum at -60 ^{o}C confirmed the formation of **3f**[SbF_6]. The tube was warmed to 0 ^{o}C and monitored by ^{1}H NMR periodically. Complex **3f**[SbF_6] was converted to **5f**[SbF_6]. The NMR resonances of **5f**[SbF_6] is very similar to **5f**[$B(C_6F_5)_4$]. The first-order rate constant for the consumption of **3f**[SbF_6] measured by the disappearance of the H_{trans} ^{1}H NMR resonance is $k_{insert,\ \mathbf{3f}} = 8.06(6) \times 10^{-4}$ s^{-1} at 0 °C. After **3f**[SbF_6] is fully consumed, the tube was warmed to 20 ^{o}C and monitored by ^{1}H NMR periodically. Complex **5f**[SbF_6] was converted to **6**[SbF_6]**.** The first-order rate constant for consumption of **5f**[SbF_6] measured by the disappearance of the PdCMe_2 resonance is $k_{\beta\text{-OSiMePh2, obs}} = 3.78(1) \times 10^{-4}$ s^{-1} at 20 °C.

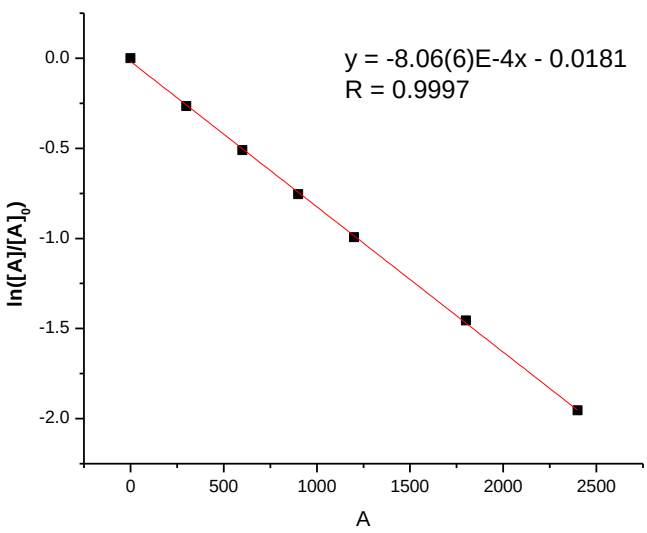

$[A]/[A]_0$	$\ln([A]/[A]_0)$	Time(s)
1	0	0
0.7667	-0.26566	300
0.6	-0.51083	600
0.4704	-0.75417	900
0.3704	-0.99317	1200
0.2333	-1.45543	1800
0.1417	-1.95404	2400

Figure 7.27. First-order consumption of **3f**[SbF_6] at 0 °C.

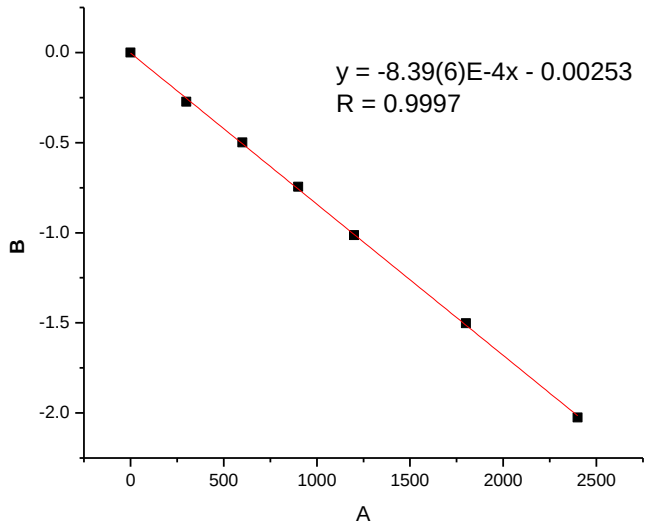

$[B]_\infty-[B]/[B]_\infty-[B]_0$	$\ln([[B]_\infty-[B])/([B]_\infty-[B]_0)]$	Time(s)
1	0	0
0.76125	-0.27279	300
0.6069	-0.49939	600
0.475	-0.74444	900
0.3631	-1.01308	1200
0.2225	-1.50283	1800
0.13188	-2.02586	2400

Figure 7.28. First-order consumption of **3f**[SbF_6] at 0 °C based on increase of **4**. B = $\ln([[B]_\infty-[B])/([B]_\infty-[B]_0)]$.

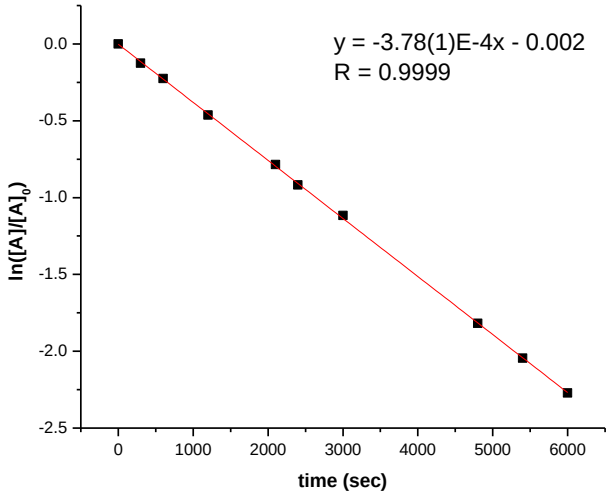

$[A]/[A]_0$	$\ln([A]/[A]_0)$	Time(s)
1	0	0
0.882749	-0.12471	300
0.798281	-0.22529	600
0.629823	-0.46232	1200
0.456056	-0.78514	2100
0.399218	-0.91825	2400
0.327244	-1.11705	3000
0.162217	-1.81882	4800
0.129278	-2.04579	5400
0.103203	-2.27106	6000

Figure 7.29. First-order consumption of **5f**[SbF_6] at 20 °C.

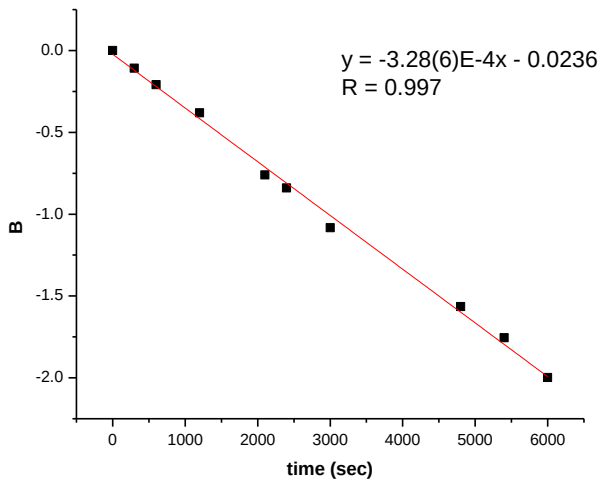

$[B]_\infty-[B]/[B]_\infty-[B]_0$	$\ln[([B]_\infty-[B])/([B]_\infty-[B]_0)]$	Time(s)
1	0	0
0.898	-0.10759	300
0.8109	-0.20961	600
0.6828	-0.38155	1200
0.46766	-0.76001	2100
0.4316	-0.84026	2400
0.3383	-1.08382	3000
0.209	-1.56542	4800
0.1729	-1.75504	5400
0.1356	-1.99805	6000

Figure 7.30. First-order consumption of **5f**[SbF_6] at 20 °C based on increase of **6**[SbF_6]. B = $\ln[([B]_\infty-[B])/([B]_\infty-[B]_0)]$.

7.8 Insertion of [(α-diimine)PdMe(CH_2=CHOPh)][SbF_6] (3g[SbF_6]). An NMR tube was charged with **1**[SbF_6] (14.6 mg, 0.0176 mmol) and **1g** (0.043 mmol). CD_2Cl_2 was added by vacuum transfer at -196 ^oC. The tube was warmed to 0 ^oC and monitored by ^1H NMR

periodically. Complex **3g**[SbF_6] was cleanly converted to **6**[SbF_6]. No intermediates were detected. The first-order rate constant for the consumption of **3g**[SbF_6] measured by the disappearance of the H_{trans} ^{1}H NMR resonance is $k_{insert,\ \mathbf{3e}}$ = 1.50(4) × 10^{-3} s^{-1} at 0 °C.

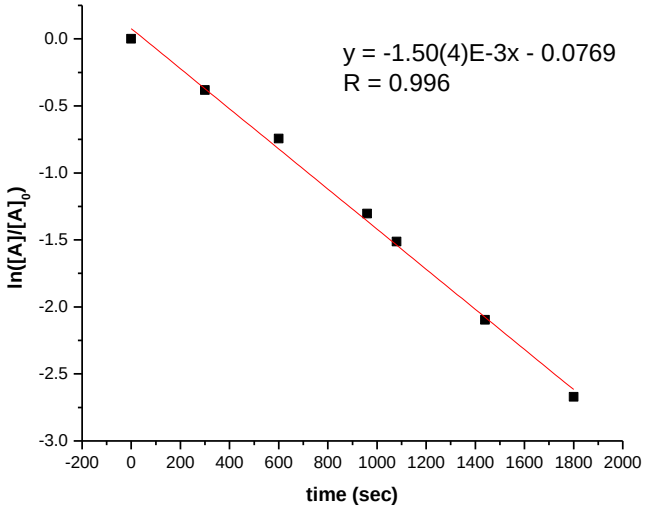

$[A]/[A]_0$	$\ln([A]/[A]_0)$	Time(s)
1	0	0
0.682813	-0.38153	300
0.475405	-0.74359	600
0.271596	-1.30344	960
0.220456	-1.51206	1080
0.122825	-2.09699	1440
0.069136	-2.67168	1800

Figure 7.31. First-order consumption of **3g**[SbF_6] at 0 °C.

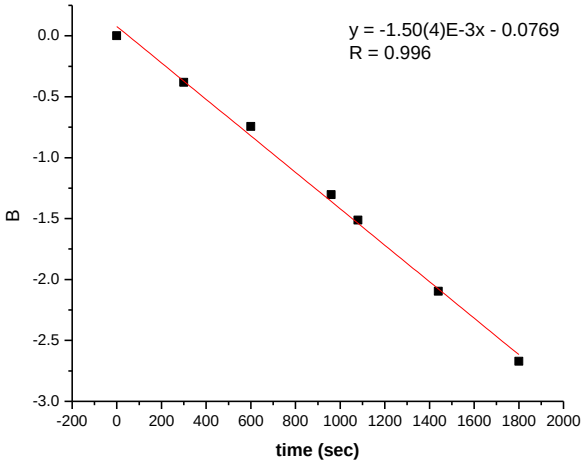

$[B]_\infty$-[B]/ $[B]_\infty$-$[B]_0$	$\ln([[B]_\infty$-[B])/ ($[B]_\infty$-$[B]_0$)]	Time(s)
1	0	0
0.7591	-0.3815	300
0.3664	-0.7436	600
0.3078	-1.3034	960
0.2433	-1.5121	1080
0.1701	-2.097	1440
0.133	-2.6717	1800

Figure 7.32. First-order consumption of **3g**[SbF_6] at 0 °C based on the increase of **6**[SbF_6]. B = $\ln([[B]_\infty$-[B])/($[B]_\infty$-$[B]_0$)].

7.9 Construction of the energy diagram for competitive binding of vinyl ethers and insertion of 3a-g (Figure 1 in manuscript).

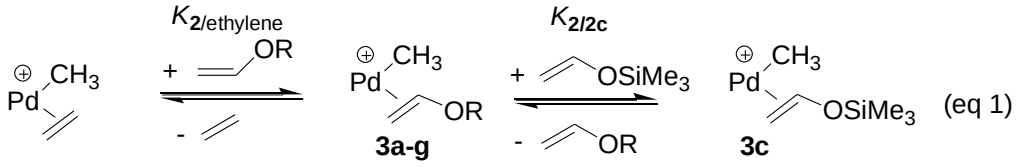

The competitive binding of ethylene and CH_2=CHOR (**2a-c**) (eq 1) was quantified by measuring $K_{\mathbf{2}/\text{ethylene}}$ = [**3**][CH_2=CH_2][(α-diimine)PdMe(CH_2=CH_2)$^+$]$^{-1}$[**2**]$^{-1}$. The $K_{\mathbf{2a/2c}}$ was determined according to equation i-iii. $K_{\mathbf{2b/2c}}$ was determined in an analogous manners and the results are shown in Tables 2 and 3.

$K_{\mathbf{2a}/\text{ethylene}}$ = [**3a**][CH_2=CH_2][(α-diimine)PdMe(CH_2=CH_2)$^+$]$^{-1}$[**2a**]$^{-1}$ (i)

$K_{\mathbf{2c}/\text{ethylene}}$ = [**3c**][CH_2=CH_2][(α-diimine)PdMe(CH_2=CH_2)$^+$]$^{-1}$[**2c**]$^{-1}$ (ii)

$K_{\mathbf{2a/2c}}$ = [**3a**][**2c**][**3c**]$^{-1}$[**2a**]$^{-1}$ = $K_{\mathbf{2a}/\text{ethylene}}/K_{\mathbf{2c}/\text{ethylene}}$ (iii)

ΔG for (α-diimine)PdMe(CH_2=CHOR)$^+$ (**3a-g**) versus **3c** was determined by equation (iv).

$\Delta G = -RT\ln K$ (iv)

The free energy barrier for the insertion of **3a-g** ($\Delta G^{\neq}$) was calculated by Erying equation (v). The results are compared in Figure 1.

$\Delta G^{\neq} = -RT\ln(k_{\text{insert},\mathbf{3}}h/k_BT)$ (v)

7.10 Insertion of [{(2,6-^{i}Pr$_2$-C$_6$H$_3$)N=CAnCAn=N(2,6-^{i}Pr$_2$-C$_6$H$_3$)}PdMe(CH$_2$=CHOSiPh$_3$)][SbF$_6$] (3h) and β-OSiPh$_3$ elimination of 5h. A NMR tube was charged with {(2,6-^{i}Pr$_2$-C$_6$H$_3$)N=C(An)-C(An)=N(2,6-^{i}Pr$_2$-C$_6$H$_3$)}PdMeCl (19.2 mg, 29.0 μmol), AgSbF$_6$ (10 mg, 29.1 μmol) and CH$_2$=CHOSiPh$_3$ (8.8 mg, 29.1 μmol), and CD_2Cl_2 (0.4 mL) was added by vacuum transfer at –78 °C. The tube was shaken to dissolve and thoroughly mix the components. NMR spectra at 23 °C showed that **3h**[SbF$_6$] (90 %) had formed. Key NMR Data for **5d**: ^{1}H NMR (CD_2Cl_2, 23 °C) δ 8.20 (d, *J* = 8, 1H, An: H$_p$), 8.16 (d, *J* = 8, 1H, An: H$_{p'}$), 7.58-7.25 (m, 23 H, An: H$_m$, H$_{m'}$, 6 H$_{aryl}$, 15 H$_{aryl}$ from SiPh$_3$), 6.58 (d, *J* = 8, 2H, An: H$_o$), 3.35 (m, 2H, C*H*Me$_2$), 3.16 (m, 2H, C*H*Me$_2$), 1.32 (d, *J* = 7, 6H, CH*Me$_2$*), 1.14 (d, *J* = 7, 6H, CH*Me$_2$*), 0.98 (d, *J* = 7, 6H, CH*Me$_2$*), 0.88 (d, *J* = 7, 6H, CH*Me$_2$*), 0.47 (s, 6H, PdC*Me$_2$*(OSiPh$_3$)). ^{13}C NMR (CD_2Cl_2, -20 ^{o}C) data: δ171.8 (N=*C*Me), 168.8 (N=*C*Me), 141.7 (CH$_2$=*C*HOSiPh$_3$), 144.9, 143.3, 142.9, 138.0, 137.3, 135.1, 135.0, 133.4, 132.9, 131.8, 131.4, 129.8, 129.5, 128.8, 128.6, 128.1, 126.3, 126.1, 125.6, 125.5, 125.3 and 124.8 (An 4 quaternary C, C$_o$, C$_o$', C$_m$, C$_m$', C$_p$, C$_p$'; Ar, Ar' C$_{ipso}$, C$_{ipso}$', C$_o$, C$_o$', C$_m$, C$_m$', C$_p$, C$_p$'; SiPh C$_{ipso}$, C$_o$, C$_m$, C$_p$,) , 87.9 (Pd*C*Me$_2$(OSiPh$_3$)), 29.5 (*C*HMe$_2$), 29.2 (*C*HMe$_2$), 26.4, 24.7, 23.4, 23.2 and 23.1 (4 CH*Me$_2$* and PdC*Me$_2$*(OSiPh$_3$)).

The first-order rate constant for the consumption of [{(2,6-^{i}Pr$_2$-C$_6$H$_3$)N=CAnCAn=N(2,6-^{i}Pr$_2$-C$_6$H$_3$)}PdMe(CH$_2$=CHOSiPh$_3$)][SbF$_6$] measured by the disappearance of the H$_{trans}$ ^{1}H NMR resonance is $k_{insert,\mathbf{3h}}$ = 1.98(2) × 10^{-4} s^{-1} at 0 °C. After [{(2,6-^{i}Pr$_2$-C$_6$H$_3$)N=CAnCAn=N(2,6-^{i}Pr$_2$-C$_6$H$_3$)}PdMe(CH$_2$=CHOSiPh$_3$)][SbF$_6$] is fully consumed, the tube was warmed to 20 ^{o}C and monitored by ^{1}H NMR periodically. Complex

[{(2,6-^{i}Pr$_2$-C$_6$H$_3$)N=CAnCAn=N(2,6-^{i}Pr$_2$-C$_6$H$_3$)}PdCMe$_2$(OSiPh$_3$)][SbF$_6$] was converted to **6**[SbF$_6$]**.** The first-order rate constant for consumption of [{(2,6-^{i}Pr$_2$-C$_6$H$_3$)N=CAnCAn=N(2,6-^{i}Pr$_2$-C$_6$H$_3$)}PdCMe$_2$(OSiPh$_3$)][SbF$_6$] (**5h**) measured by the disappearance of the PdC*Me$_2$* resonance is $k_{\beta\text{-OSiPh3, obs}}$ = 1.37(1) × 10^{-4} s^{-1} at 20 °C.

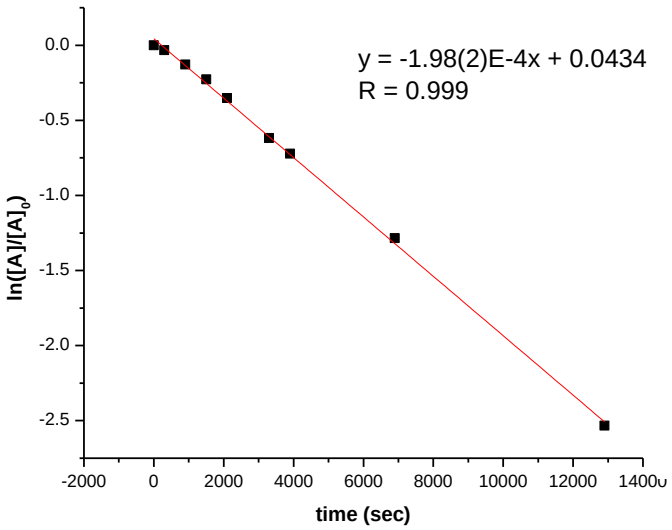

[A]/[A]$_0$	ln([A]/[A]$_0$)	Time(s)
1	0	0
0.96719	-0.0334	300
0.87999	-0.1278	900
0.79683	-0.2271	1500
0.70328	-0.352	2100
0.539	-0.618	3300
0.48576	-0.722	3900
0.2766	-1.2852	6900
0.0794	-2.533	12900

Figure 7.33. First-order consumption of **3h** at 0 °C.

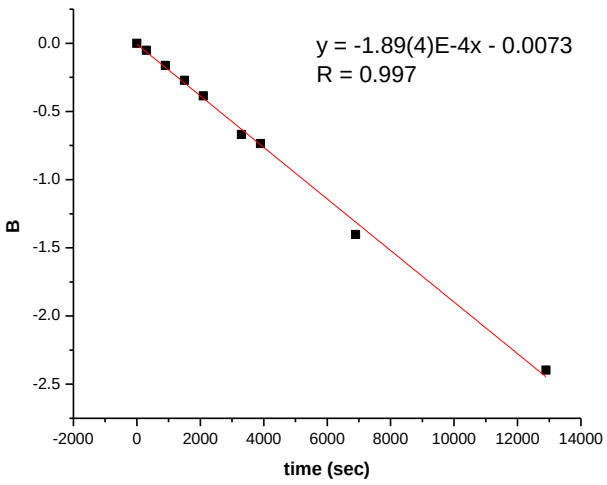

$[B]_\infty-[B]/[B]_\infty-[B]_0$	$\ln[([B]_\infty-[B])/([B]_\infty-[B]_0)]$	Time(s)
1	0	0
0.9501	-0.05119	300
0.85	-0.16252	900
0.7613	-0.27273	1500
0.6793	-0.38669	2100
0.512	-0.66943	3300
0.4791	-0.73585	3900
0.2459	-1.40283	6900
0.091	-2.3969	12900

Figure 7.34. First-order consumption of **3h** at 0 °C based on increase of insertion product. B = $\ln[([B]_\infty-[B])/([B]_\infty-[B]_0)]$.

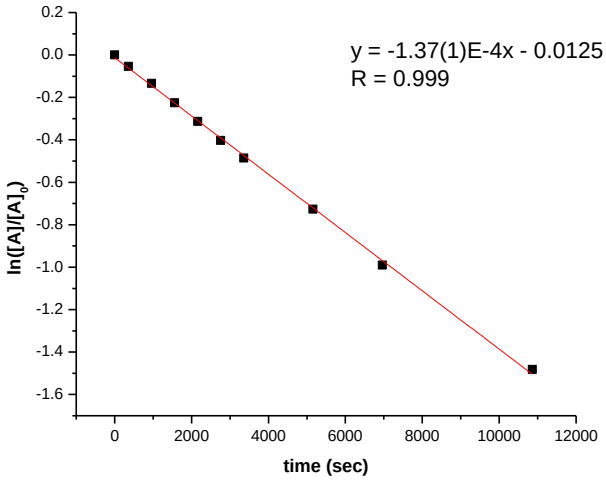

$[A]/[A]_0$	$\ln([A]/[A]_0)$	Time(s)
1	0	0
0.946778	-0.05469	360
0.86224	-0.14822	960
0.78397	-0.24338	1560
0.7057	-0.34857	2160
0.64308	-0.44149	2760
0.58986	-0.52787	3360
0.48341	-0.72689	5160
0.3713	-0.99074	6960
0.2273	-1.48148	10860

Figure 7.35. First-order consumption of [{(2,6-^{i}Pr$_2$-C$_6$H$_3$)N=CAnCAn=N(2,6-^{i}Pr$_2$-C$_6$H$_3$)}PdCMe$_2$(OSiPh$_3$)][SbF$_6$][SbF$_6$] at 20 °C.

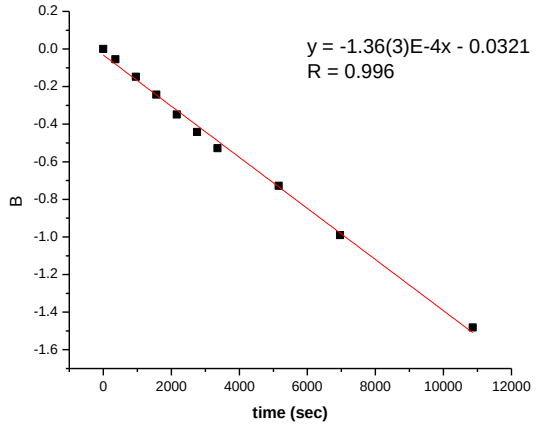

$[B]_\infty$-[B]/ $[B]_\infty$-$[B]_0$	ln(($[B]_\infty$-[B])/ ($[B]_\infty$-$[B]_0$)]	Time(s)
1	0	0
0.9471	-0.05435	360
0.875	-0.13353	960
0.7981	-0.22552	1560
0.7308	-0.31362	2160
0.6683	-0.40302	2760
0.6154	-0.48548	3360
0.5096	-0.67413	5160
0.4086	-0.89502	6960
0.2933	-1.22656	10860

Figure 7.36. First-order consumption of [{(2,6-$^{i}Pr_2$-C_6H_3)N=CAnCAn=N(2,6-$^{i}Pr_2$-C_6H_3)}PdCMe$_2$(OSiPh$_3$)][SbF_6][SbF_6] at 20 °C based on increase of the allyl product. B = ln(($[B]_\infty$-[B])/($[B]_\infty$-$[B]_0$)].

7.11 Insertion of [{(4-Me-C_6H_5)N=CMeCMe=N(4-Me-C_6H_5)}PdMe(CH_2=CHOSiPh_3)][SbF_6] (3i).

The first-order rate constant for the consumption of **3i** measured by the disappearance of the H_{trans} ^{1}H NMR resonance is $k_{insert,\ \mathbf{3i}}$ = 1.76(4) × 10^{-4} s^{-1} at 0 °C.

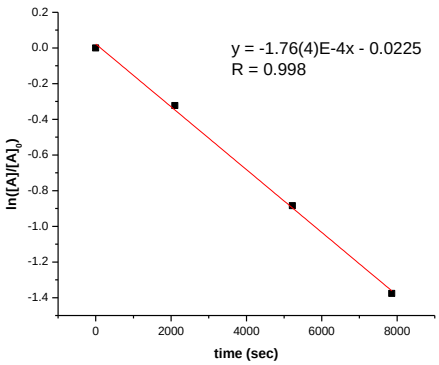

$[A]/[A]_0$	ln($[A]/[A]_0$)	Time(s)
1	0	0
0.724343	-0.32249	2100
0.413114	-0.88403	5220
0.252423	-1.37665	7860

Figure 7.37. First-order consumption of **3i** at 0 °C.

8. X-Ray Crystallography.

8.1 [(α-diimine)Pd(η^3-C_3H_5)][$B(C_6F_5)_4$](6[$B(C_6F_5)_4$]). Single crystals of **6[$B(C_6F_5)_4$]** were obtained by slow diffusion of hexanes into the concentrated CH_2Cl_2 solution at room temperature. The molecular structure of **6[$B(C_6F_5)_4$]** was determined by X-ray diffraction and is shown in Figure 8.1 and the crystallographic data are summarized in Table 8.1. Data were collected on a Bruker Smart Apex diffractometer using Mo Kα radiation (0.71073 Å). Direct methods were used to locate The Pd atom as well as many C atoms from the E-map. Repeated difference Fourier maps allowed recognition of all expected non-H atoms. Following anisotropic refinement of all non-hydrogen atoms, ideal H atom positions were calculated. Final refinement was anisotropic for Pd, N, B F and C and isotropic-riding for H atoms. Positional disorder was apparent for C29, C30 and C31. C30 was spit into two atoms, C30A and C30B each with occupancies of 0.5. C30A and C30B were refined as isotropic atoms while the displacement parameters for C29 and C31 showed elongation due to the positional disorder. No other anomalous bond lengths or thermal parameters were noted. All ORTEP diagrams have been drawn with 50% probability ellipsoids.

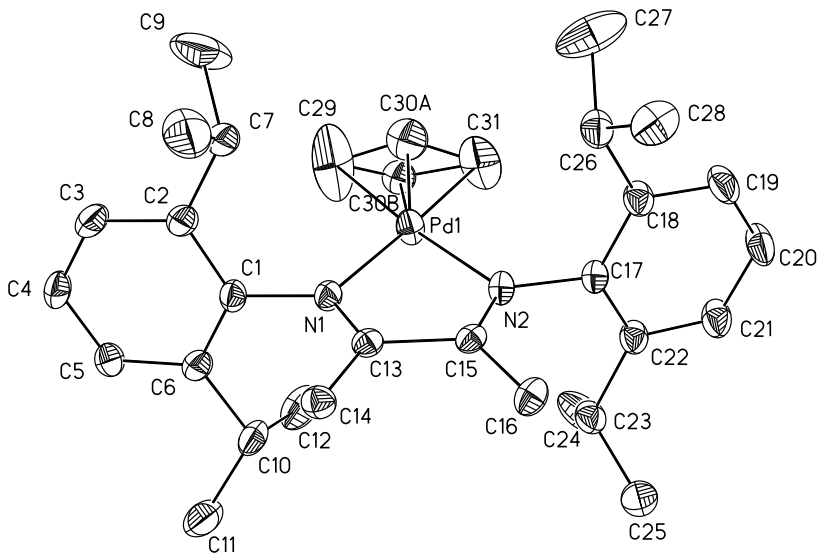

Figure 8.1. Molecular structure of **6[B(C_6F_5)$_4$]**. Hydrogen atoms and the anion are omitted for clarity.

Table 8.1. Summary of X-Ray Diffraction Data for **6[B(C_6F_5)$_4$]**.

formula	$C_{31}H_{45}N_2Pd + C_{24}BF_{20}$
formula weight	1226.10 (including solvent)
crystal system	Monoclinic
space group	$P2_1/c$
a (Å)	15.922(3)
b (Å)	20.076(4)
c (Å)	19.176(3)
β (^{o})	121.573(10)
V (Å^3)	5222.3(16)
Z	4
T (K)	100
crystal color, habit	yellow, fragment
GOF on F^2	1.018
R indices [$I > 2\sigma(I)$]^a	R1 = 0.0435, wR2 = 0.0972
R indices (all data)^a	R1 = 0.0664, wR2 = 0.1042

^{a}R1 = $\Sigma||F_o| - |F_c||/\Sigma|F_o|$; wR2 = $[\Sigma[w(F_o^2 - F_c^2)^2]/ \Sigma[w(F_o^2)^2]]^{1/2}$, where $w = q[\sigma^2(F_o^2) + (aP)^2 + bP]^{-1}$

9. DFT Calculations.

9.1 DFT studies of the structure of 4a and 5a. DFT studies at the B3LYP level using the 6-31G* (for C, H, N, O) and Lanl2DZ (for Pd) basis sets provide additional evidence for the O-chelated structures in **4a** and **5a**.[10] The optimized structures of **4a** and **5a** are shown in Figure 9.1. The calculated Pd-O distances are 2.19 Å (**4a**) and 2.15 Å (**5a**), which are typical for Pd(II)-OR_2 distances.[11] DFT studies show that the energy difference between **4a** and **5a** is

small ($E_{\mathbf{4a}} - E_{\mathbf{5a}}$ = 0.2 ± 1.0 kcal/mol), which is consistent with the fact that both isomers are observed.

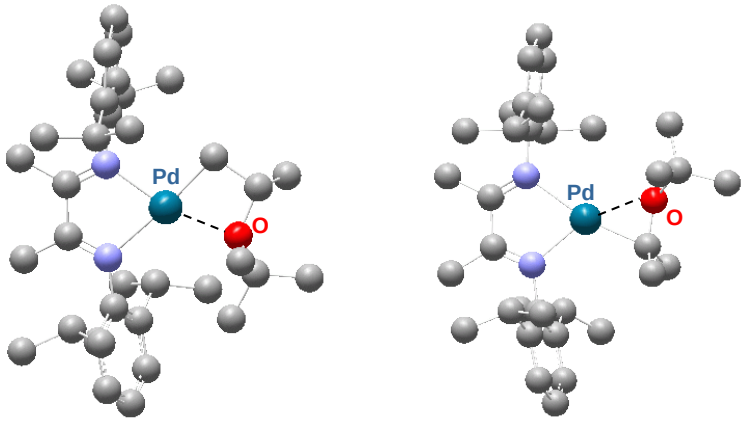

4a cation **5a** cation

Figure 9.1. Optimized structures of the **4a** and **5a** cations. Hydrogens are omitted.

9.2 DFT studies of the structure of 4c and 5c.

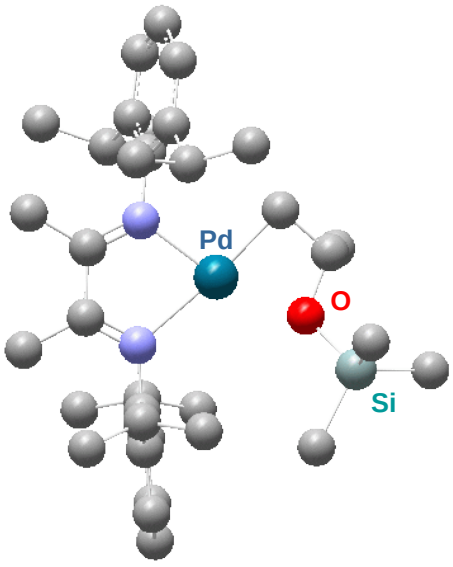

Figure 9.2. Optimized structure of the (α-diimine)Pd{$CH_2CH(OSiMe_3)CH_3$})$^+$ (**4c**) cation.

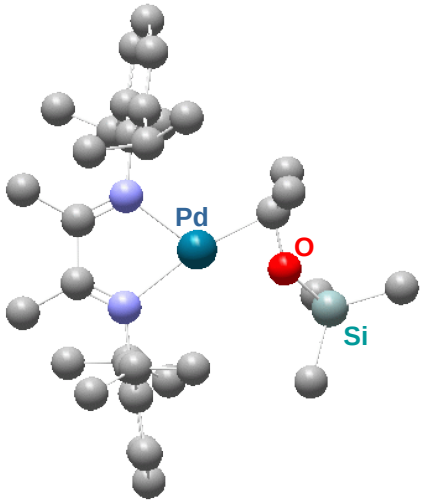

Figure 9.3. Optimized structure of the (α-diimine)Pd{$CMe_2(OSiMe_3)$})$^+$ (**5c**) cation.

10. NMR Spectra for Cationic Polymers and Kinetics Studies.

10. 1 Spectra of -[$CH_2CH(O^tBu)]_n$- homopolymer.

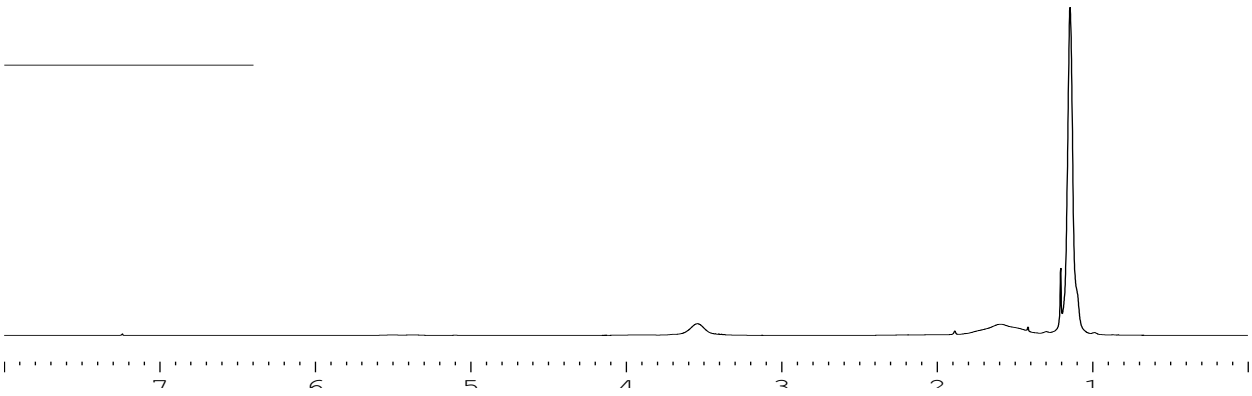

Figure 10-1a. ^{1}H NMR of -[$CH_2CH(O^tBu)]_n$- homopolymer ($CDCl_3$): full spectrum.

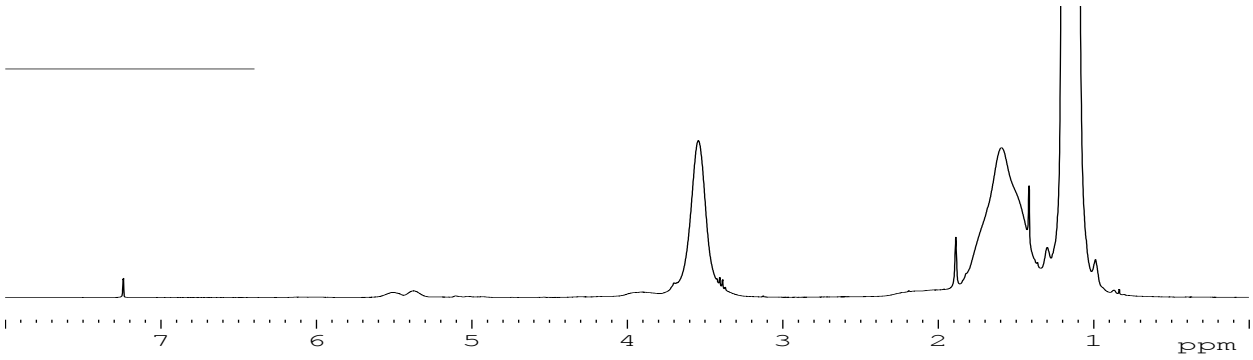

Figure 10-1b. ^{1}H NMR of -[$CH_2CH(O^tBu)]_n$- homopolymer ($CDCl_3$): vertical expansion.

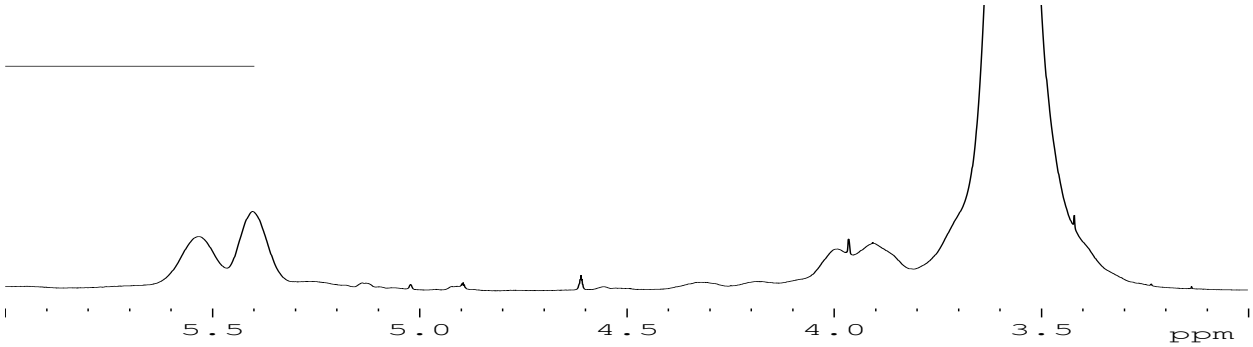

Figure 10-1c. ^{1}H NMR of -[$CH_2CH(O^tBu)]_n$- homopolymer ($CDCl_3$): expansion of the δ 6.0-3.0 region.

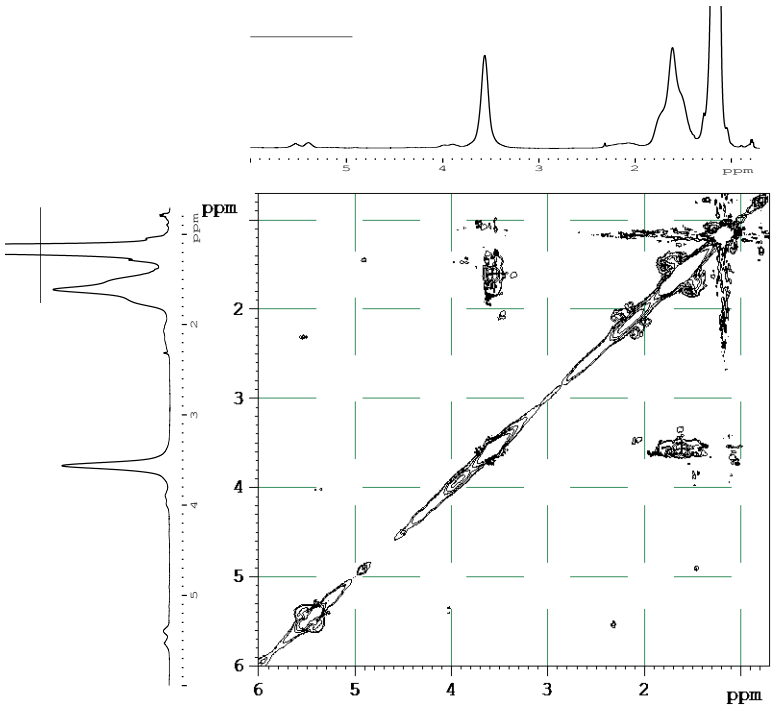

Figure 10-1d. COSY NMR of -[$CH_2CH(O^tBu)]_n$- homopolymer ($CDCl_3$): expansion of the δ 6.0-0.7; 6.0-0.7 region.

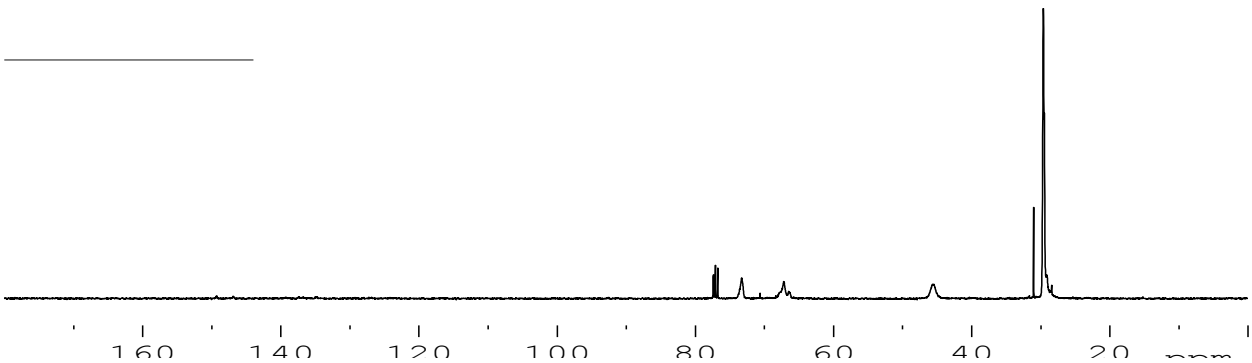

Figure 10-1e. ^{13}C NMR of -[$CH_2CH(O^tBu)]_n$- homopolymer ($CDCl_3$): full spectrum.

Figure 10-1f. ^{13}C NMR of -$[CH_2CH(O^tBu)]_n$- homopolymer ($CDCl_3$): expansion of the δ 75-65 region. The sharp signal at δ 70.6 is from HO^tBu.

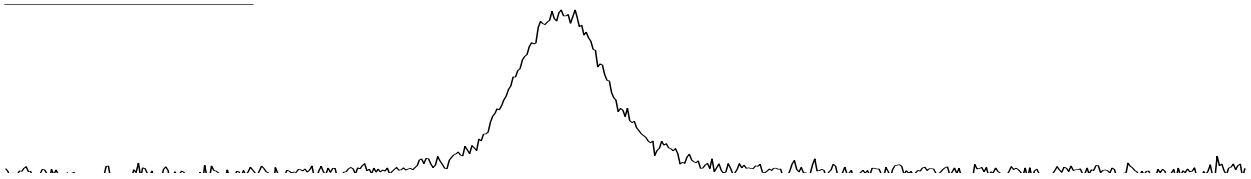

Figure 10-1g. ^{13}C NMR of -$[CH_2CH(O^tBu)]_n$- homopolymer ($CDCl_3$): expansion of the δ 50-40 region. The sharp signal at δ 31.0 is from HO^tBu.

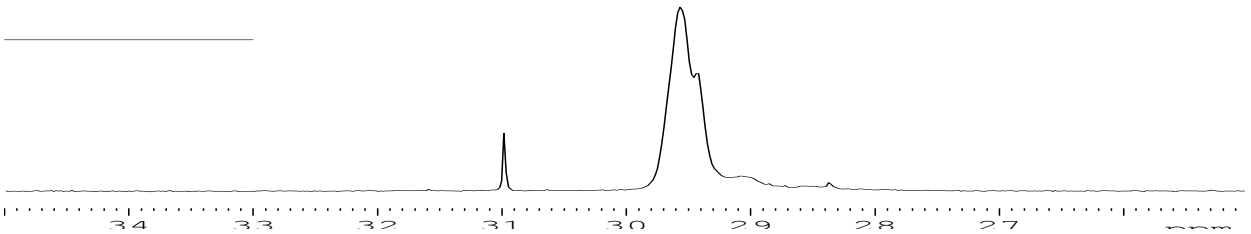

Figure 10-1h. ^{13}C NMR of -$[CH_2CH(O^tBu)]_n$- homopolymer ($CDCl_3$): expansion of the δ 35-25 region.

10.2 Spectra of -$[CH_2CH(OSiMe_3)]_n$- homopolymer and attempted polymerization of CH_2=CHOSiPh_3 and CH_2=CHOPh.

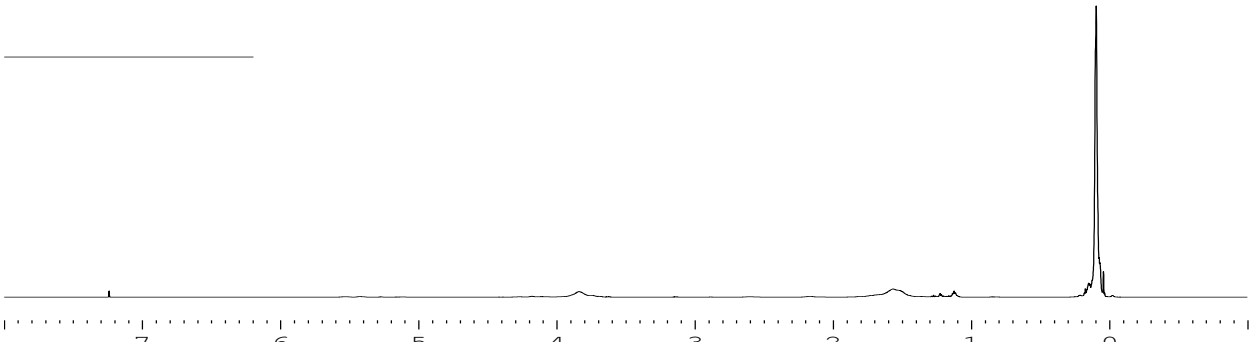

Figure 10-2a. ^1H NMR of -$[CH_2CH(OSiMe_3)]_n$- homopolymer ($CDCl_3$): full spectrum.

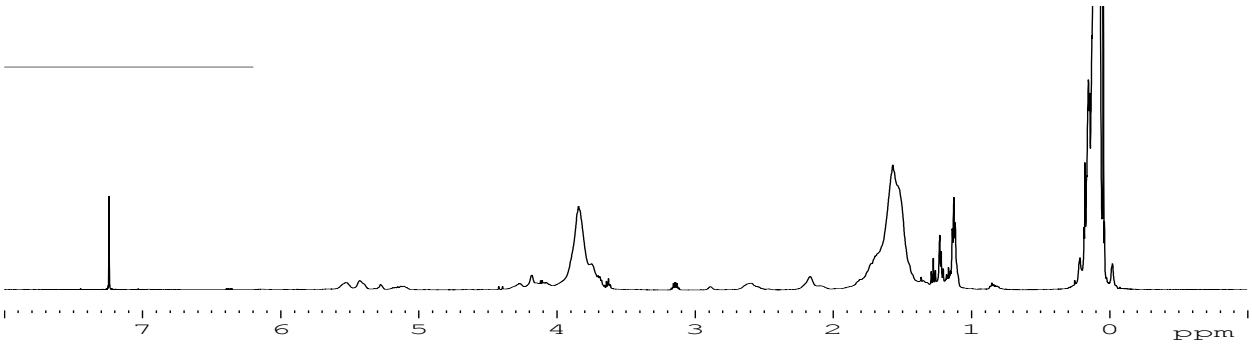

Figure 10-2b. ^{1}H NMR of -[$CH_2CH(OSiMe_3)]_n$- homopolymer ($CDCl_3$): vertical expansion.

Figure 10-2c. ^{1}H NMR of -[$CH_2CH(OSiMe_3)]_n$- homopolymer ($CDCl_3$): expansion of the δ 4.3-3.4 region.

Figure 10-2d. ^{1}H NMR of -[$CH_2CH(OSiMe_3)]_n$- homopolymer ($CDCl_3$): expansion of the δ 1.8-0.5 region.

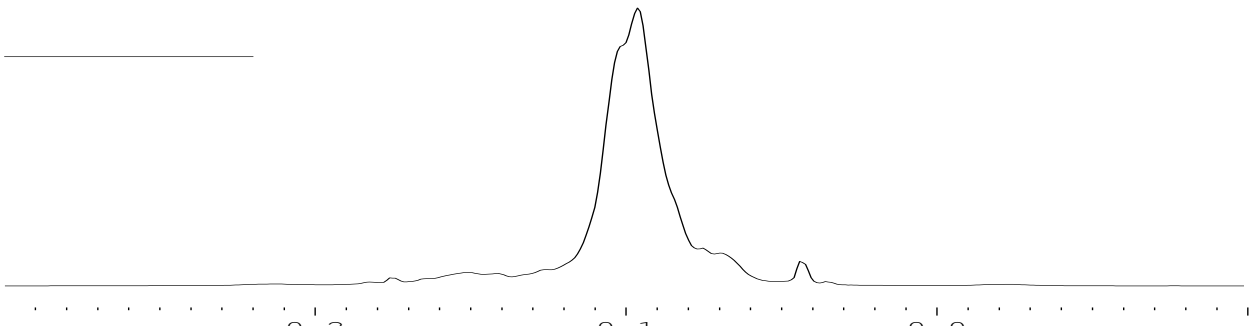

Figure 10-2e. ^{1}H NMR of -$[CH_2CH(OSiMe_3)]_n$- homopolymer ($CDCl_3$): expansion of the δ 0.3 - -0.1 region.

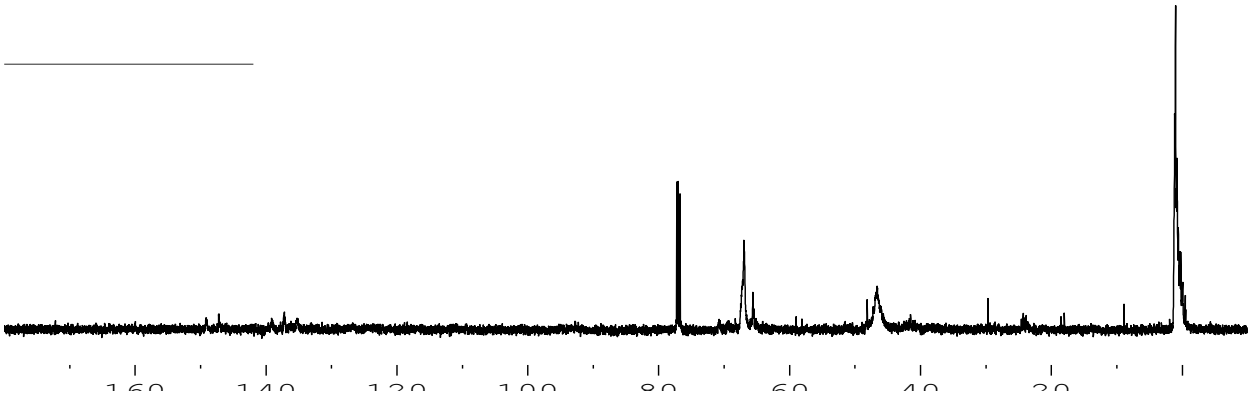

Figure 10-2f. ^{13}C NMR of -$[CH_2CH(OSiMe_3)]_n$- homopolymer ($CDCl_3$): full spectrum.

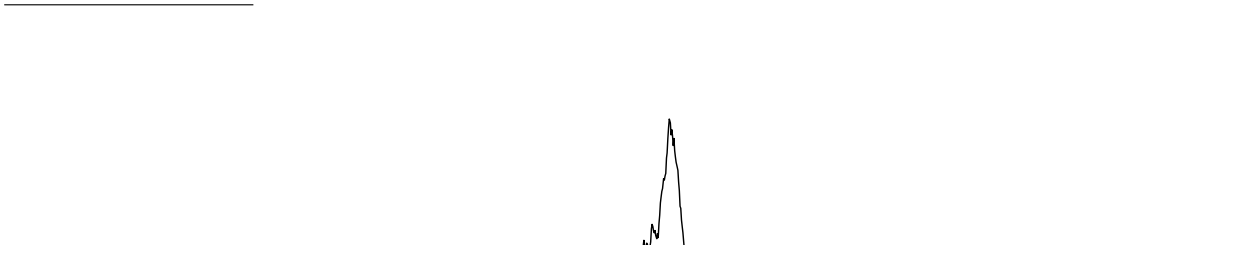

Figure 10-2g. ^{13}C NMR of -$[CH_2CH(OSiMe_3)]_n$- ($CDCl_3$): expansion of the δ 75-60 region.

Figure 10-2h. ^{13}C NMR of -[$CH_2CH(OSiMe_3)]_n$- homopolymer ($CDCl_3$): expansion of the δ 50-40 region.

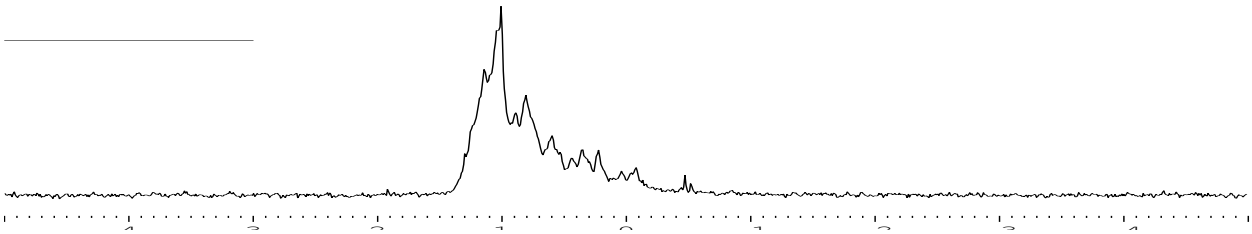

Figure 10-2i. ^{13}C NMR of -[$CH_2CH(OSiMe_3)]_n$- homopolymer ($CDCl_3$): expansion of the δ 5 - -5 region.

10.3 Selected ^{1}H NMR spectra for CH_2=CHO^{t}Bu case:

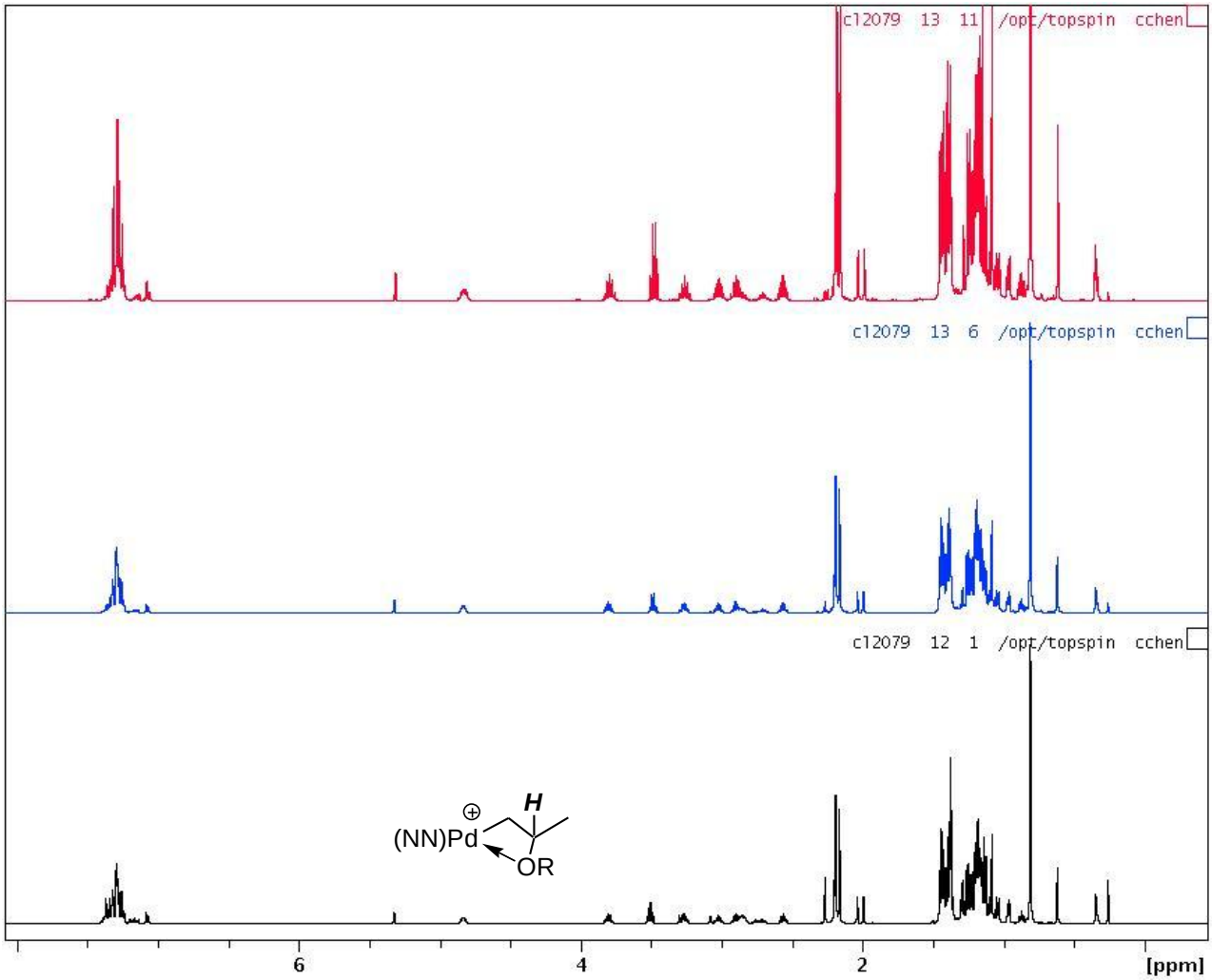

Figure 10-3a. Selected spectra for the insertion of [(α-diimine)PdMe(CH_2=CHO^{t}Bu)][B(C_6F_5)$_4$] (**3a**) to produce [(α-diimine)Pd{CH_2CHMe(O^{t}Bu)}][B(C_6F_5)$_4$] (**4b**) and [(α-diimine)Pd{CMe_2(O^{t}Bu)}][B(C_6F_5)$_4$] (**5b**) at 0 °C: full spectra. The bottom spectrum is the is the starting point of the reaction, the middle spectrum corresponds to ca. 50% completion and the top spectrum corresponds to ca. 90% completion. For kinetics analysis see Figure 5.1 and Figure 5.2.

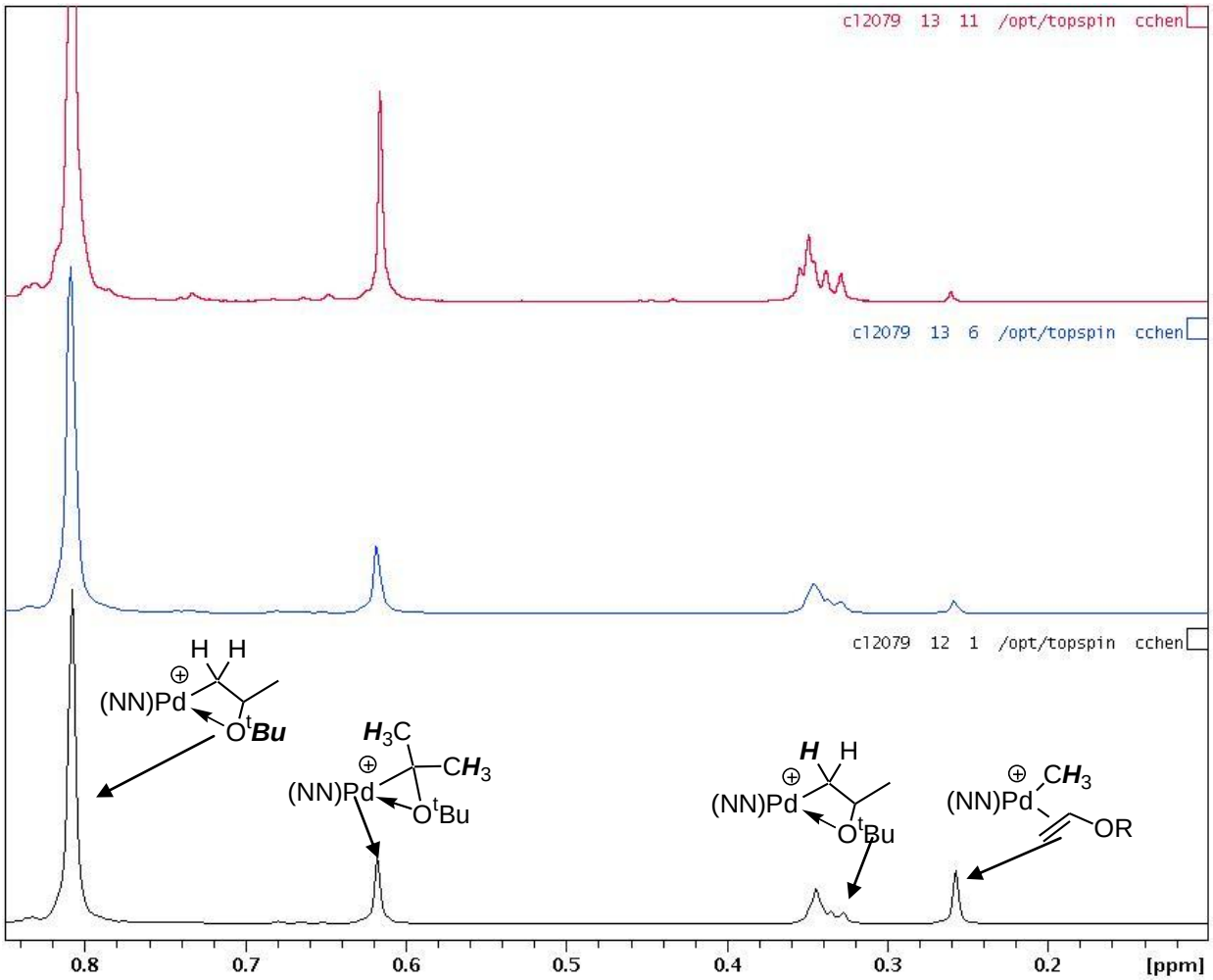

Figure 10-3b. Selected spectra for the first-order consumption of [(α-diimine)PdMe(CH_2=CHO^{t}Bu)][$B(C_6F_5)_4$] (**3a**) at 0 °C: expansion of δ 0.8-0.1 . The peak at 0.35 is [{(α-diimine)PdMe}$_2$(μ-Cl)][$B(C_6F_5)_4$]. The bottom spectrum is the is the starting point of the reaction, the middle spectrum corresponds to ca. 50% completion and the top spectrum corresponds to ca. 90% completion. For kinetics analysis see Figure 5.1 and Figure 5.2.

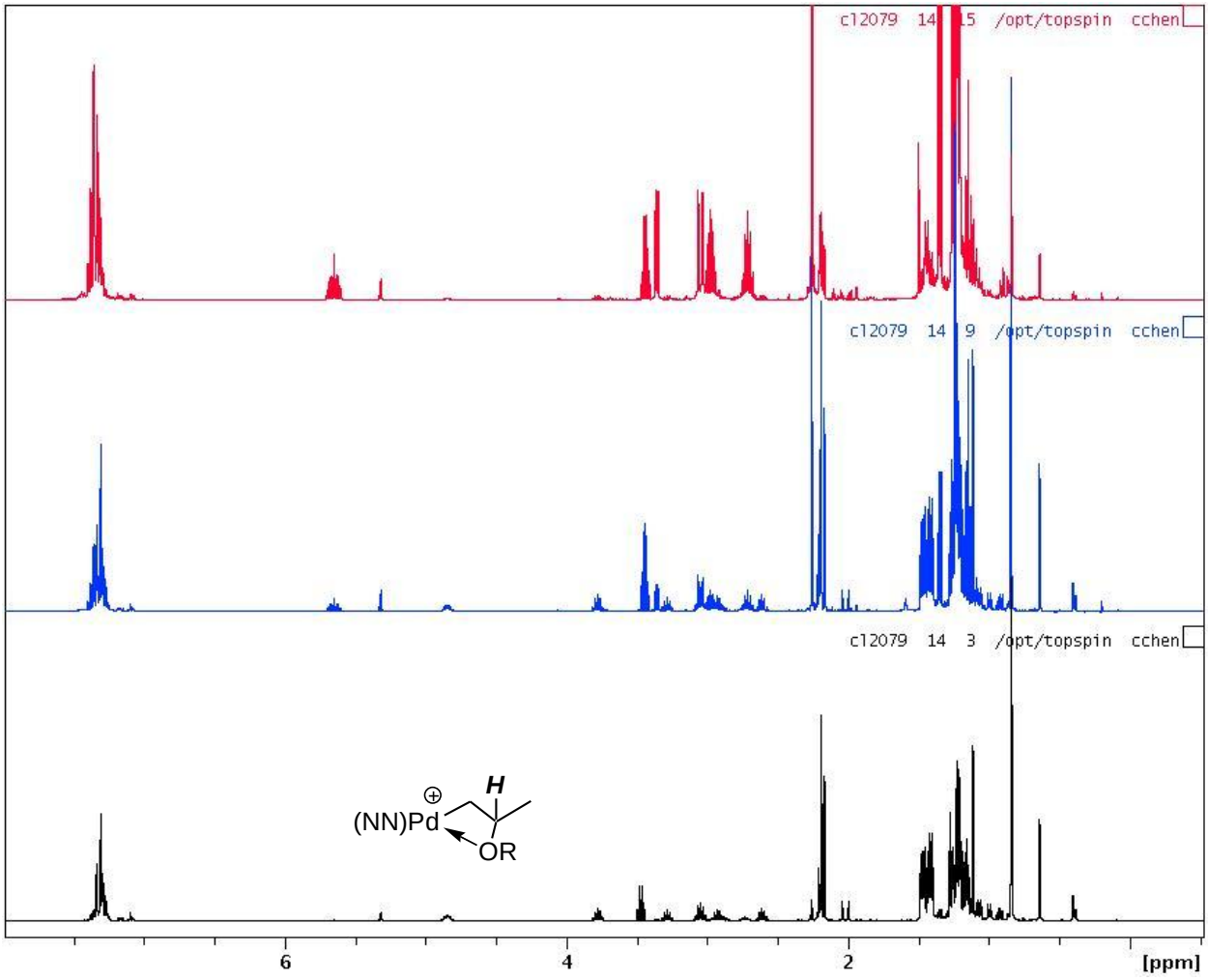

Figure 10-3c. Selected spectra for the first-order consumption of [(α-diimine)Pd{$CH_2CHMe(O^tBu)$}][$B(C_6F_5)_4$] (**4b**) and [(α-diimine)Pd{$CMe_2(O^tBu)$}][$B(C_6F_5)_4$] (**5b**) at 20 °C: full spectra. The bottom spectrum is the is the starting point of the reaction, the middle spectrum corresponds to ca. 50% completion and the top spectrum corresponds to ca. 90% completion. For kinetics analysis see Figure 5.5 and Figure 5.6.

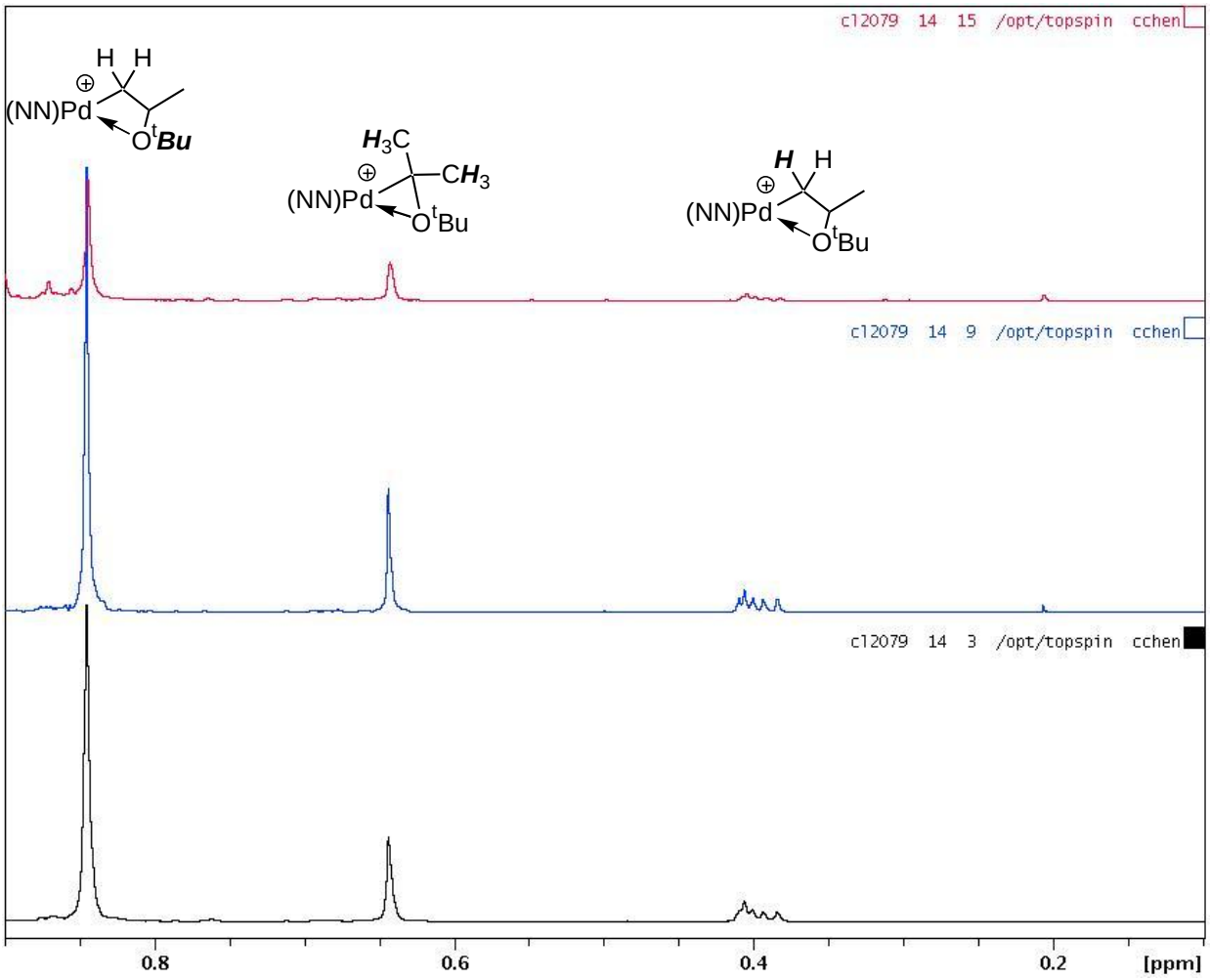

Figure 10-3d. Selected spectra for the first-order consumption of [(α-diimine)Pd{$CH_2CHMe(O^tBu)$}][$B(C_6F_5)_4$] (**4b**) and [(α-diimine)Pd{$CMe_2(O^tBu)$}][$B(C_6F_5)_4$] (**5b**) at 20 °C: expansion of δ 0.8-0.1. The peak at ca. 0.4 is [{(α-diimine)PdMe}$_2$(μ-Cl)][$B(C_6F_5)_4$]. The bottom spectrum is the is the starting point of the reaction, the middle spectrum corresponds to ca. 50% completion and the top spectrum corresponds to ca. 90% completion. For kinetics analysis see Figure 5.5 and Figure 5.6.

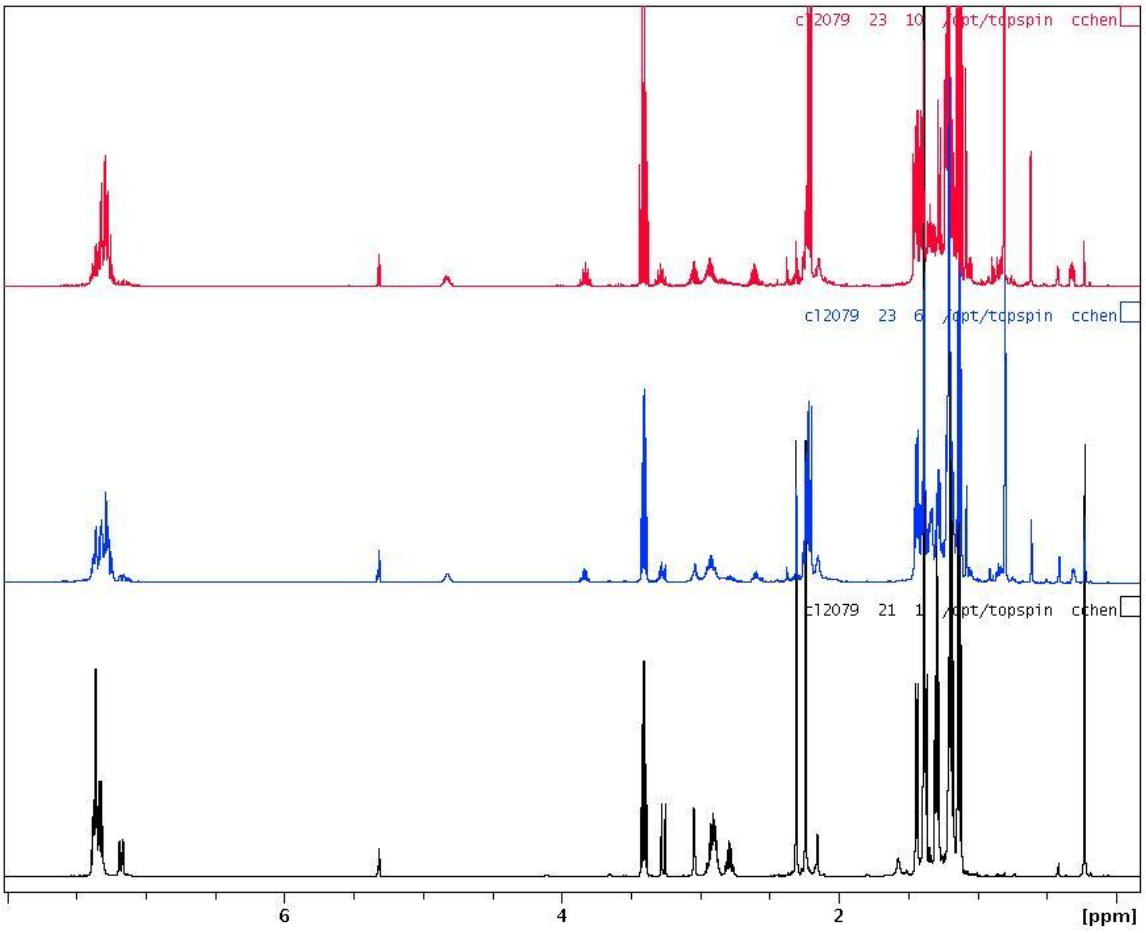

Figure 10-3e. Selected spectra for the first-order consumption of [(α-diimine)PdMe(CH_2=CHO^{t}Bu)][SbF_6] (**3a**) at 0 °C: full spectra. The bottom spectrum is the is the starting point of the reaction, the middle spectrum corresponds to ca. 50% completion and the top spectrum corresponds to ca. 90% completion. For kinetics analysis see Figure 7.1 and Figure 7.2.

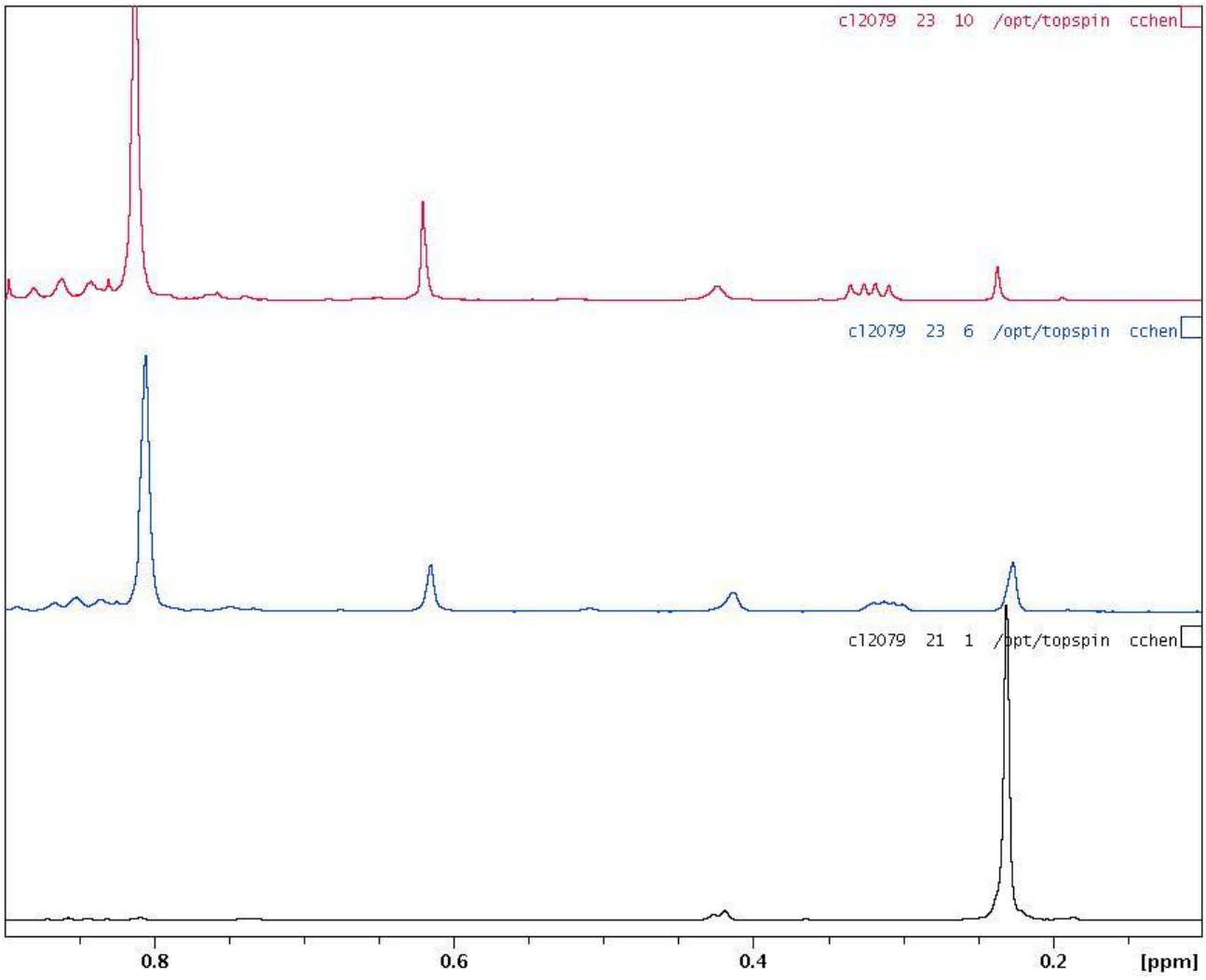

Figure 10-3f. Selected spectra for the first-order consumption of [(α-diimine)PdMe(CH_2=CHO^{t}Bu)][SbF_6] (**3a**) at 0 °C: expansion of δ 0.9-0.1. The bottom spectrum is the is the starting point of the reaction, the middle spectrum corresponds to ca. 50% completion and the top spectrum corresponds to ca. 90% completion. For kinetics analysis see Figure 7.1 and Figure 7.2.

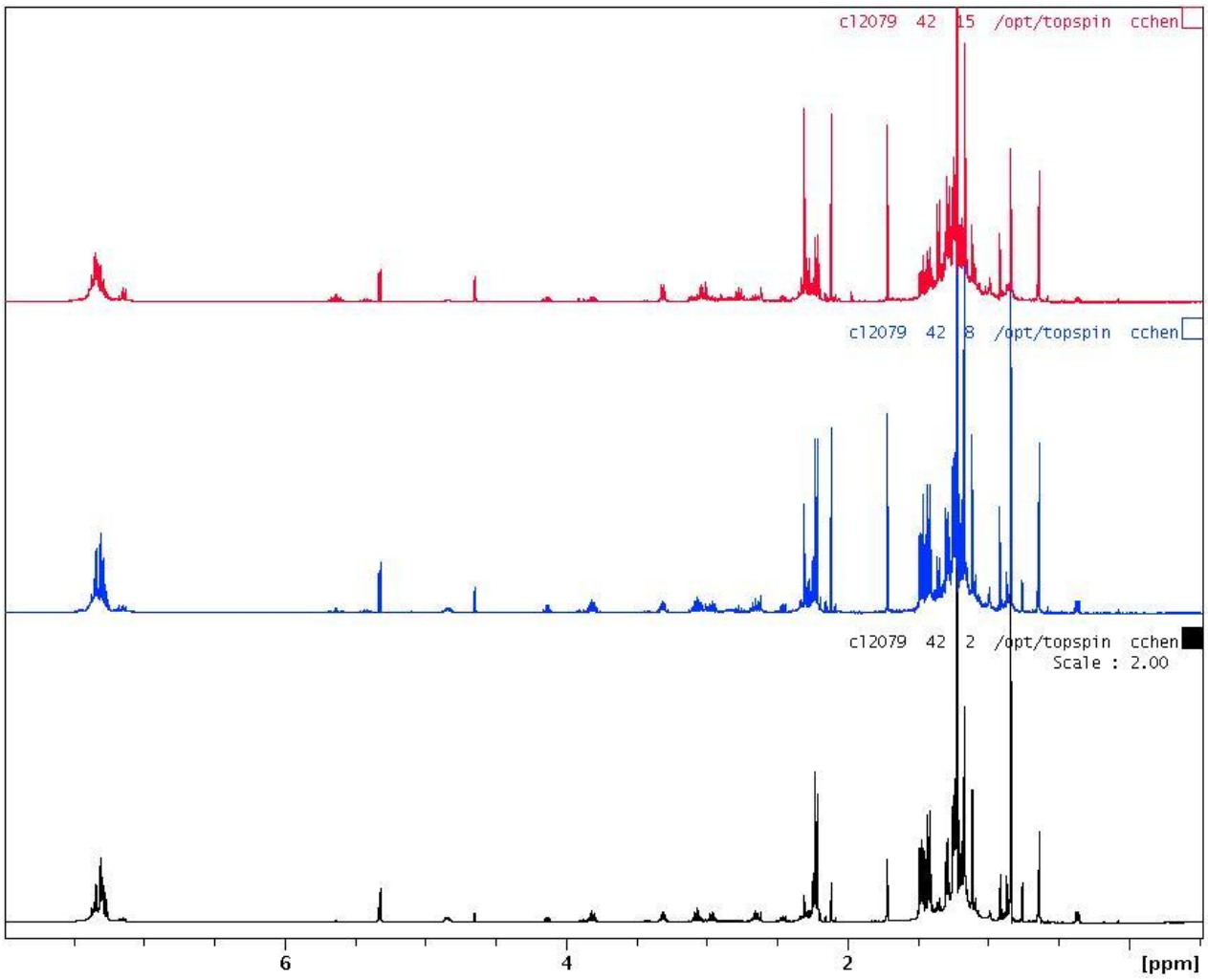

Figure 10-3g. Selected spectra for the first-order consumption of [(α-diimine)Pd{$CH_2CHMe(O^tBu)$}][SbF_6] (**4a**) and [(α-diimine)Pd{$CMe_2(O^tBu)$}][SbF_6] (**5a**) at 20 °C: full spectra. The bottom spectrum is the is the starting point of the reaction, the middle spectrum corresponds to ca. 50% completion and the top spectrum corresponds to ca. 90% completion. For kinetics analysis see Figure 7.5 and Figure 7.6.

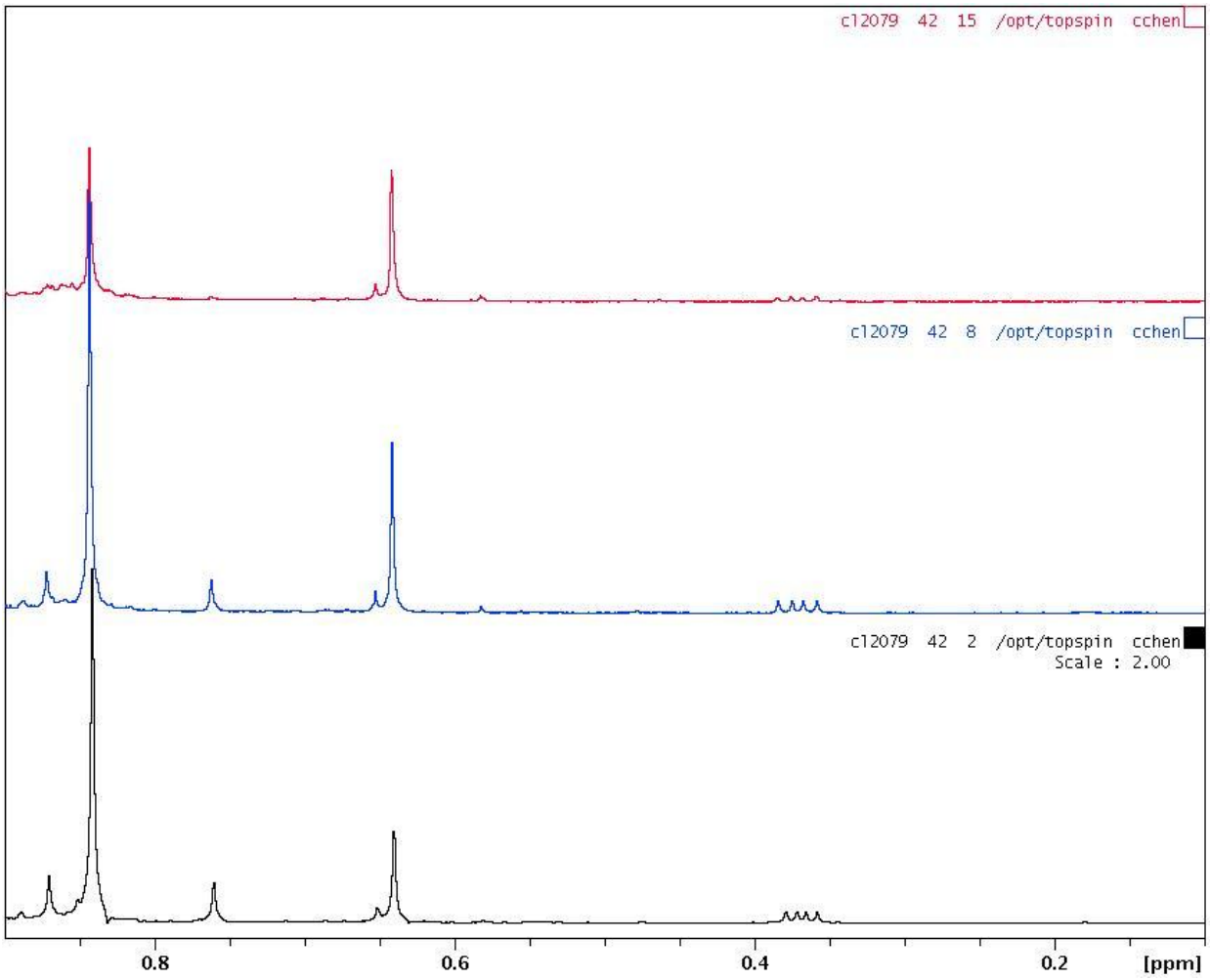

Figure 10-3h. Selected spectra for the first-order consumption of [(α-diimine)Pd{$CH_2CHMe(O^tBu)$}][SbF_6] (**4a**) and [(α-diimine)Pd{$CMe_2(O^tBu)$}][SbF_6] (**5a**) at 20 °C: expansion of δ 0.9-0.1. The bottom spectrum is the is the starting point of the reaction, the middle spectrum corresponds to ca. 50% completion and the top spectrum corresponds to ca. 90% completion. For kinetics analysis see Figure 7.5 and Figure 7.6.

10.4 Selected ^{1}H NMR spectra for CH_2=CHOEt case:

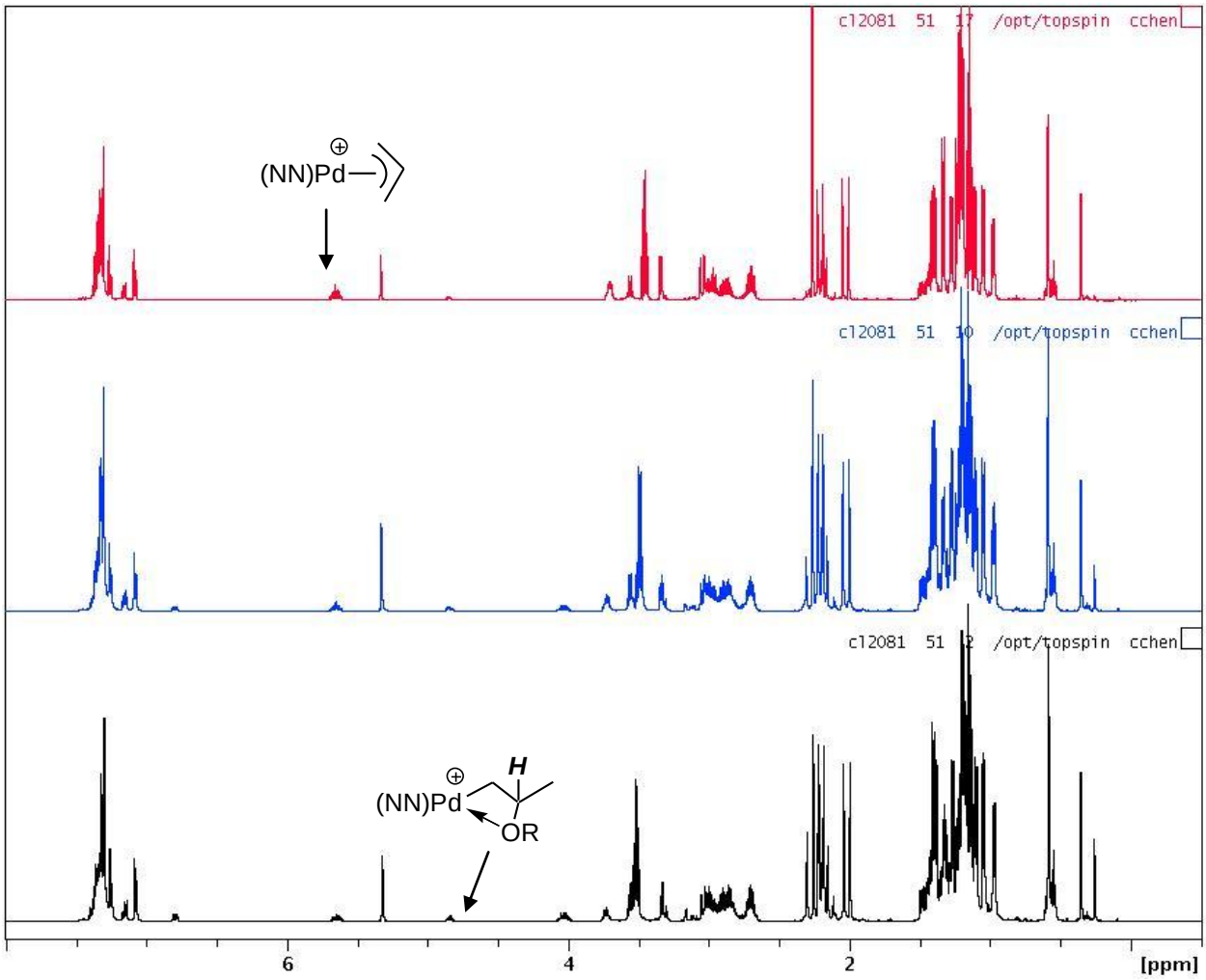

Figure 10-4a. Selected spectra for the first-order consumption of [(α-diimine)PdMe(CH_2=CHOEt)][$B(C_6F_5)_4$] (**3b**) at 0 °C: full spectra. The bottom spectrum is the is the starting point of the reaction, the middle spectrum corresponds to ca. 50% completion and the top spectrum corresponds to ca. 90% completion. For kinetics analysis see Figure 6.1 and Figure 6.2.

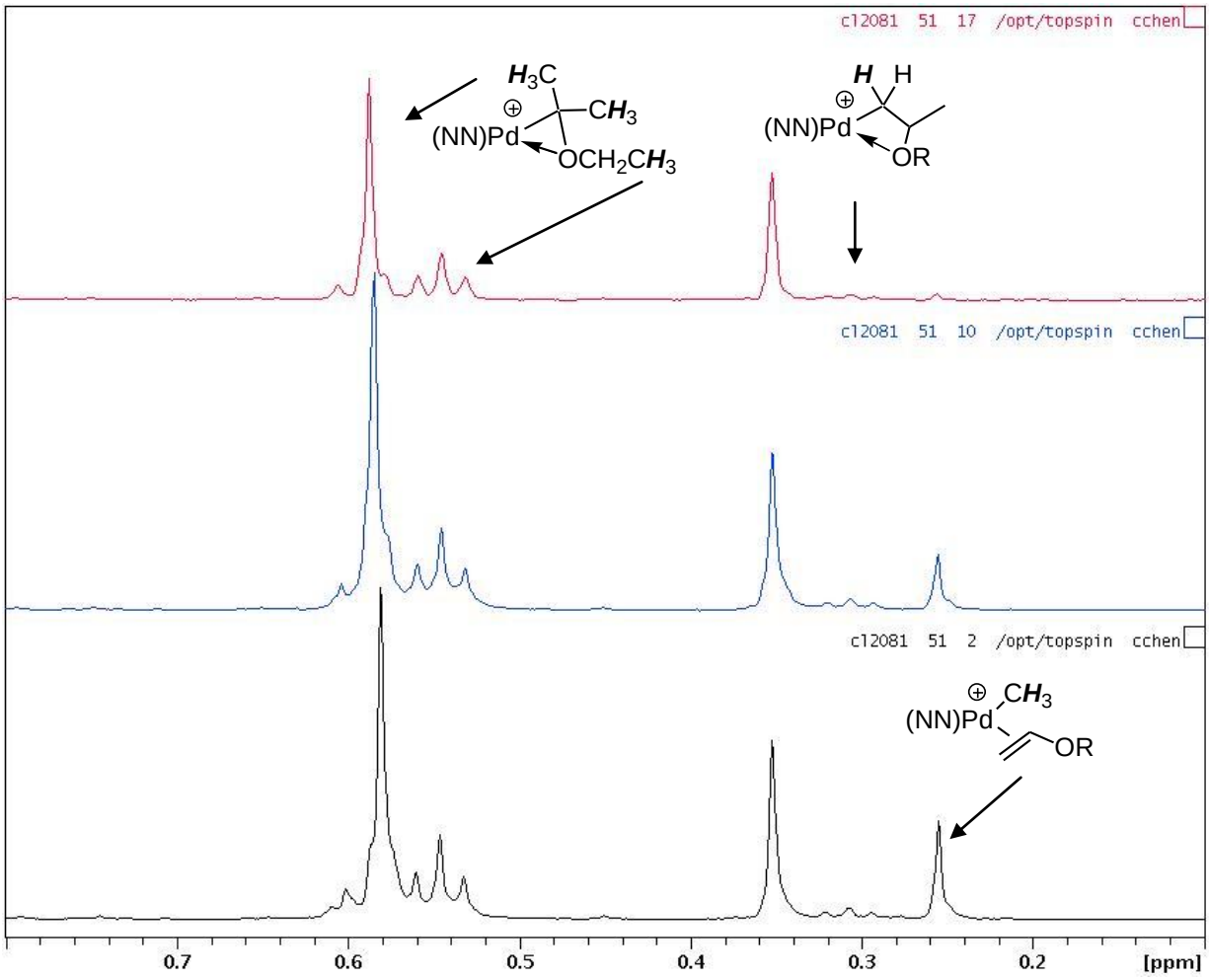

Figure 10-4b. Selected spectra for the first-order consumption of [(α-diimine)PdMe(CH_2=CHOEt)][$B(C_6F_5)_4$] (**3b**) at 0 °C: expansion of δ 0.8-0.1. The peak at 0.35 is [{(α-diimine)PdMe}$_2$(μ-Cl)][$B(C_6F_5)_4$]. The bottom spectrum is the is the starting point of the reaction, the middle spectrum corresponds to ca. 50% completion and the top spectrum corresponds to ca. 90% completion. For kinetics analysis see Figure 6.1 and Figure 6.2.

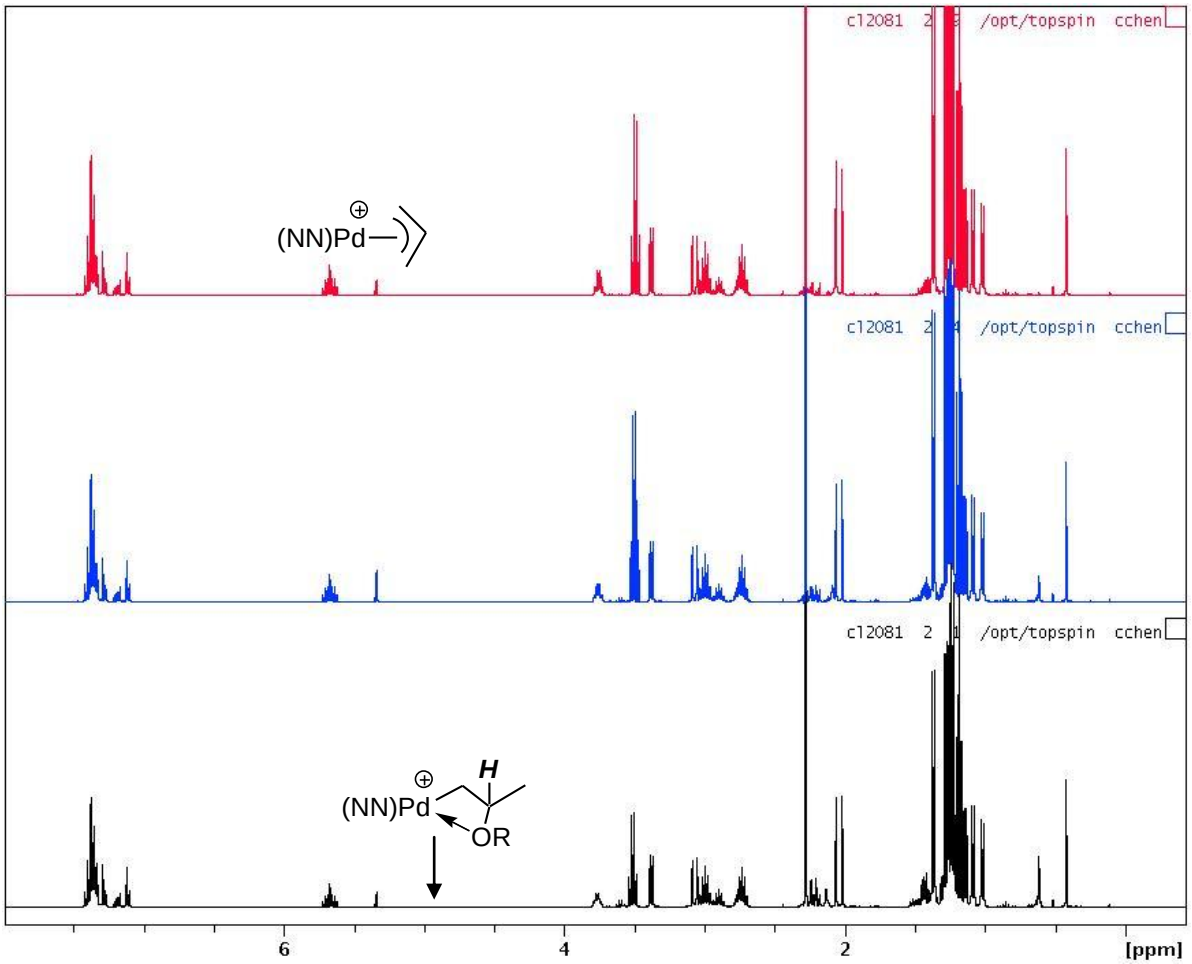

Figure 10-4c. Selected spectra for the first-order consumption of [(α-diimine)Pd{$CH_2CHMe(OEt)$}][$B(C_6F_5)_4$] (**4b**) and [(α-diimine)Pd{$CMe_2(OEt)$}][$B(C_6F_5)_4$] (**5b**) at 20 °C: full spectra. The bottom spectrum is the is the starting point of the reaction, the middle spectrum corresponds to ca. 50% completion and the top spectrum corresponds to ca. 90% completion. For kinetics analysis see Figure 6.5 and Figure 6.6.

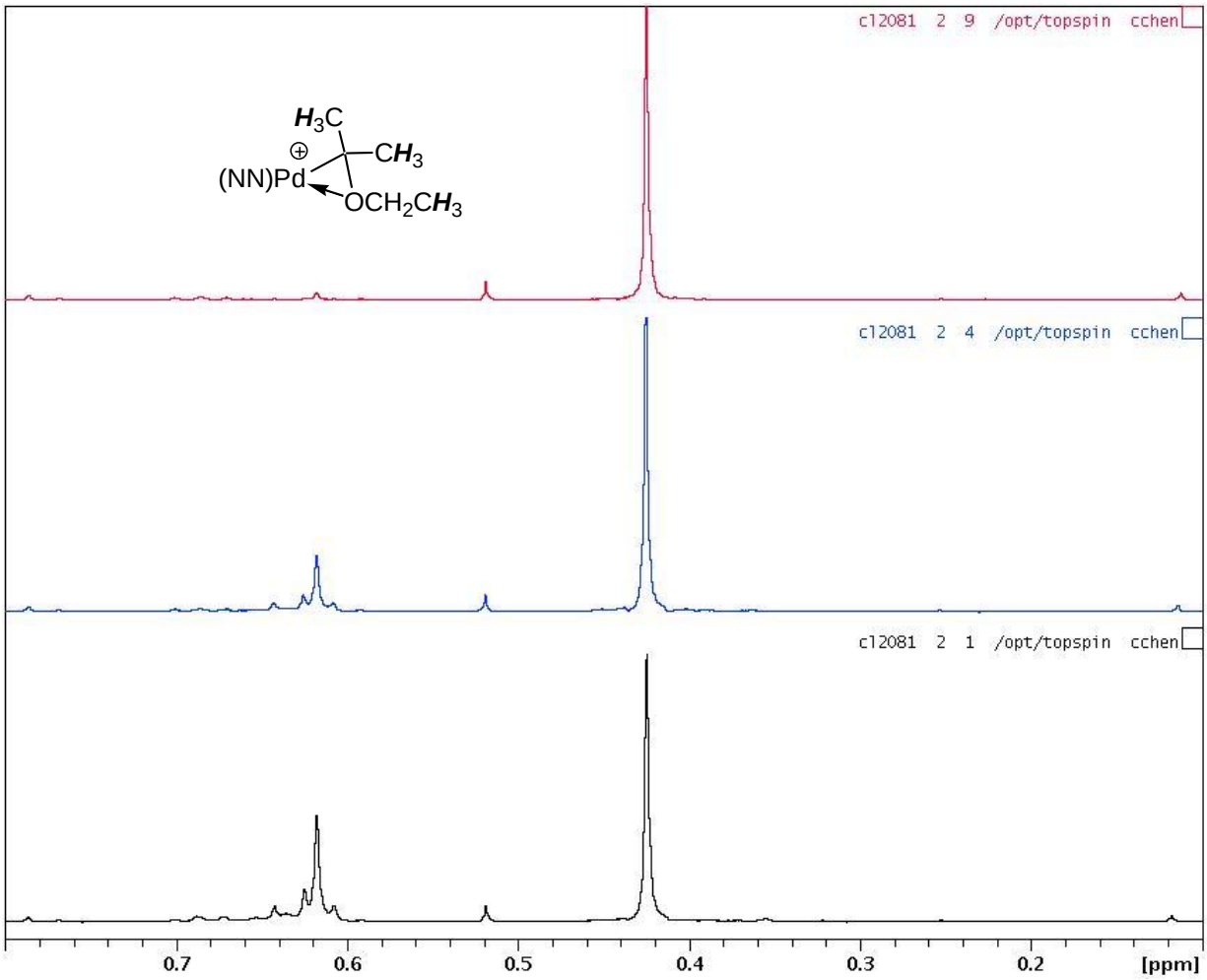

Figure 10-4d. Selected spectra for the first-order consumption of [(α-diimine)Pd{$CH_2CHMe(OEt)$}][$B(C_6F_5)_4$] (**4b**) and [(α-diimine)Pd{$CMe_2(OEt)$}][$B(C_6F_5)_4$] (**5b**) at 20 °C: expansion of δ 0.8-0.1. The peak at 0.42 is [{(α-diimine)PdMe}$_2$(μ-Cl)][$B(C_6F_5)_4$]. The bottom spectrum is the is the starting point of the reaction, the middle spectrum corresponds to ca. 50% completion and the top spectrum corresponds to ca. 90% completion. For kinetics analysis see Figure 6.5 and Figure 6.6.

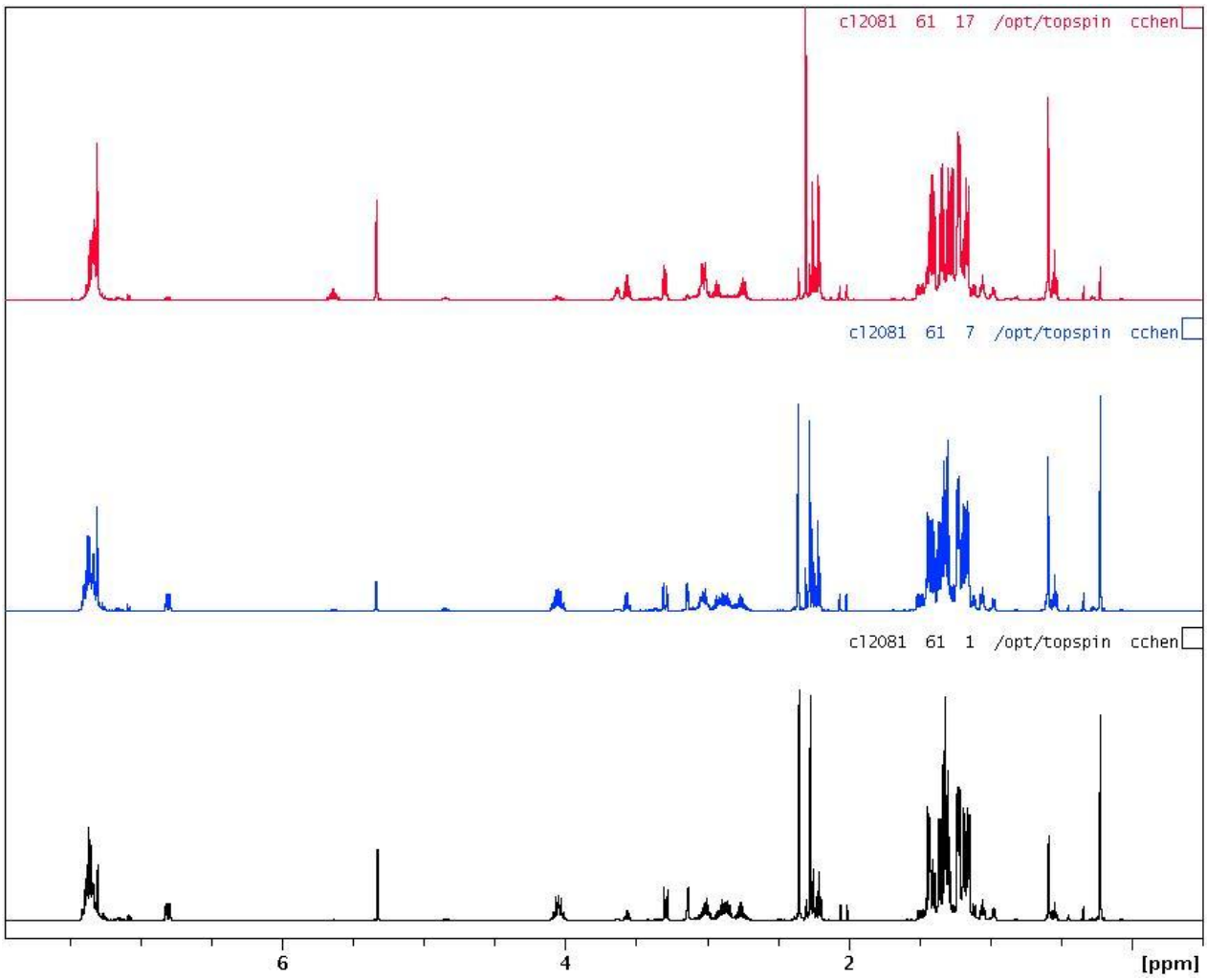

Figure 10-4e. Selected spectra for the first-order consumption of [(α-diimine)PdMe(CH_2=CHOEt)][SbF_6] (**3b**) at 0 °C: full spectra. The bottom spectrum is the is the starting point of the reaction, the middle spectrum corresponds to ca. 50% completion and the top spectrum corresponds to ca. 90% completion. For kinetics analysis see Figure 7.7 and Figure 7.8.

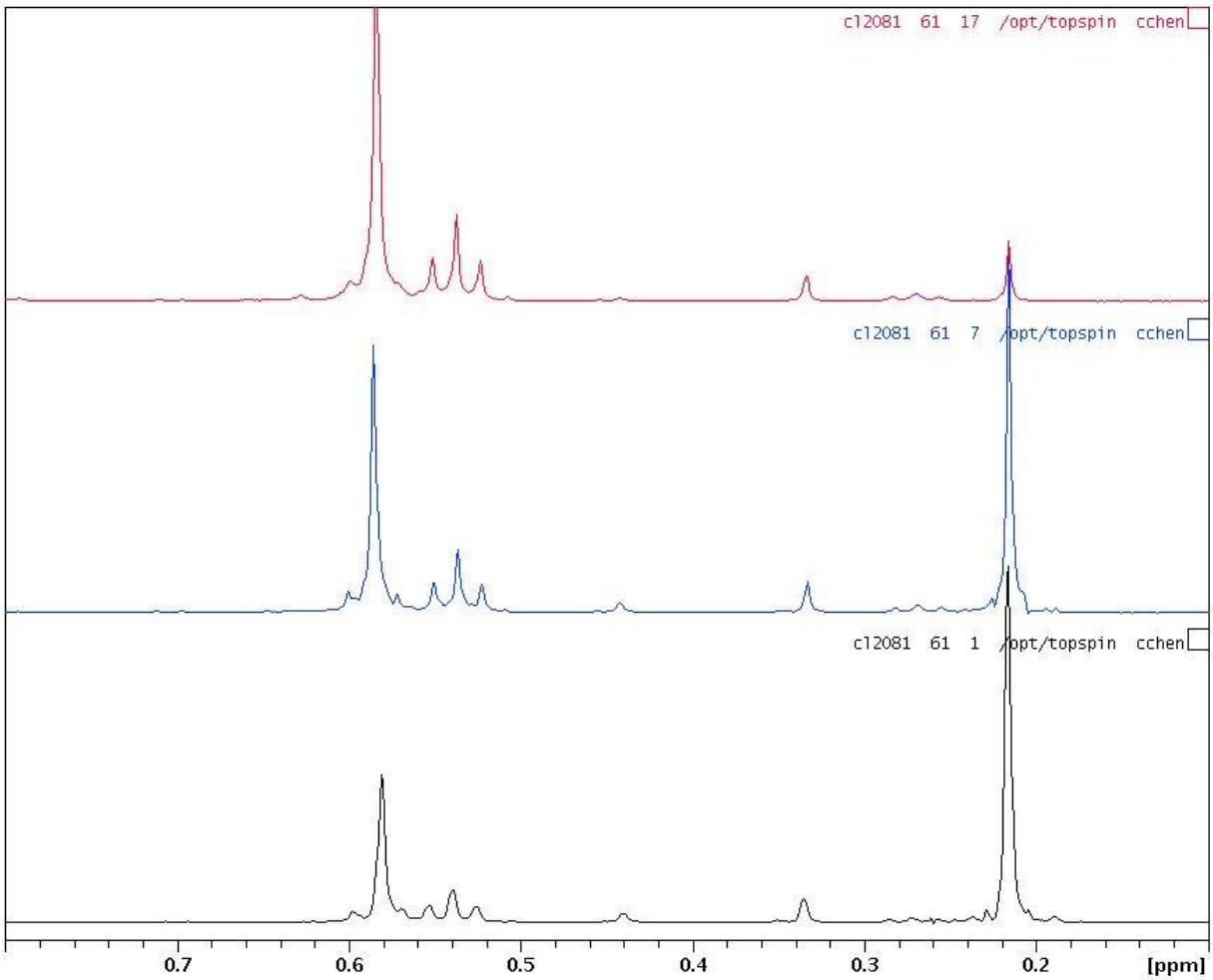

Figure 10-4f. Selected spectra for the first-order consumption of [(α-diimine)PdMe(CH_2=CHOEt)][SbF_6] (**3b**) at 0 °C: expansion of δ 0.8-0.1. The bottom spectrum is the is the starting point of the reaction, the middle spectrum corresponds to ca. 50% completion and the top spectrum corresponds to ca. 90% completion. For kinetics analysis see Figure 7.7 and Figure 7.8.

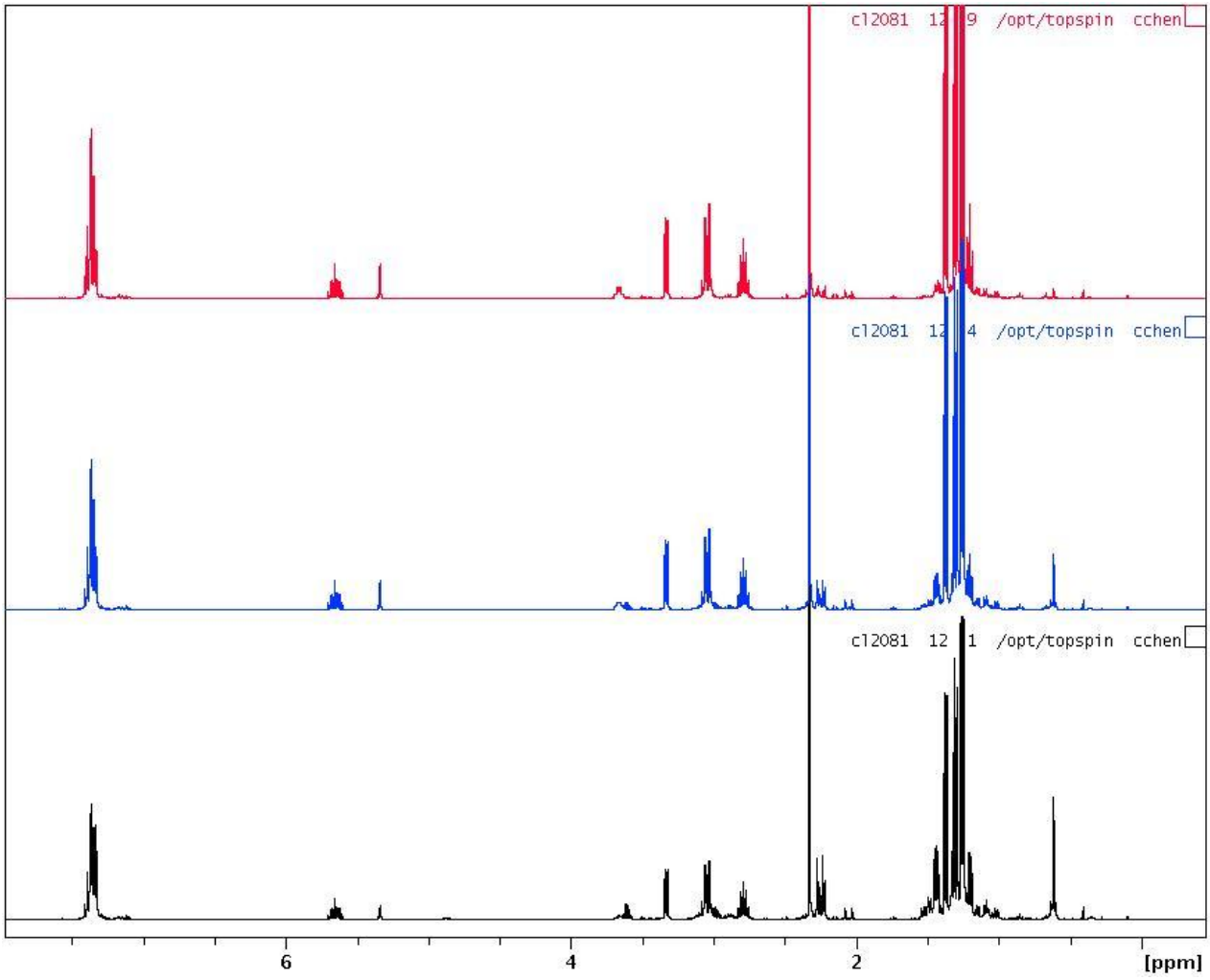

Figure 10-4g. Selected spectra for the first-order consumption of [(α-diimine)Pd{$CH_2CHMe(OEt)$}][SbF_6] (**4b**) and [(α-diimine)Pd{$CMe_2(OEt)$}][SbF_6] (**5b**) at 20 °C: full spectra. The bottom spectrum is the is the starting point of the reaction, the middle spectrum corresponds to ca. 50% completion and the top spectrum corresponds to ca. 90% completion. For kinetics analysis see Figure 7.11 and Figure 7.12.

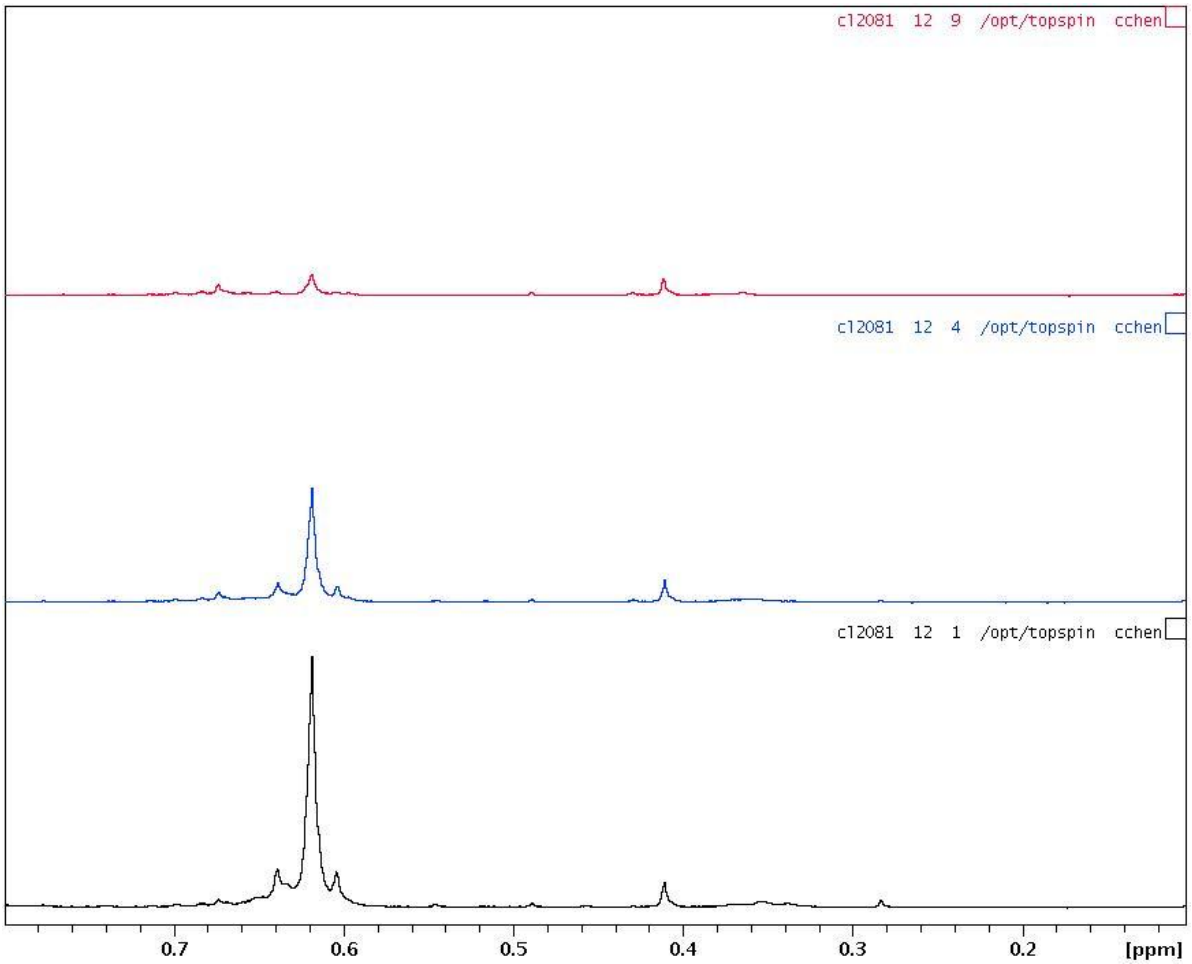

Figure 10-4h. Selected spectra for the first-order consumption of [(α-diimine)Pd{$CH_2CHMe(OEt)$}][SbF_6] (**4b**) and [(α-diimine)Pd{$CMe_2(OEt)$}][SbF_6] (**5b**) at 20 °C: expansion of δ 0.8-0.1. The bottom spectrum is the is the starting point of the reaction, the middle spectrum corresponds to ca. 50% completion and the top spectrum corresponds to ca. 90% completion. For kinetics analysis see Figure 7.11 and Figure 7.12.

10. 5 Selected ^{1}H NMR spectra for CH_2=CHOSiMe$_3$ case:

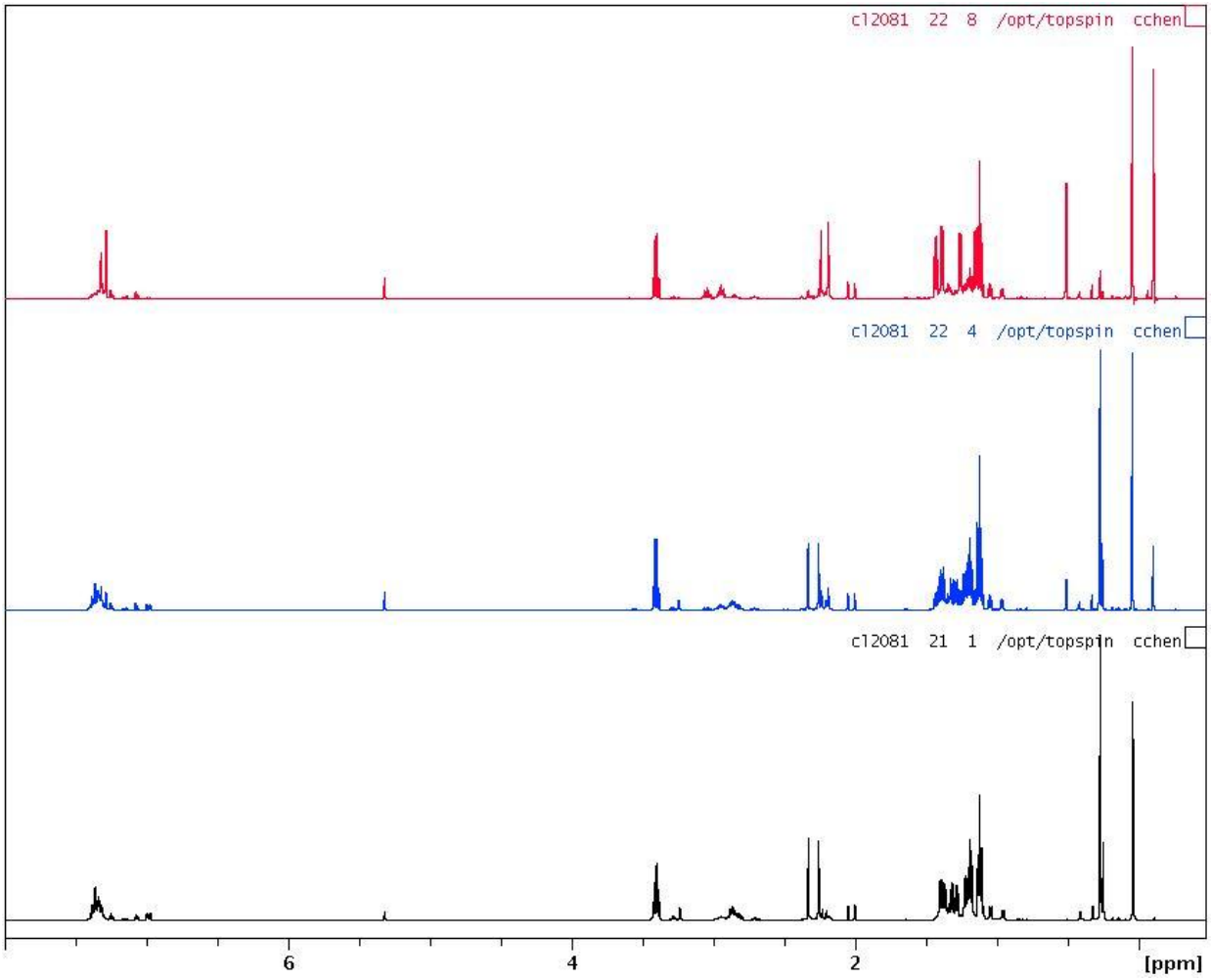

Figure 10-5a. Selected spectra for the first-order consumption of [(α-diimine)PdMe(CH_2=CHOSiMe$_3$)][SbF_6] (**3c**) at 0 °C: expansion of δ 0.8-0.1. The bottom spectrum is the is the starting point of the reaction, the middle spectrum corresponds to ca. 50% completion and the top spectrum corresponds to ca. 90% completion. For kinetics analysis see Figure 6.15 and Figure 6.16.

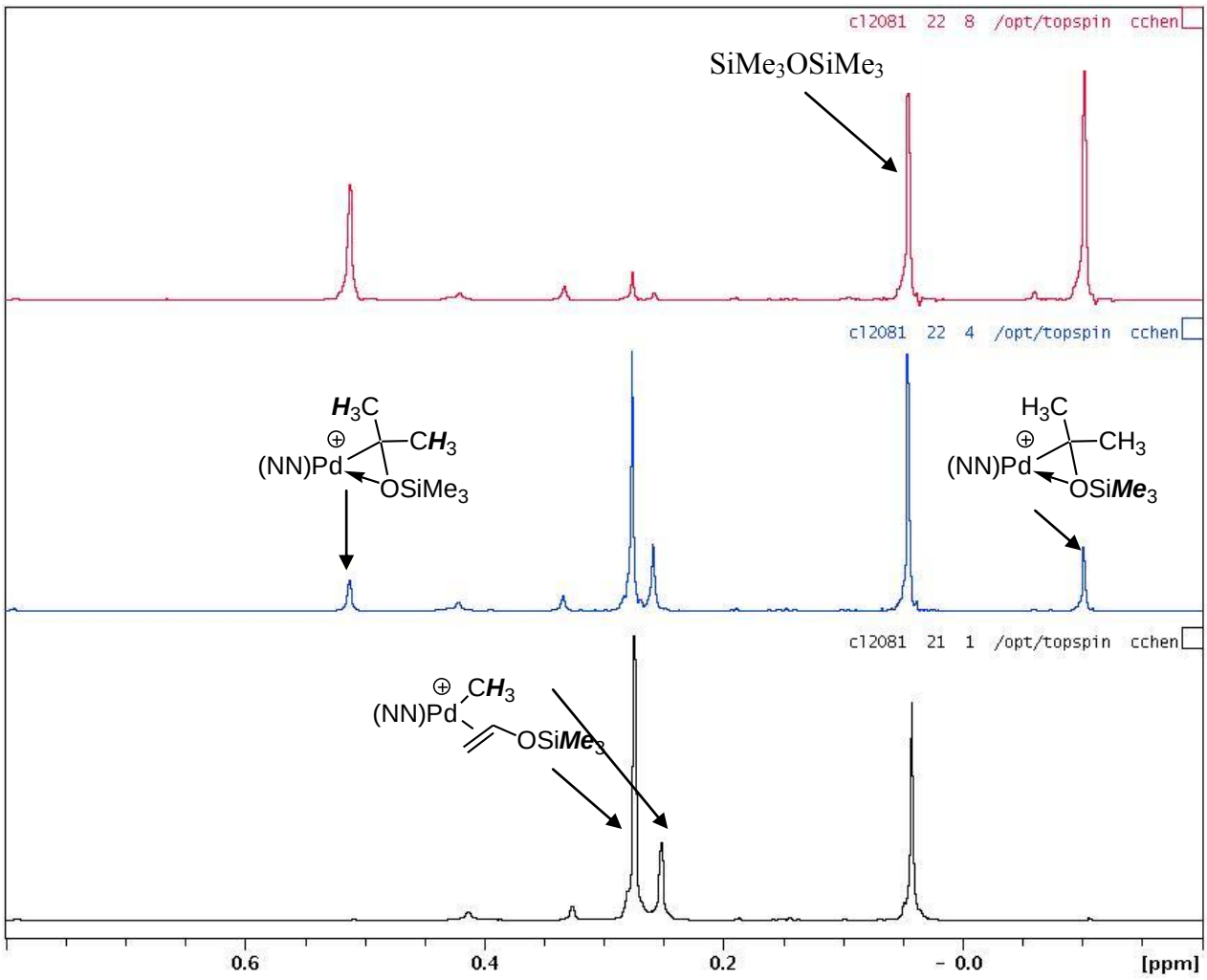

Figure 10-5b. Selected spectra for the first-order consumption of [(α-diimine)PdMe(CH_2=CHOSiMe_3)][SbF_6] (**3c**) at 0 °C: expansion of δ 0.8 - -0.2. The bottom spectrum is the is the starting point of the reaction, the middle spectrum corresponds to ca. 50% completion and the top spectrum corresponds to ca. 90% completion. For kinetics analysis see Figure 6.15 and Figure 6.16.

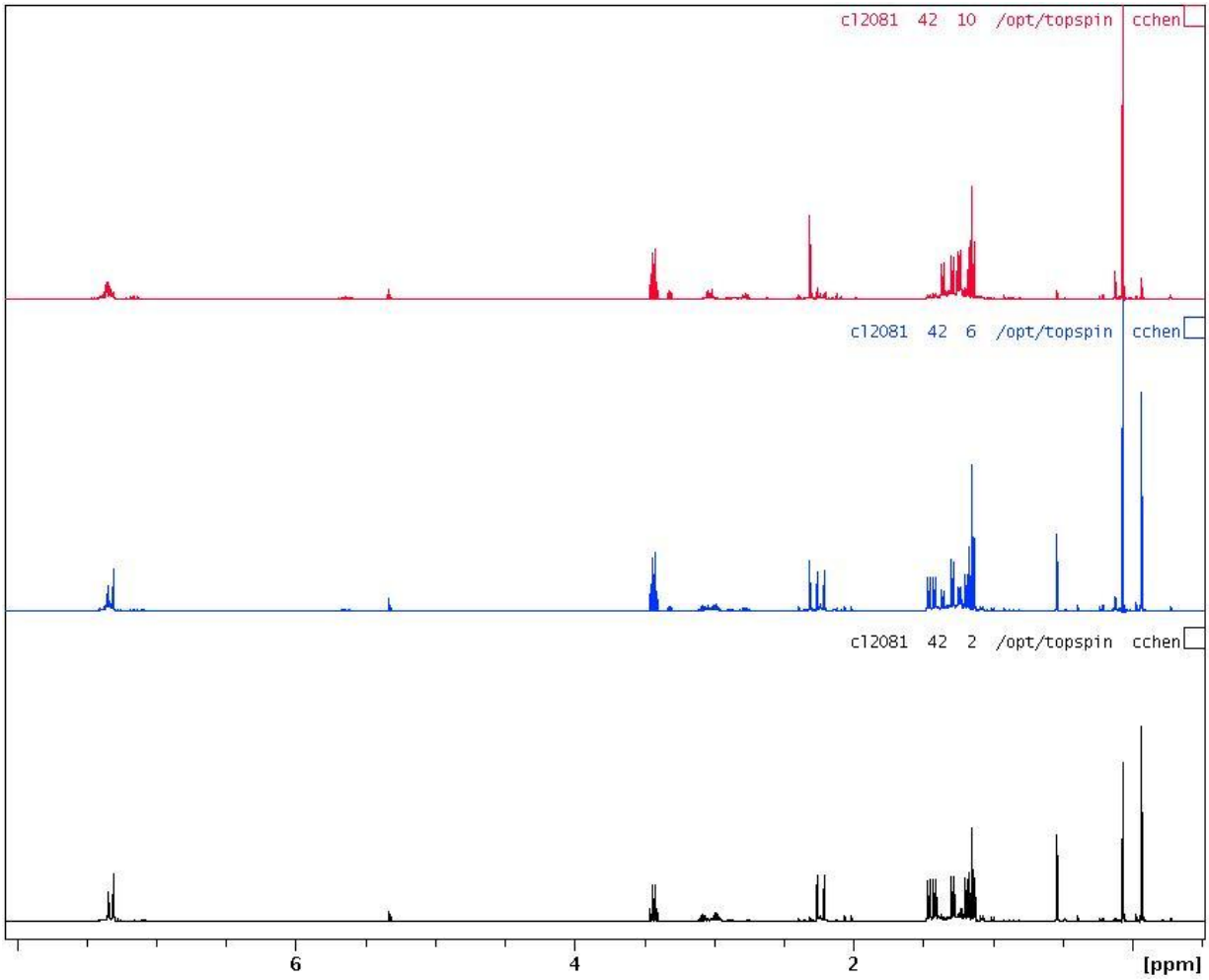

Figure 10-5c. Selected spectra for the first-order consumption of [(α-diimine)Pd{$CMe_2(OSiMe_3)$}][SbF_6] (**5c**) at 20 °C: full spectra. The bottom spectrum is the is the starting point of the reaction, the middle spectrum corresponds to ca. 50% completion and the top spectrum corresponds to ca. 90% completion. For kinetics analysis see Figure 6.17 and Figure 6.18.

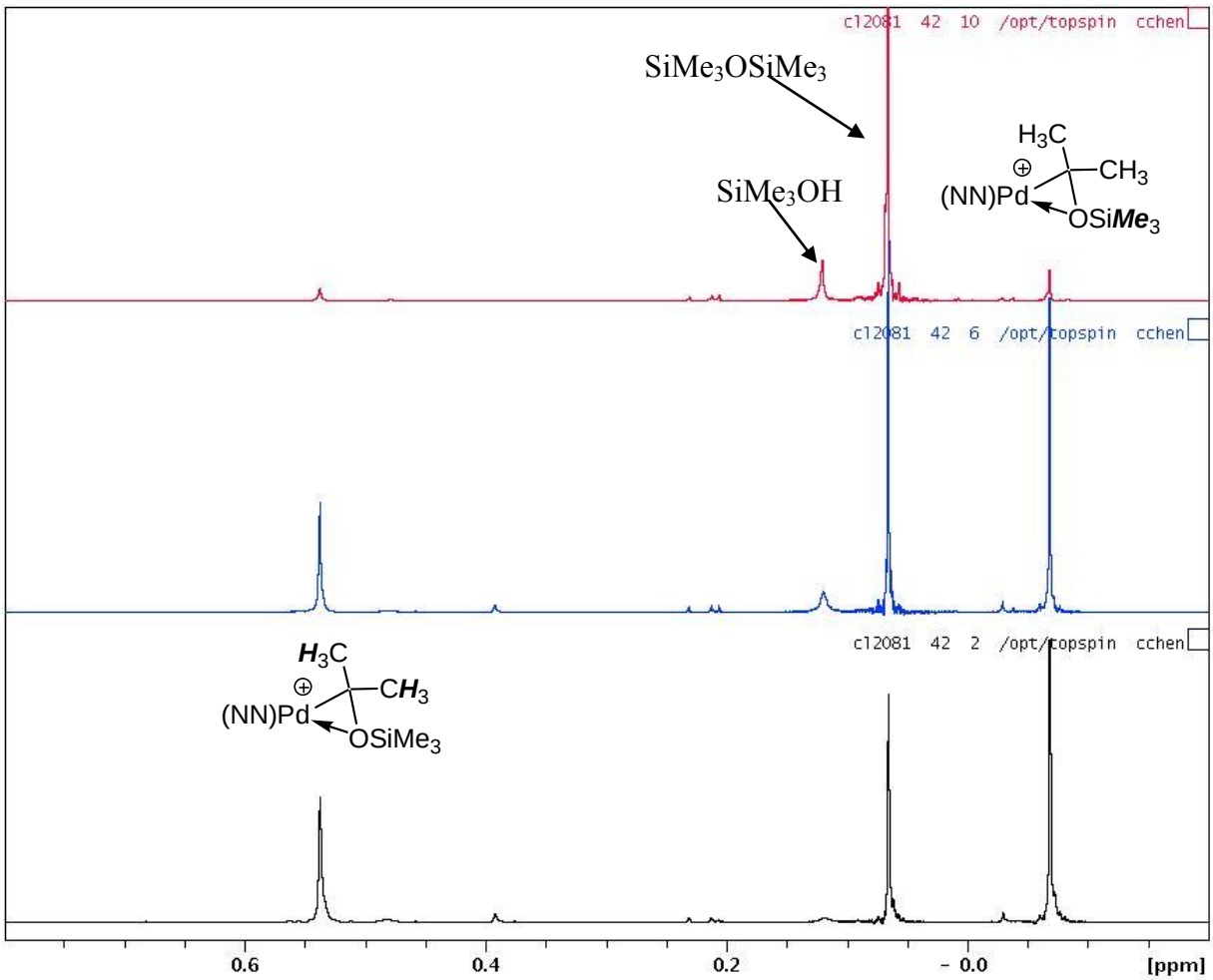

Figure 10-5d. Selected spectra for the first-order consumption of [(α-diimine)Pd{$CMe_2(OSiMe_3)$}][SbF_6] (**5c**) at 20 °C: expansion of δ 0.8 - -0.2. The bottom spectrum is the is the starting point of the reaction, the middle spectrum corresponds to ca. 50% completion and the top spectrum corresponds to ca. 90% completion. For kinetics analysis see Figure 6.17 and Figure 6.18.

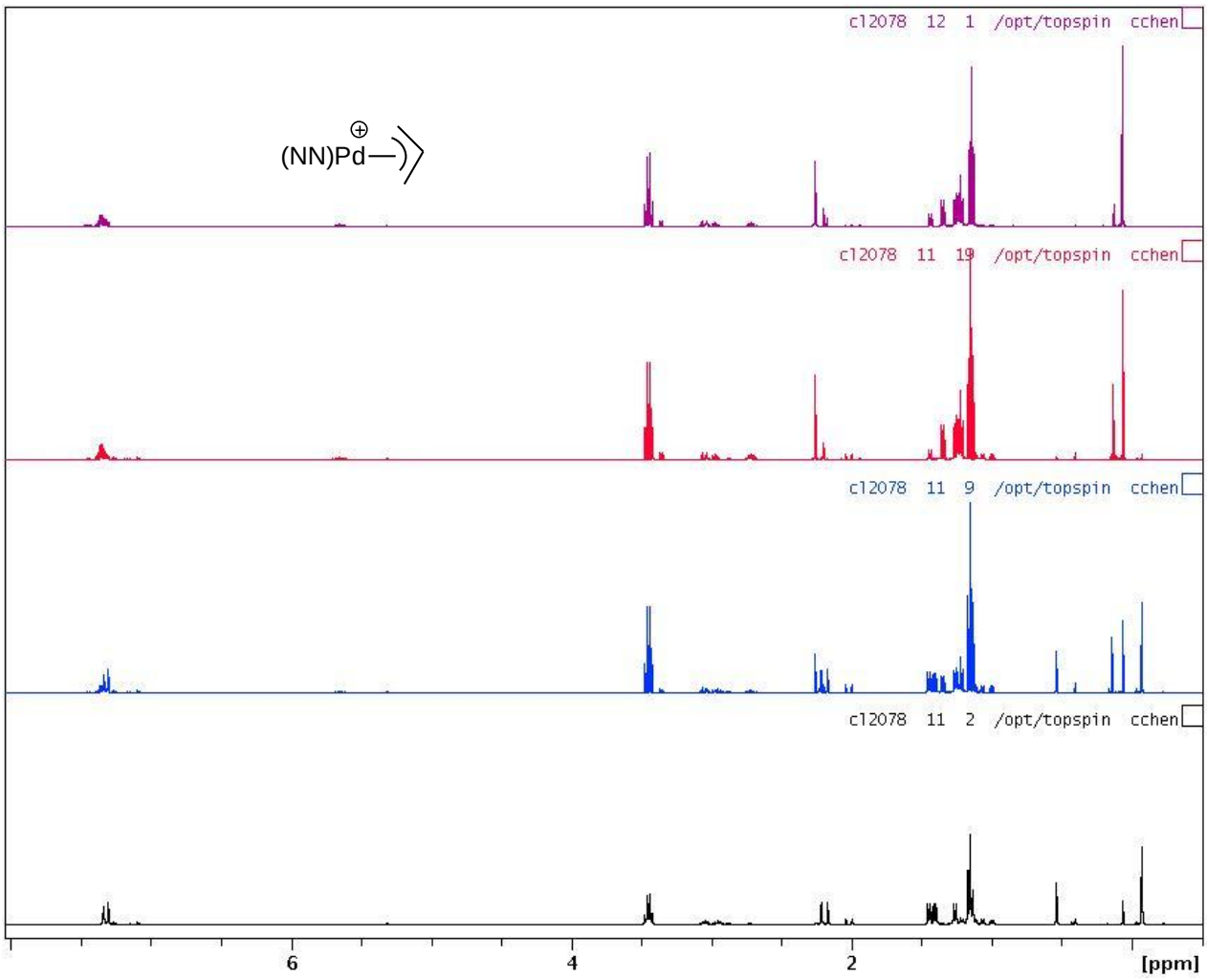

Figure 10-5e.. Selected spectra for the first-order consumption of [(α-diimine)Pd{$CMe_2(OSiMe_3)$}][$B(C_6F_5)_4$] (**5c**) at 20 °C: full spectra. The bottom spectrum is the is the starting point of the reaction, the second to the bottom spectrum corresponds to ca. 50% completion and the second to the top spectrum corresponds to ca. 90% completion. The top spectrum shows the conversion of Me_3SiOH to $Me_3SiOSiMe_3$. For kinetics analysis see Figure 6.7 and Figure 6.8.

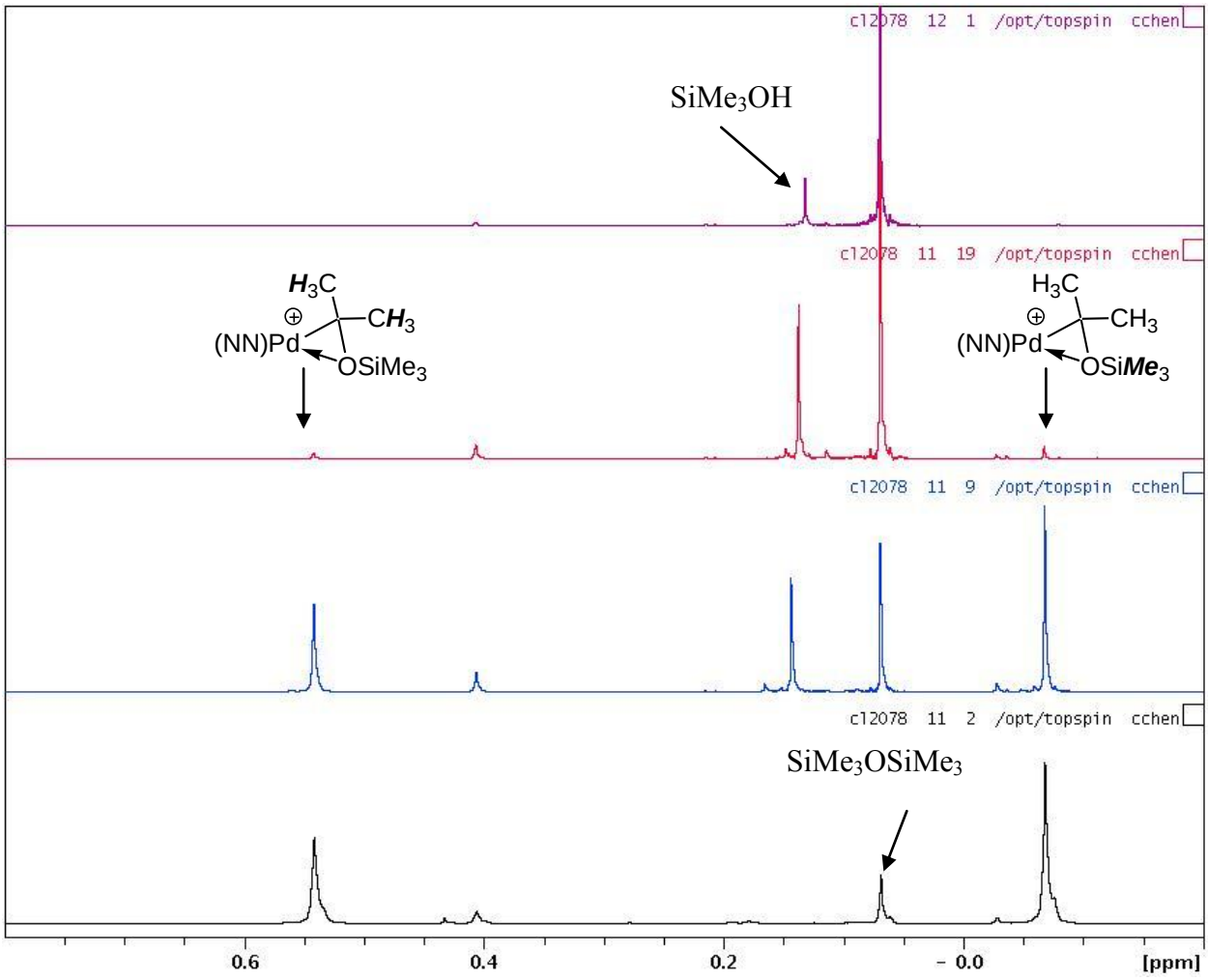

Figure 10-5f. Selected spectra for the first-order consumption of [(α-diimine)Pd{$CMe_2(OSiMe_3)$}][$B(C_6F_5)_4$] (**5c**) at 20 °C: expansion of δ 0.8 - -0.2. The bottom spectrum is the is the starting point of the reaction, the second to the bottom spectrum corresponds to ca. 50% completion and the second to the top spectrum corresponds to ca. 90% completion. The top spectrum shows the conversion of Me_3SiOH to $Me_3SiOSiMe_3$. For kinetics analysis see Figure 6.7 and Figure 6.8.

10.6 Selected ^{1}H NMR spectra for CH_2=$CHSiMe_2Ph$ case.

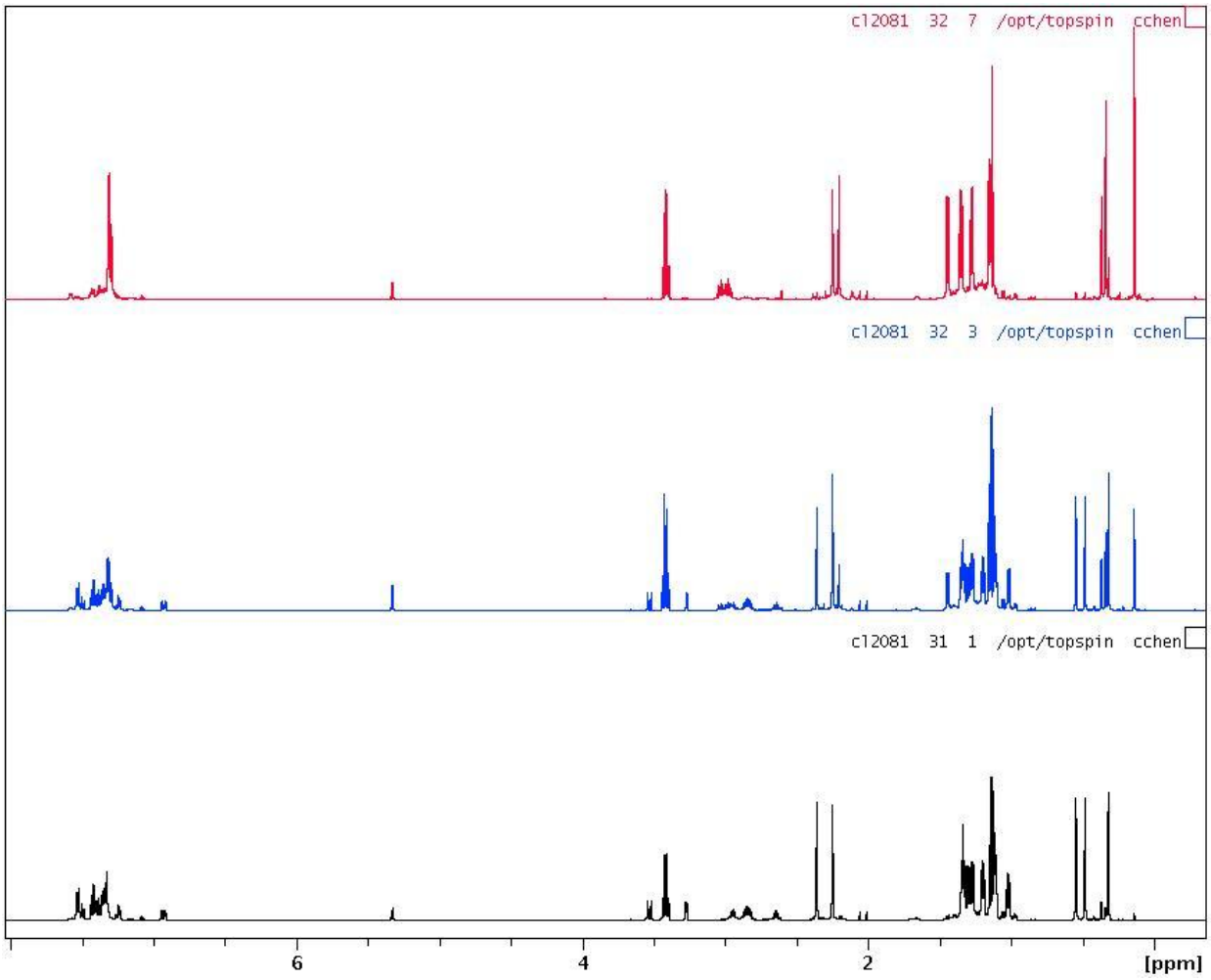

Figure 10-6a. Selected spectra for the first-order consumption of [(α-diimine)PdMe(CH_2=$CHOSiMe_2Ph$)][SbF_6] (**3d**) at 0 °C: full spectra. The bottom spectrum is the is the starting point of the reaction, the middle spectrum corresponds to ca. 50% completion and the top spectrum corresponds to ca. 90% completion. For kinetics analysis see Figure 6.19 and Figure 6.20.

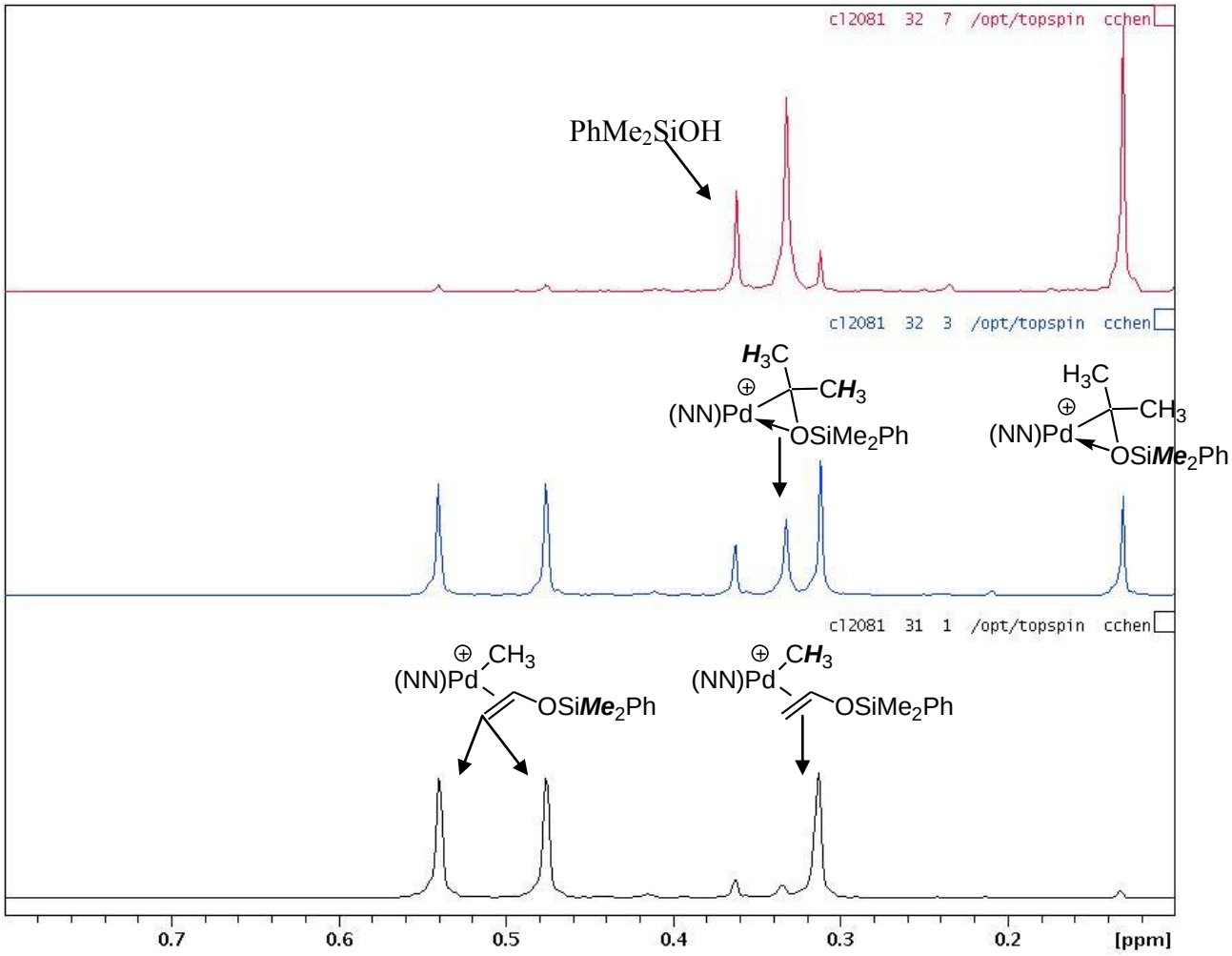

Figure 10-6b. Selected spectra for the first-order consumption of [(α-diimine)PdMe(CH_2=CHOSiMe_2Ph)][SbF_6] (**3d**) at 0 °C: expansion of δ 0.8-0.1. The bottom spectrum is the is the starting point of the reaction, the middle spectrum corresponds to ca. 50% completion and the top spectrum corresponds to ca. 90% completion. For kinetics analysis see Figure 6.19 and Figure 6.20.

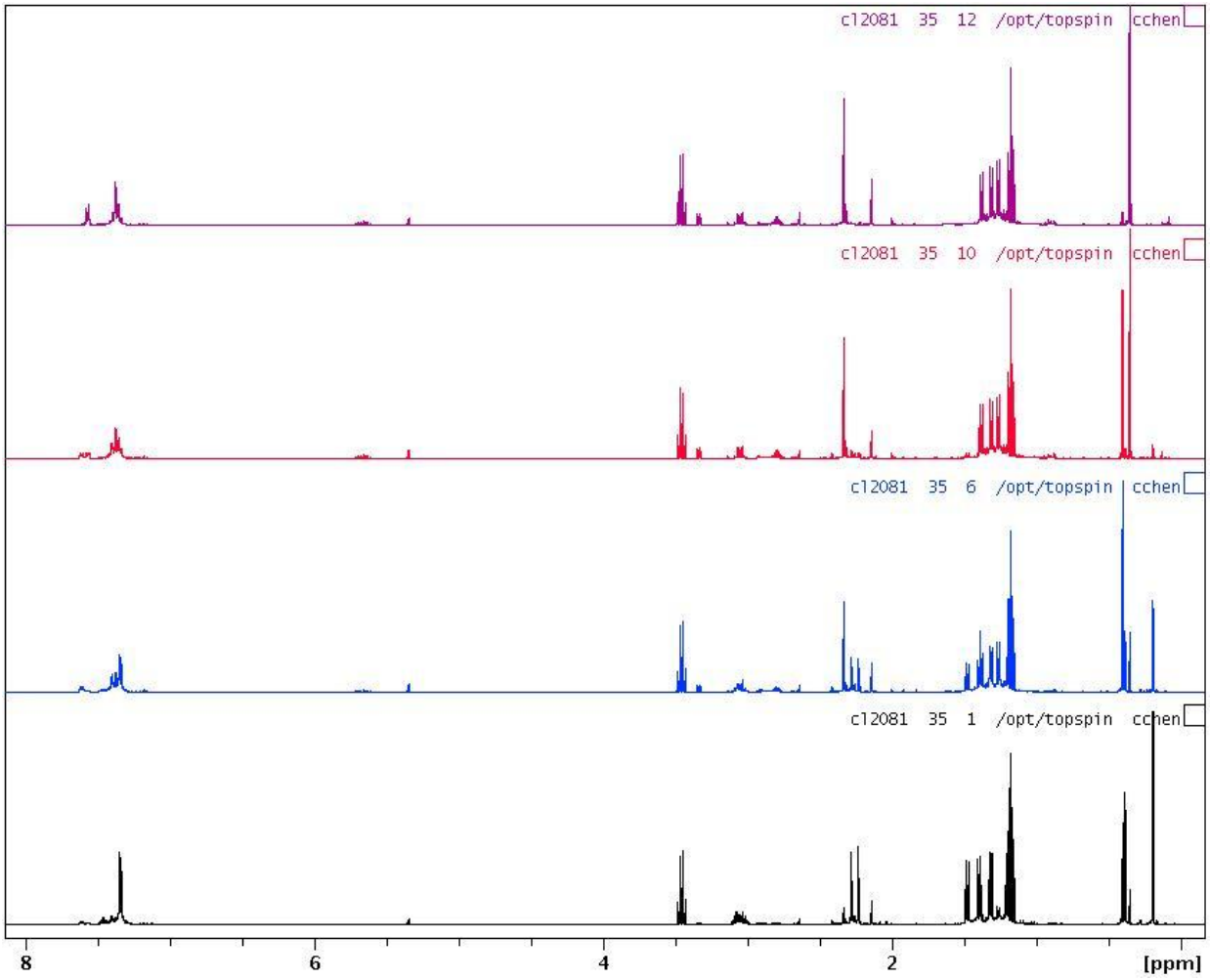

Figure 10-6c. Selected spectra for the first-order consumption of [(α-diimine)Pd{$CMe_2(OSiMe_2Ph)$}][SbF_6] (**5d**) at 20 °C: full spectra. The bottom spectrum is the is the starting point of the reaction, the second to the bottom spectrum corresponds to ca. 50% completion and the second to the top spectrum corresponds to ca. 90% completion. The top spectrum shows the conversion of $PhMe_2SiOH$ to $PhMe_2SiOSiMe_2Ph$. For kinetics analysis see Figure 6.21 and Figure 6.22.

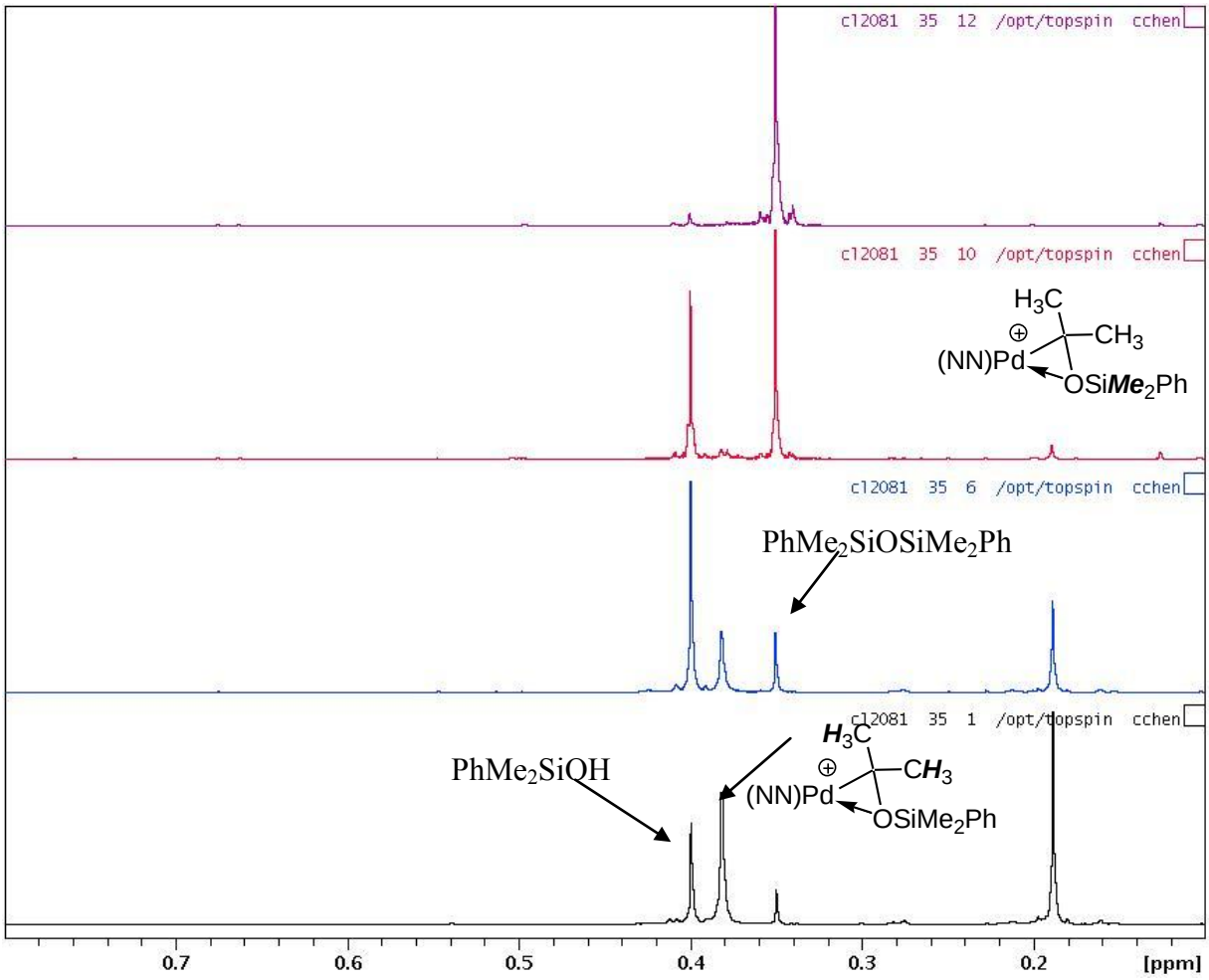

Figure 10-6d. Selected spectra for the first-order consumption of [(α-diimine)Pd{CMe_2($OSiMe_2Ph$)}][SbF_6] (**5d**) at 20 °C: expansion of δ 0.8-0.1. The bottom spectrum is the is the starting point of the reaction, the second to the bottom spectrum corresponds to ca. 50% completion and the second to the top spectrum corresponds to ca. 90% completion. The top spectrum shows the conversion of $PhMe_2SiOH$ to $PhMe_2SiOSiMe_2Ph$. For kinetics analysis see Figure 6.21 and Figure 6.22.

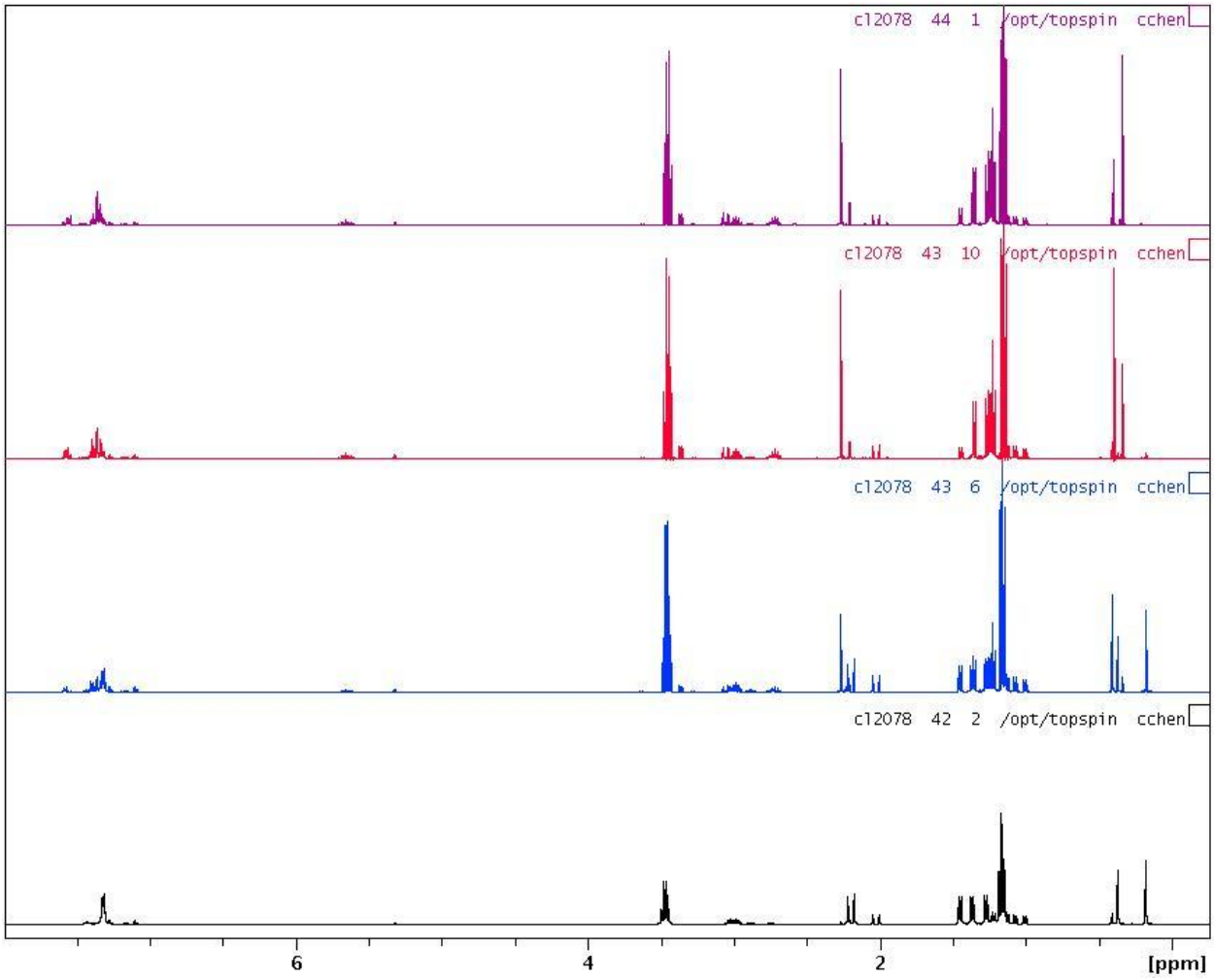

Figure 10-6e. Selected spectra for the first-order consumption of [(α-diimine)Pd{$CMe_2(OSiMe_2Ph)$}][$B(C_6F_5)_4$] (**5d**) at 20 °C: full spectra. The bottom spectrum is the is the starting point of the reaction, the second to the bottom spectrum corresponds to ca. 50% completion and the second to the top spectrum corresponds to ca. 90% completion. The top spectrum shows the conversion of $PhMe_2SiOH$ to $PhMe_2SiOSiMe_2Ph$. For kinetics analysis see Figure 6.9 and Figure 6.10.

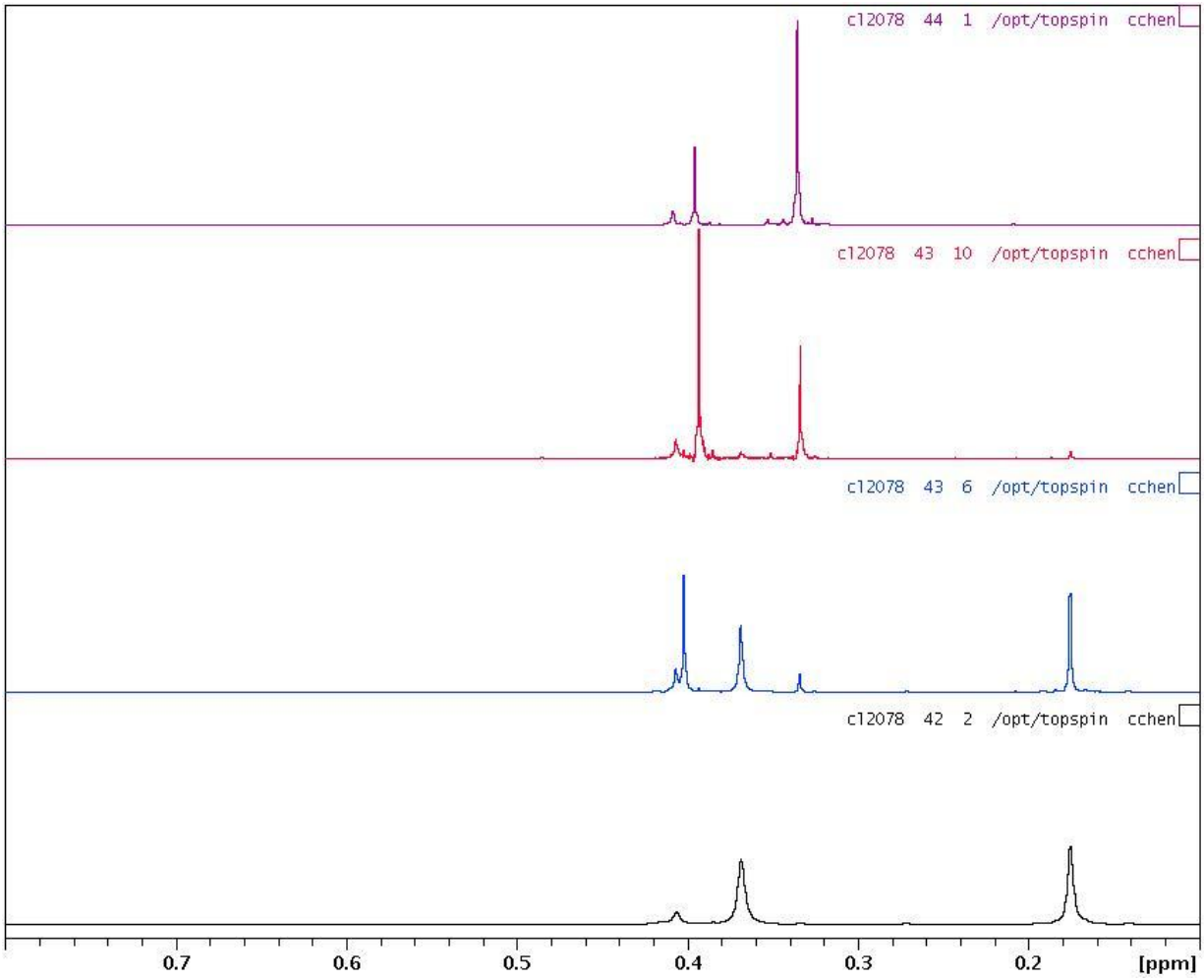

Figure 10-6f. Selected spectra for the first-order consumption of [(α-diimine)Pd{$CMe_2(OSiMe_2Ph)$}][$B(C_6F_5)_4$] (**5d**) at 20 °C: expansion of δ 0.8-0.1. The bottom spectrum is the is the starting point of the reaction, the second to the bottom spectrum corresponds to ca. 50% completion and the second to the top spectrum corresponds to ca. 90% completion. The top spectrum shows the conversion of $PhMe_2SiOH$ to $PhMe_2SiOSiMe_2Ph$. For kinetics analysis see Figure 6.9 and Figure 6.10.

10.7 Selected ^{1}H NMR spectra for CH_2=CHSiMe$_2$Ph case.

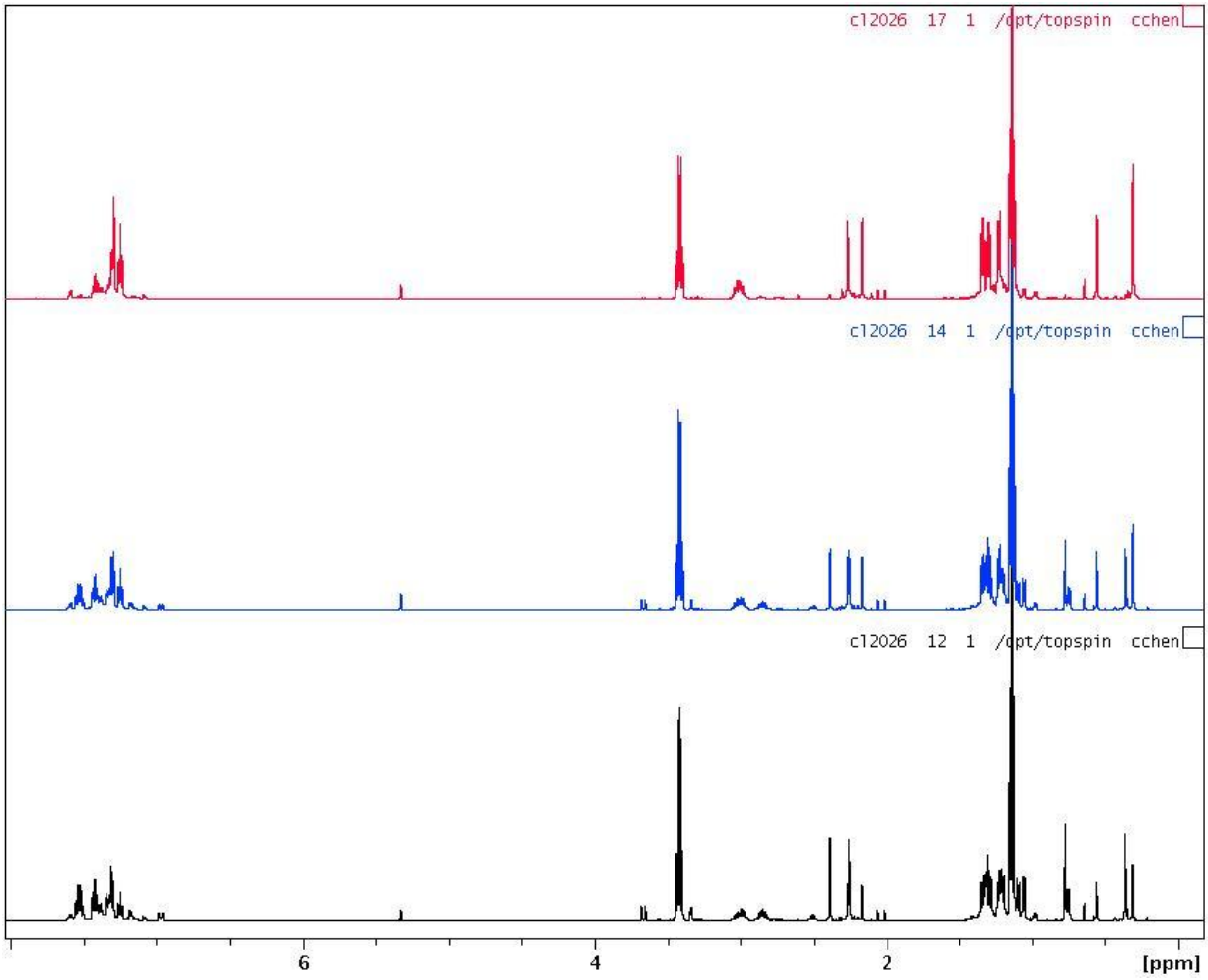

Figure 10-7a. Selected spectra for the first-order consumption of [(α-diimine)PdMe(CH_2=CHOSiMePh$_2$)][SbF_6] (**3e**) at 0 °C: full spectra. The bottom spectrum is the is the starting point of the reaction, the middle spectrum corresponds to ca. 50% completion and the top spectrum corresponds to ca. 90% completion. For kinetics analysis see Figure 6.23 and Figure 6.24.

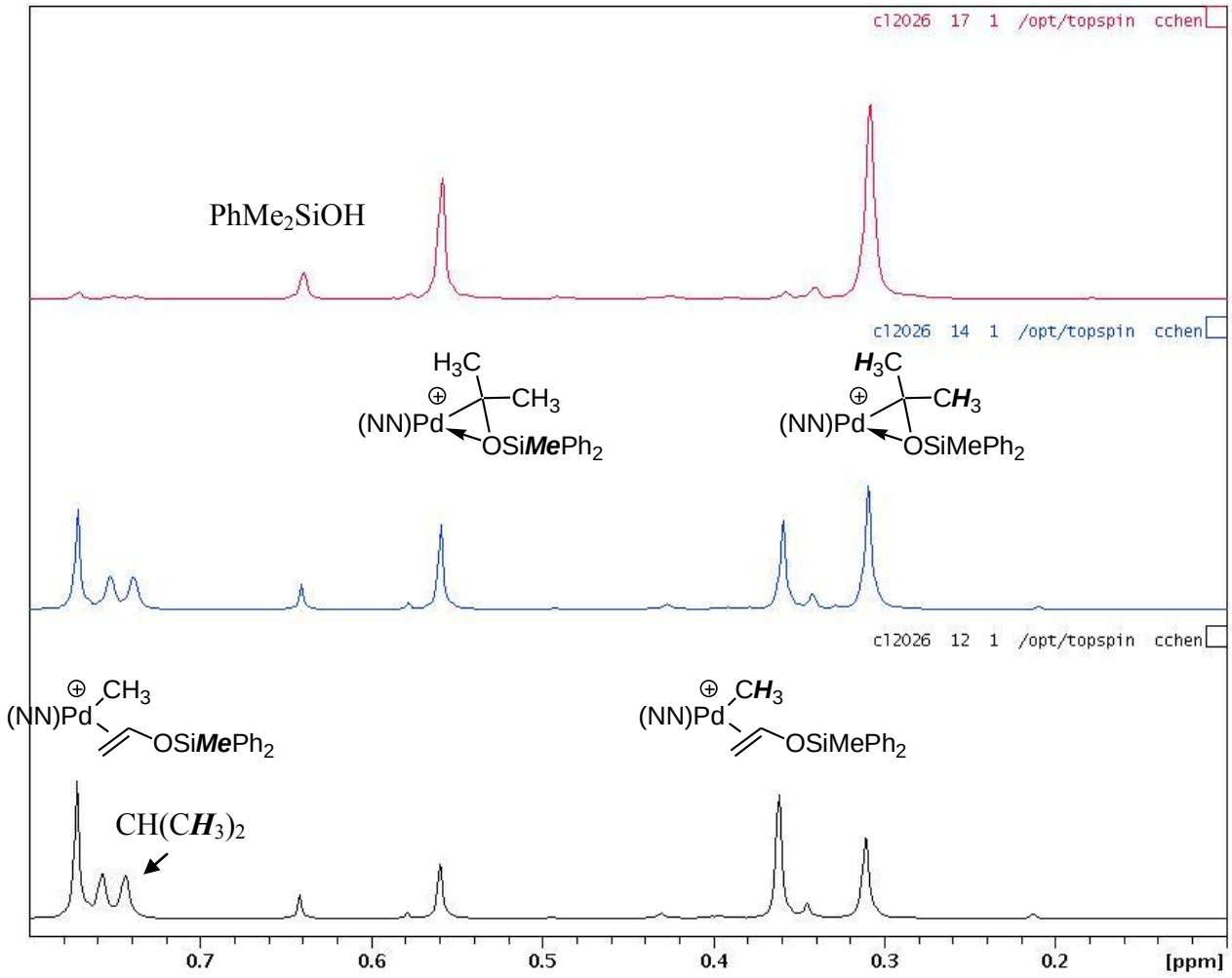

Figure 10-7b. Selected spectra for the first-order consumption of [(α-diimine)PdMe(CH_2=CHOSiMePh_2)][SbF_6] (**3e**) at 0 °C: expansion of δ 0.8-0.1. The bottom spectrum is the is the starting point of the reaction, the middle spectrum corresponds to ca. 50% completion and the top spectrum corresponds to ca. 90% completion. For kinetics analysis see Figure 6.23 and Figure 6.24.

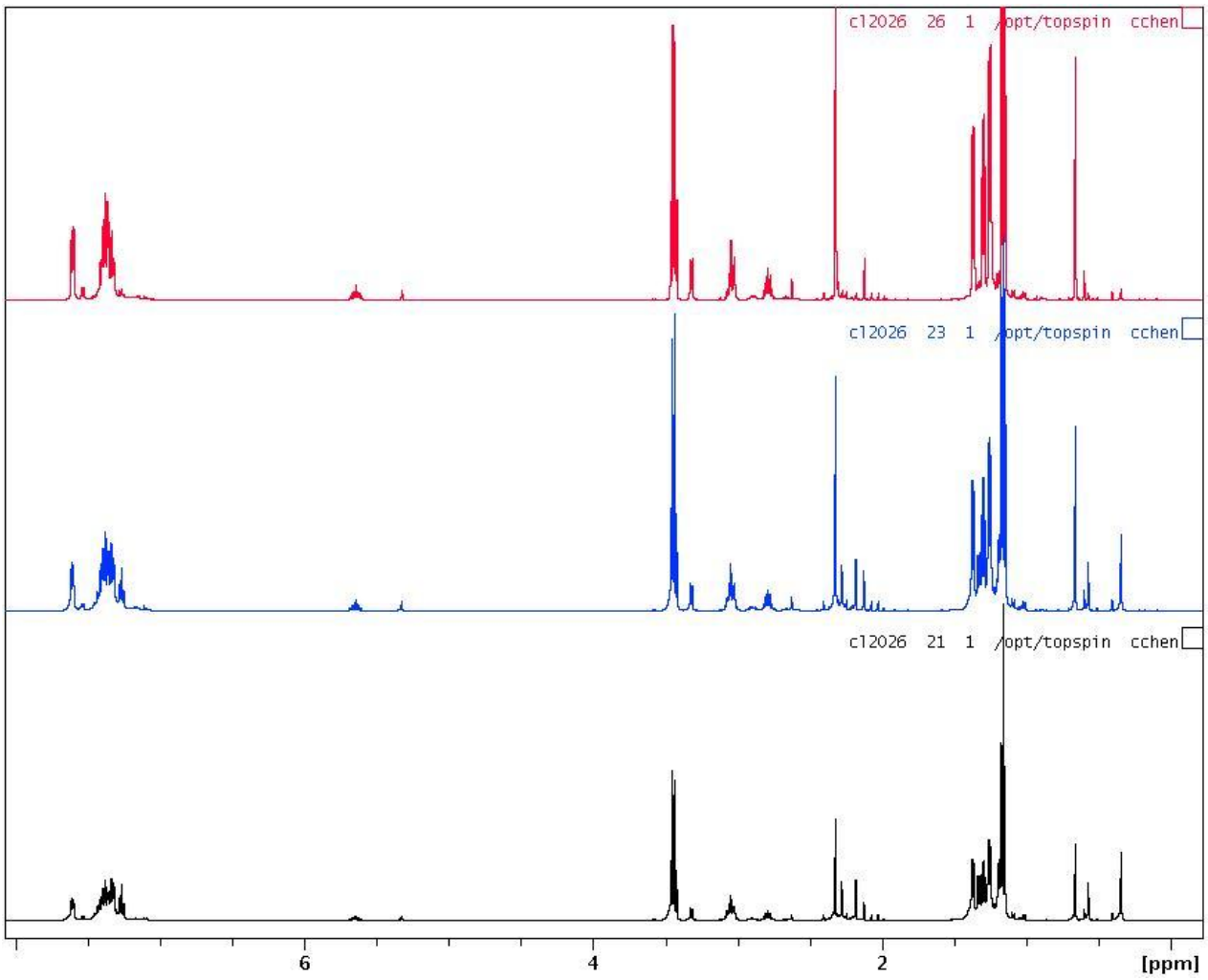

Figure 10-7c. Selected spectra for the first-order consumption of [(α-diimine)Pd{CMe_2($OSiMePh_2$)}][SbF_6] (**5e**) at 20 °C: full spectra. The bottom spectrum is the is the starting point of the reaction, the middle spectrum corresponds to ca. 50% completion and the top spectrum corresponds to ca. 90% completion. For kinetics analysis see Figure 6.25 and Figure 6.26.

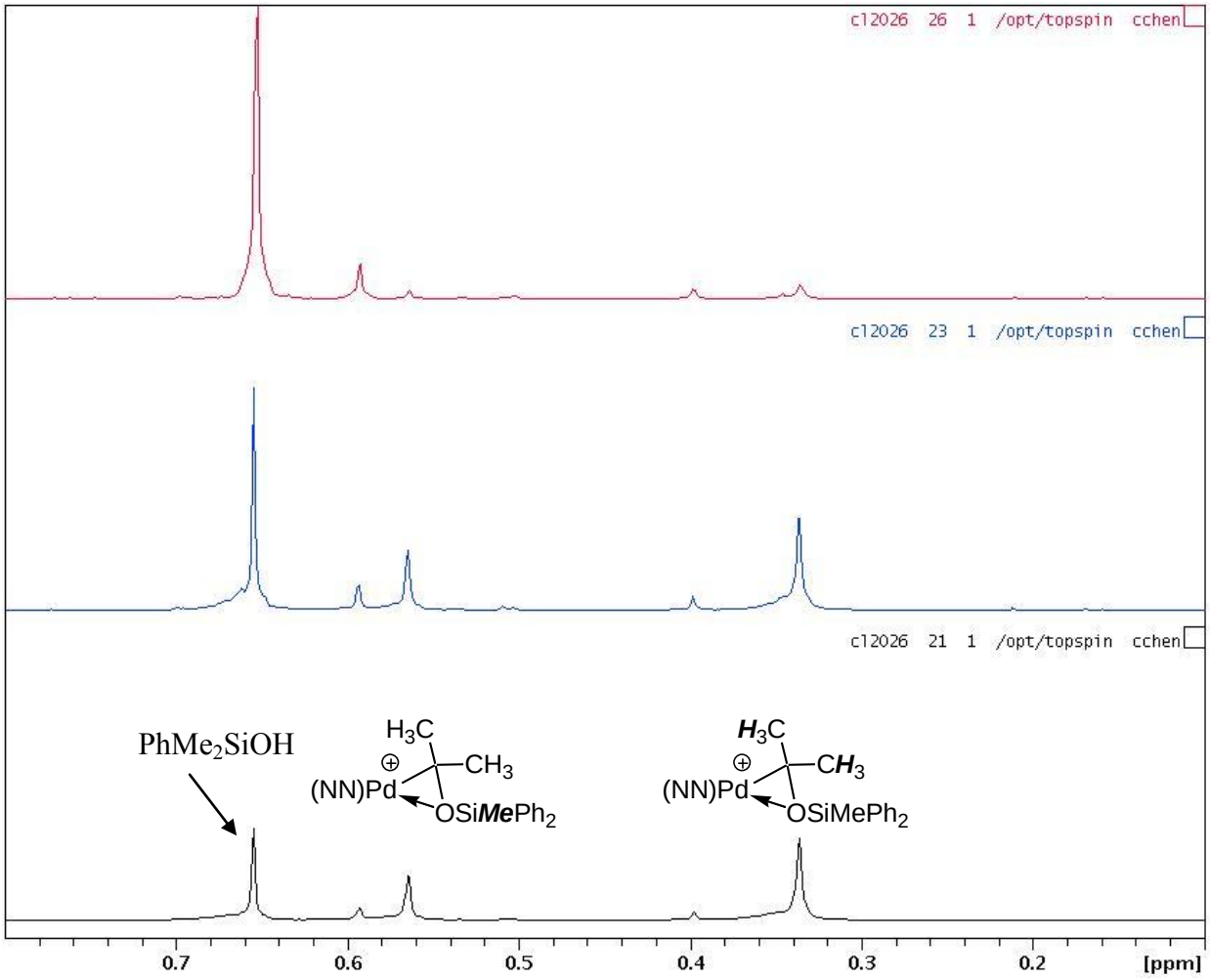

Figure 10-7d. Selected spectra for the first-order consumption of [(α-diimine)Pd{$CMe_2(OSiMePh_2)$}][SbF_6] (**5e**) at 20 °C: expansion of δ 0.8-0.1. The bottom spectrum is the is the starting point of the reaction, the middle spectrum corresponds to ca. 50% completion and the top spectrum corresponds to ca. 90% completion. For kinetics analysis see Figure 6.25 and Figure 6.26.

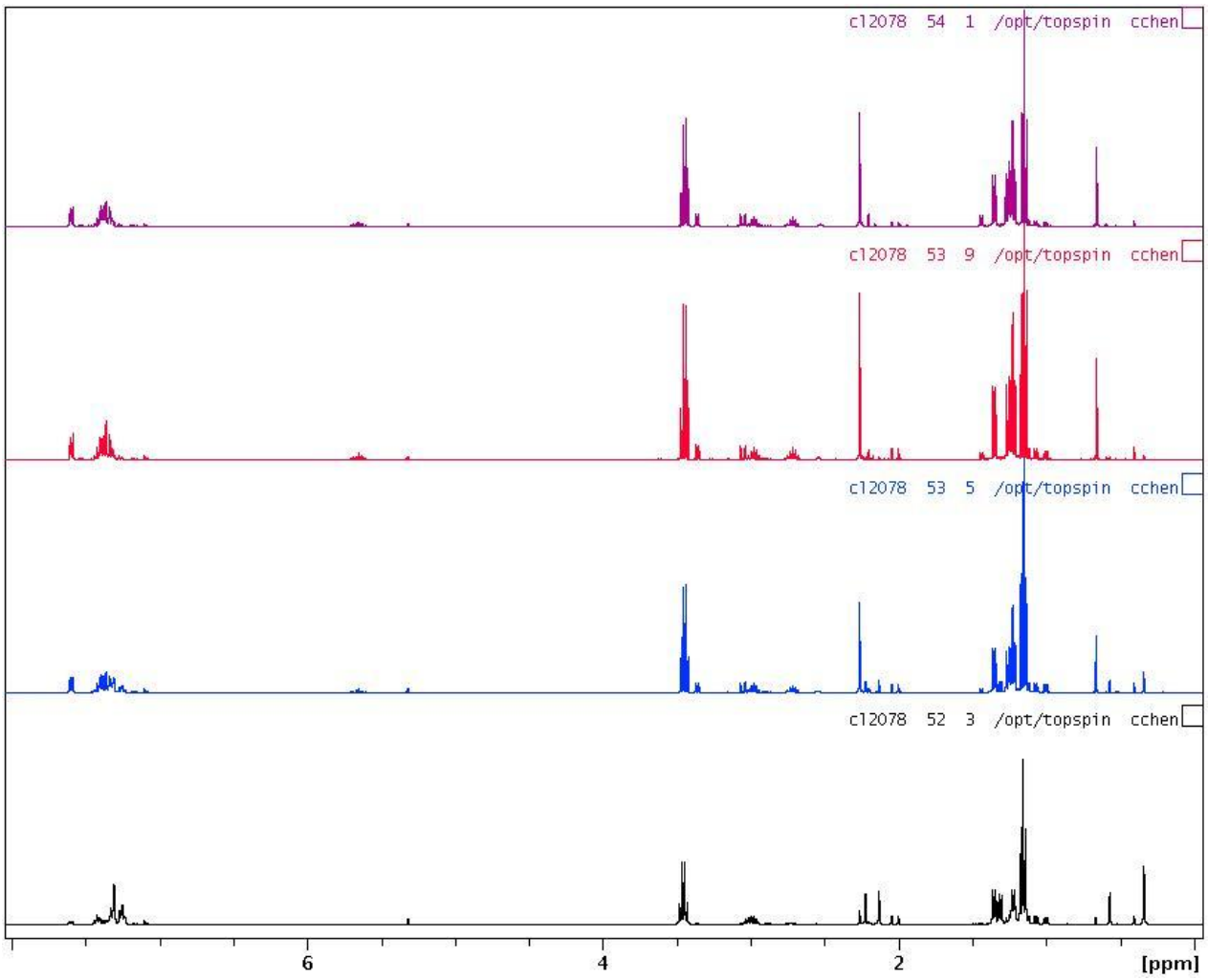

Figure 10-7e. Selected spectra for the first-order consumption of [(α-diimine)Pd{$CMe_2(OSiMePh_2)$}][$B(C_6F_5)_4$] (**5e**) at 20 °C: full spectra. The bottom spectrum is the is the starting point of the reaction, the second to the bottom spectrum corresponds to ca. 50% completion and the second to the top spectrum corresponds to ca. 90% completion. The top spectrum shows $Ph_2MeSiOH$ does not convert to $Ph_2MeSiOSiMePh_2$. For kinetics analysis see Figure 6.11, Figure 6.12 and Figure 6.13.

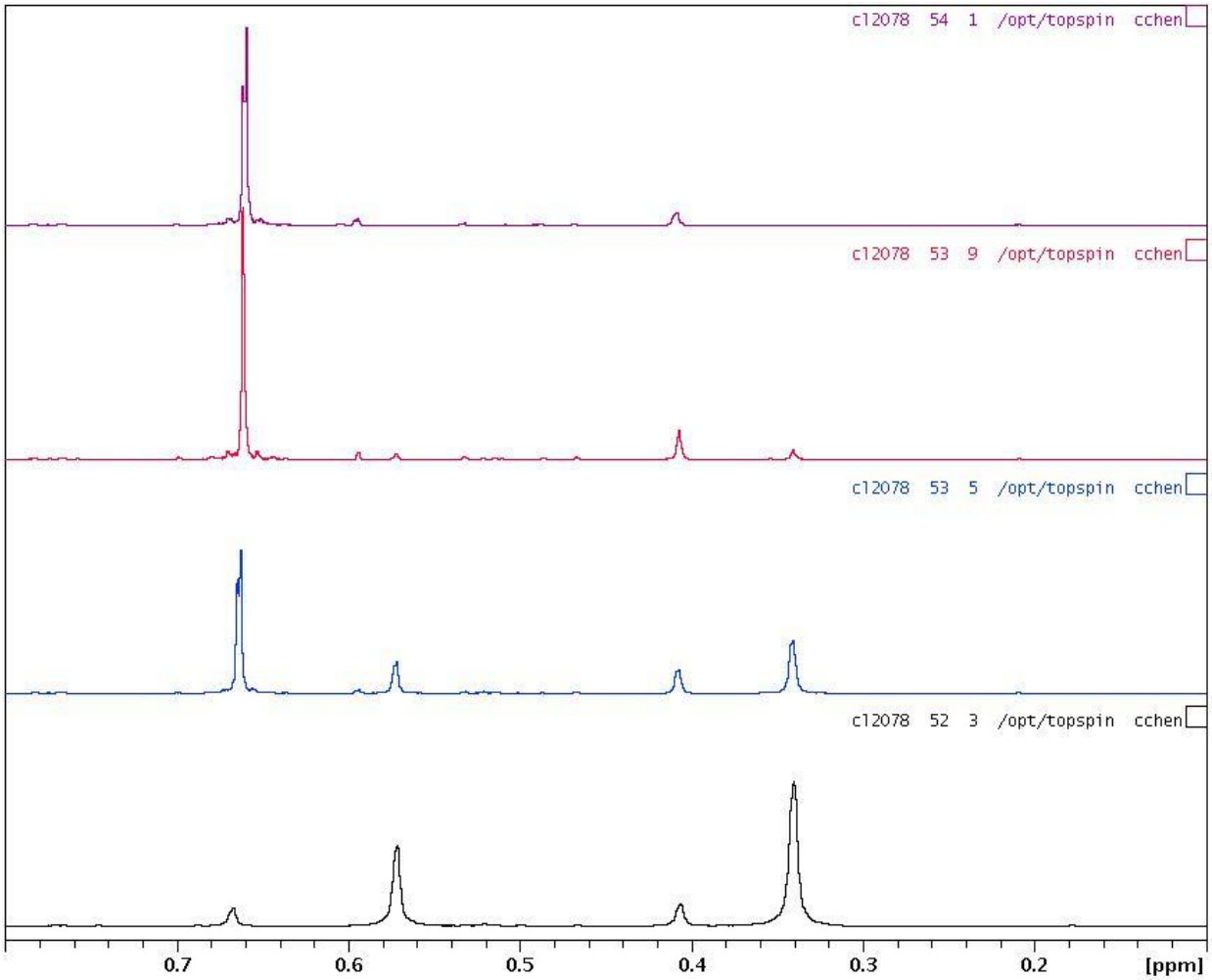

Figure 10-7f. Selected spectra for the first-order consumption of [(α-diimine)Pd{$CMe_2(OSiMePh_2)$}][$B(C_6F_5)_4$] (**5e**) at 20 °C: expansion of δ 0.8-0.1. The bottom spectrum is the is the starting point of the reaction, the second to the bottom spectrum corresponds to ca. 50% completion and the second to the top spectrum corresponds to ca. 90% completion. The top spectrum shows $Ph_2MeSiOH$ does not convert to $Ph_2MeSiOSiMePh_2$. For kinetics analysis see Figure 6.11, Figure 6.12 and Figure 6.13.

10.8 Selected ^{1}H NMR spectra for CH_2=CHSiPh_3 case:

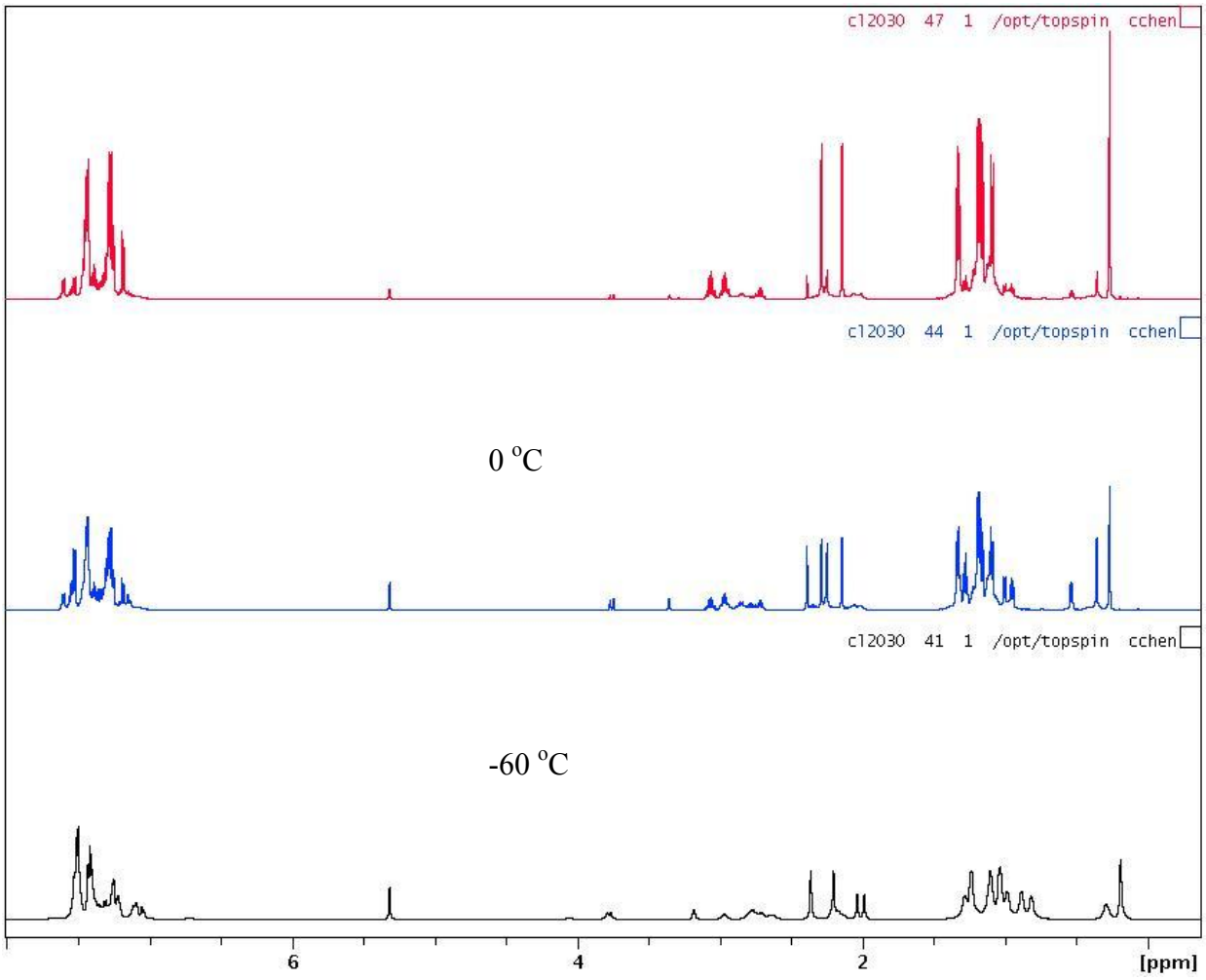

Figure 10-8a. Selected spectra for the first-order consumption of [(α-diimine)PdMe(CH_2=CHOSiPh_3)][SbF_6] (**3f**) at 0 °C: full spectra. The bottom spectrum is the starting point of the reaction at -60 °C, the middle spectrum corresponds to ca. 50% completion at 0 °C and the top spectrum corresponds to ca. 90% completion at 0 °C. For kinetics analysis see Figure 6.27 and Figure 6.28.

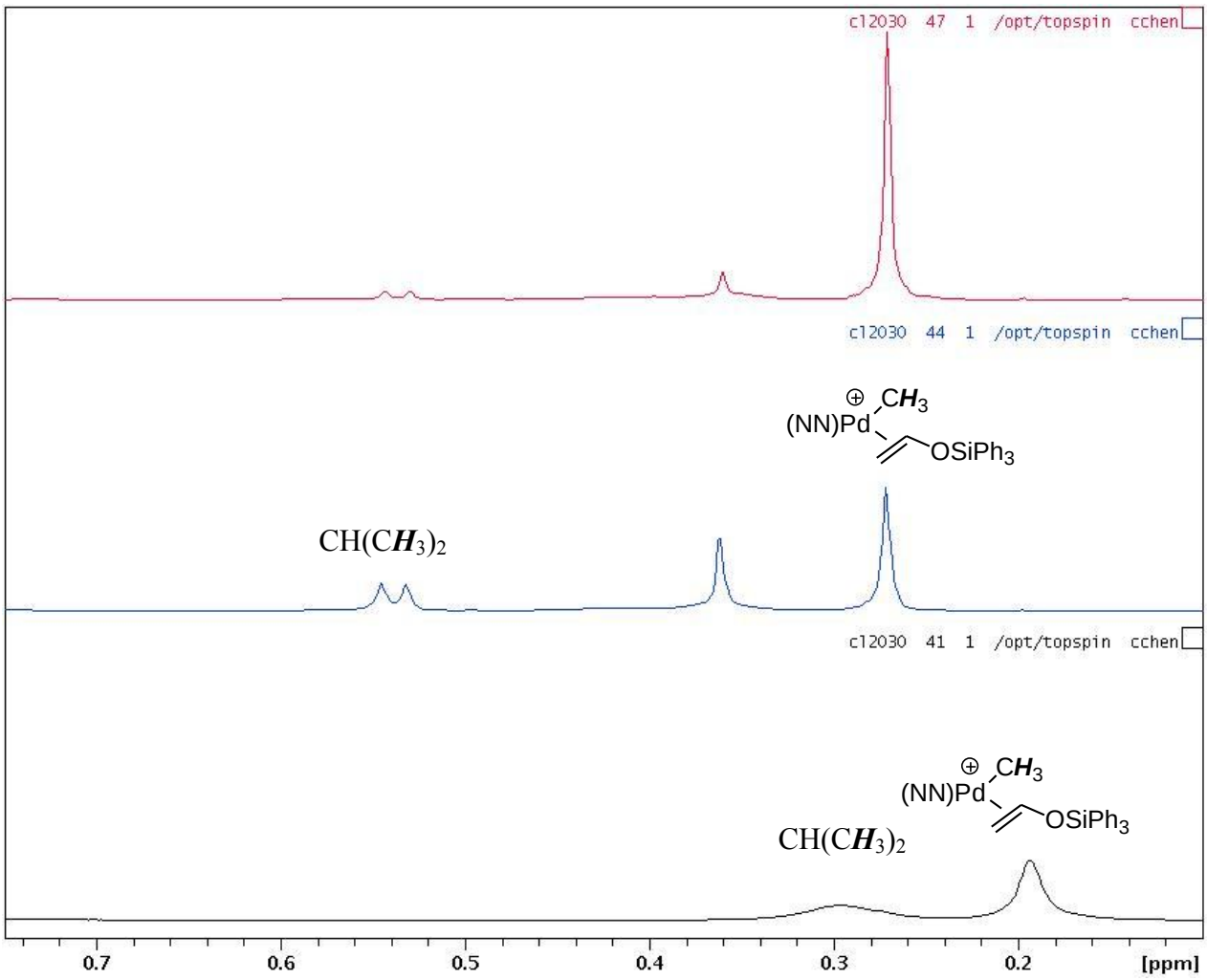

Figure 10-8b. Selected spectra for the first-order consumption of [(α-diimine)PdMe(CH_2=CHOSiPh_3)][SbF_6] (**3f**) at 0 °C: expansion of δ 0.8-0.1. The bottom spectrum is the starting point of the reaction at -60 °C, the middle spectrum corresponds to ca. 50% completion at 0 °C and the top spectrum corresponds to ca. 90% completion at 0 °C. For kinetics analysis see Figure 6.27 and Figure 6.28.

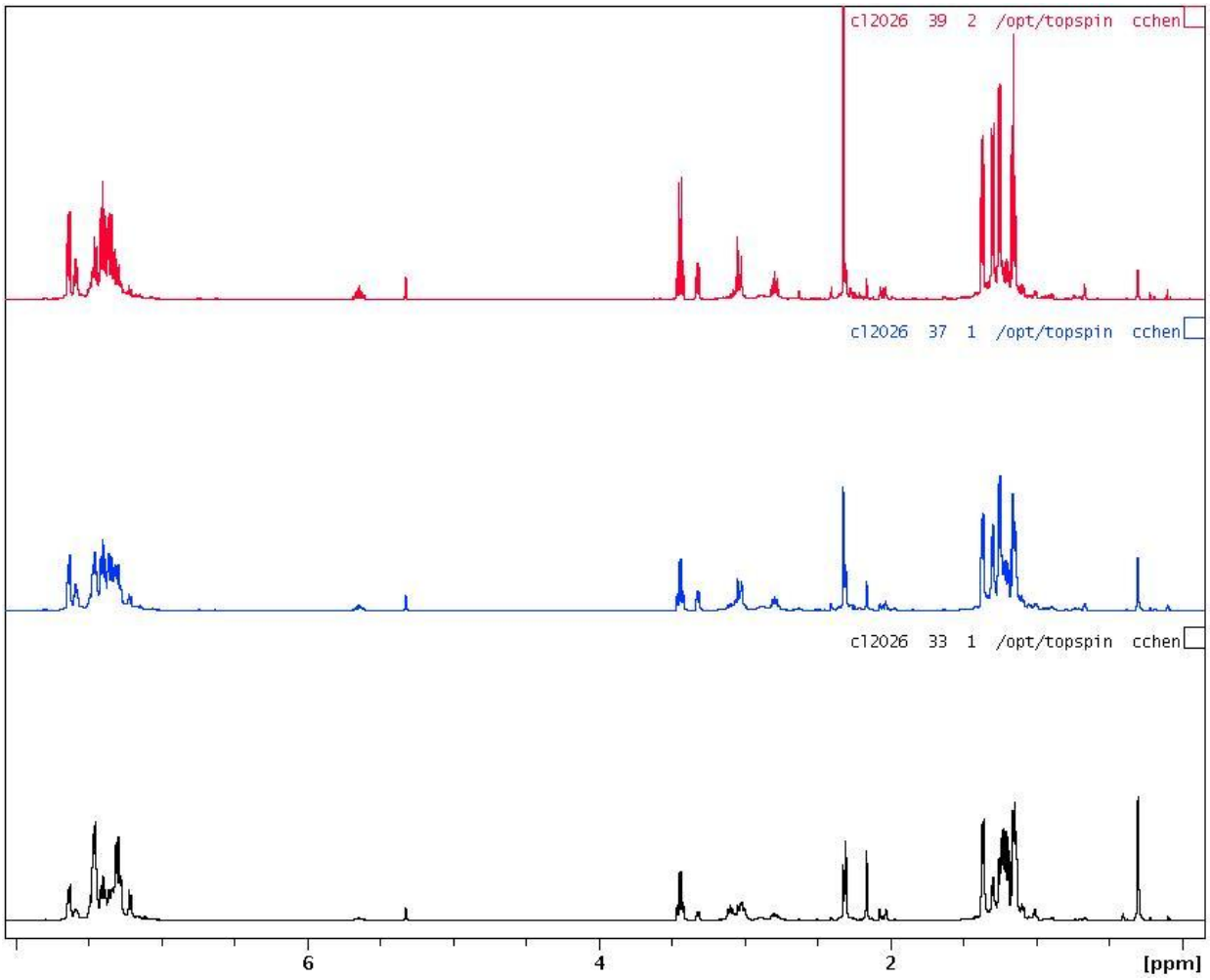

Figure 10-8c. Selected spectra for the first-order consumption of [(α-diimine)Pd{$CMe_2(OSiPh_3)$}][SbF_6] (**5f**) at 20 °C: full spectra. The bottom spectrum is the is the starting point of the reaction, the middle spectrum corresponds to ca. 50% completion and the top spectrum corresponds to ca. 90% completion. For kinetics analysis see Figure 6.29 and Figure 6.30.

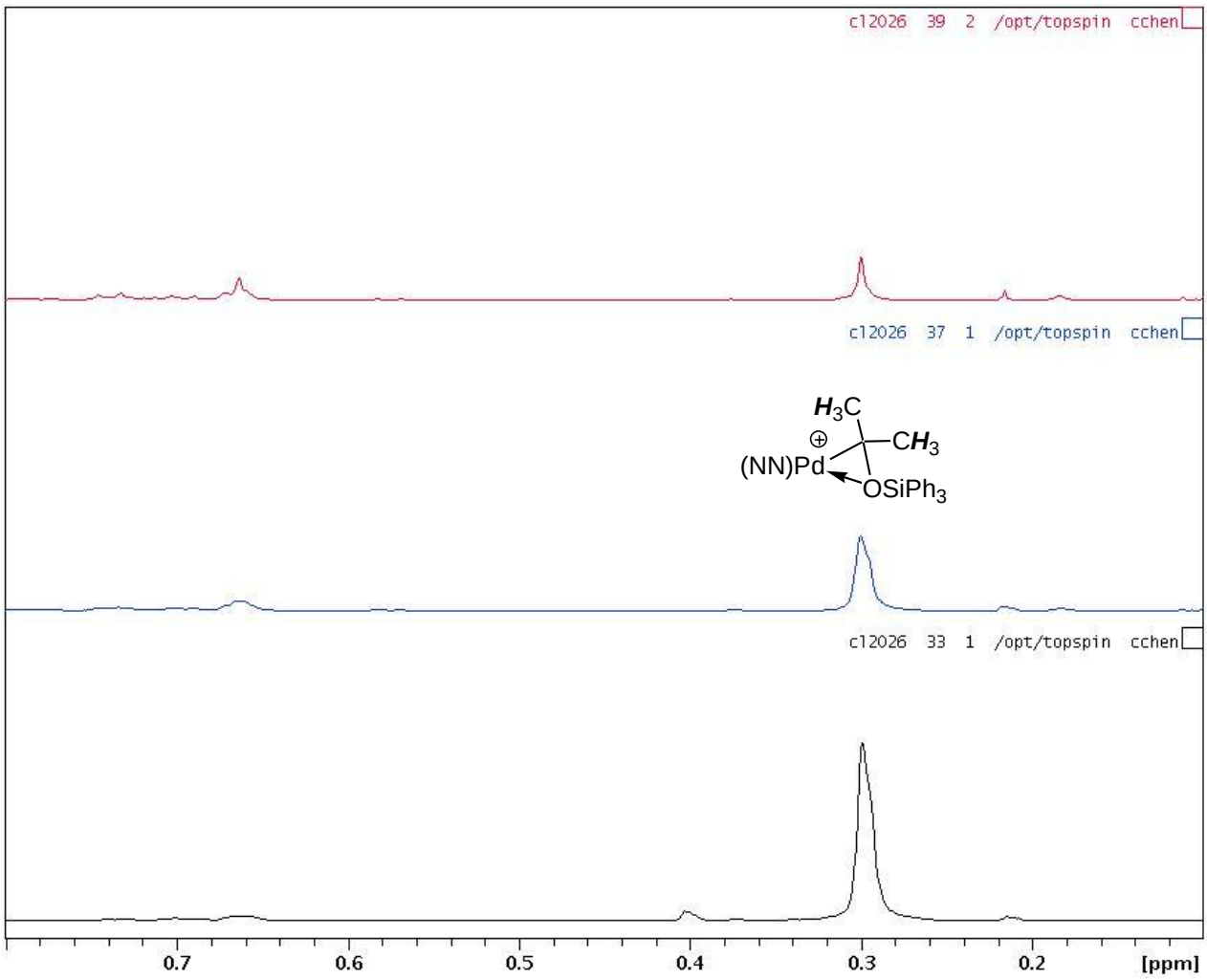

Figure 10-8d. Selected spectra for the first-order consumption of [(α-diimine)Pd{$CMe_2(OSiPh_3)$}][SbF_6] (**5f**) at 20 °C: expansion of δ 0.8-0.1. The bottom spectrum is the is the starting point of the reaction, the middle spectrum corresponds to ca. 50% completion and the top spectrum corresponds to ca. 90% completion. For kinetics analysis see Figure 6.29 and Figure 6.30.

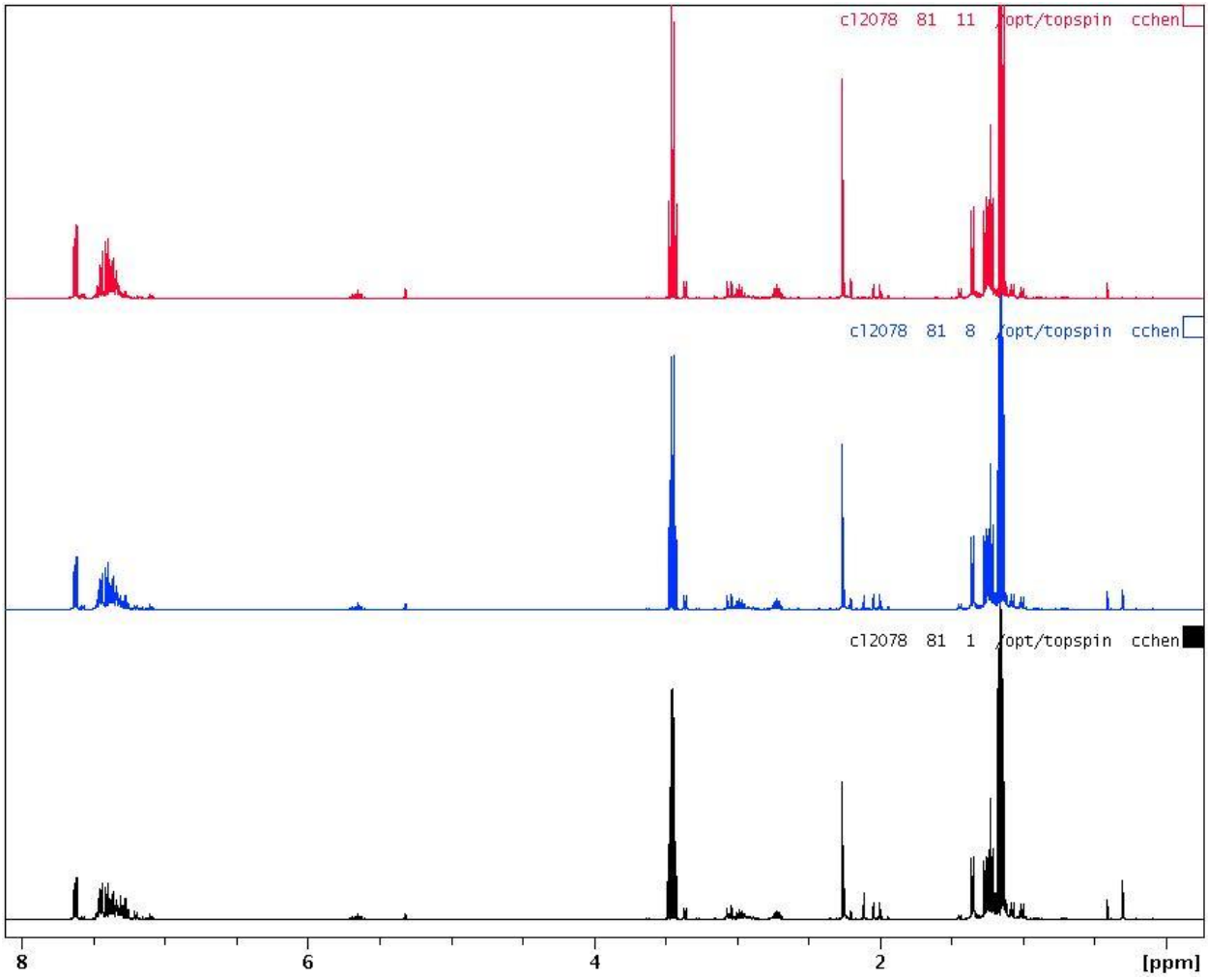

Figure 10-8e. Selected spectra for the first-order consumption of [(α-diimine)Pd{$CMe_2(OSiPh_3)$}][$B(C_6F_5)_4$] (**5f**) at 20 °C: full spectra. The bottom spectrum is the is the starting point of the reaction, the middle spectrum corresponds to ca. 50% completion and the top spectrum corresponds to ca. 90% completion. For kinetics analysis see Figure 6.14 and Figure 6.15.

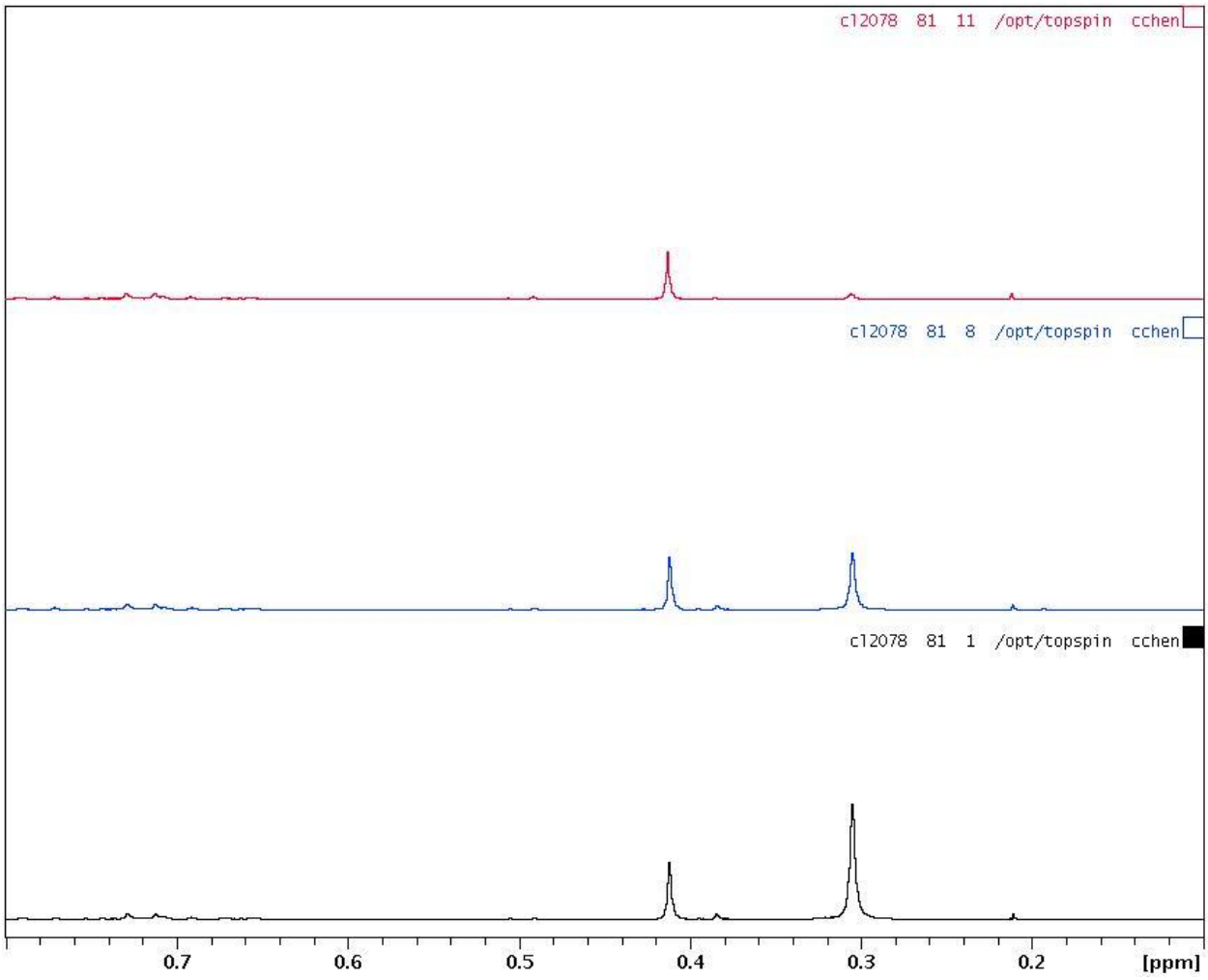

Figure 10-8f. Selected spectra for the first-order consumption of [(α-diimine)Pd{$CMe_2(OSiPh_3)$}][$B(C_6F_5)_4$] (**5f**) at 20 °C: expansion of δ 0.8-0.1. The bottom spectrum is the is the starting point of the reaction, the middle spectrum corresponds to ca. 50% completion and the top spectrum corresponds to ca. 90% completion. For kinetics analysis see Figure 6.14 and Figure 6.15.

11 References

[1] NMR tube experiments demonstrated that poly(vinyl trimethylsilyl ether) had formed prior to hydrolysis in methanol. ^{1}H NMR (C_6D_5Cl): δ 4.15 (br s, 1H, CH), 1.85 (br s, 2H, CH_2), 0.29 (br, 9H, $SiMe_3$).

[2] The C*H*$_2$=C*H*OPh resonances of **2e** were broad at -60 ^{o}C.

[3] Key NMR data for C_2H_5OH: **^{1}H NMR** (CD_2Cl_2, 20 °C): δ 3.73 (d of q, J = 6, 7 Hz, 2H, OC*H*$_2$CH$_3$), 1.71 (t, J = 6 Hz, 1H, OH), 1.17 (t, J = 6 Hz, 3H, OCH$_2$C*H*$_3$).

[4] Key NMR data for Me_3SiOH: **^{1}H NMR** (CD_2Cl_2, 20 °C): δ 2.57 ((b, SiO*H*), 0.14 (s, Si*Me*). Key NMR data for $Me_3SiOSiMe_3$: **^{1}H NMR** (CD_2Cl_2, 20 °C): δ 0.07 (s, Si*Me*).

[5] Key NMR data for $PhMe_2SiOH$: **^{1}H NMR** (CD_2Cl_2, 20 °C): δ 2.45 ((b, SiO*H*), 0.34 (s, Si*Me*). Key NMR data for $PhMe_2SiOSiMe_2Ph$: **^{1}H NMR** (CD_2Cl_2, 20 °C): δ 0.40 (s, Si*Me*).

[6] Key NMR data for $Ph_2MeSiOH$: **^{1}H NMR** (CD_2Cl_2, 20 °C): δ 2.51 ((b, SiO*H*), 0.66 (s, Si*Me*)

[7] NMR data for Ph_3SiOH: **^{1}H NMR** (CD_2Cl_2, 20 °C): δ 7.63 (t, H_{meta}), 7.44 (d, H_{ortho}), 7.39 (t, H_{para}), 2.87 (b, SiO*H*).

[8] The α-diimine aromatic signal overlap with OSi*Ph*$_3$ signals.

[9] The simulation was done by using Kintecus software. Ianni, J. *Kintecus* V3.8.

[10] Complete citation for reference 73 in the paper.

Gaussian 03, Revision C.02, Frisch, M. J.; Trucks, G. W.; Schlegel, H. B.; Scuseria, G. E.; Robb, M. A.; Cheeseman, J. R.; Montgomery, Jr., J. A.; Vreven, T.; Kudin, K. N.; Burant, J. C.; Millam, J. M.; Iyengar, S. S.; Tomasi, J.; Barone, V.; Mennucci, B.; Cossi, M.; Scalmani, G.; Rega, N.; Petersson, G. A.; Nakatsuji, H.; Hada, M.; Ehara, M.; Toyota, K.; Fukuda, R.; Hasegawa, J.; Ishida, M.; Nakajima, T.; Honda, Y.; Kitao, O.; Nakai, H.; Klene, M.; Li, X.; Knox, J. E.; Hratchian, H. P.; Cross, J. B.; Bakken, V.; Adamo, C.; Jaramillo, J.; Gomperts, R.; Stratmann, R. E.; Yazyev, O.; Austin, A. J.; Cammi, R.; Pomelli, C.; Ochterski, J. W.; Ayala, P. Y.; Morokuma, K.; Voth, G. A.; Salvador, P.; Dannenberg, J. J.; Zakrzewski, V. G.; Dapprich, S.; Daniels, A. D.; Strain, M. C.; Farkas, O.; Malick, D. K.; Rabuck, A. D.; Raghavachari, K.; Foresman, J. B.; Ortiz, J. V.; Cui, Q.; Baboul, A. G.; Clifford, S.; Cioslowski, J.; Stefanov, B. B.; Liu, G.; Liashenko, A.; Piskorz, P.; Komaromi, I.; Martin, R. L.; Fox, D. J.; Keith, T.; Al-Laham, M. A.; Peng, C. Y.; Nanayakkara, A.; Challacombe, M.; Gill, P. M. W.; Johnson, B.; Chen, W.; Wong, M. W.; Gonzalez, C.; and Pople, J. A.;

Gaussian, Inc., Wallingford CT, 2004.

[11] Pd-OR$_2$ distances in square planar Pd(II) complexes are in the range 2.11-2.20 Å. (a) Bei, X.; Uno, T.; Norris, J.; Turner, H. W.; Weinberg, W. H.; Guram, A. S. *Organometallics* **1999**, *18*, 1840. (b) Kim, Y.; Verkade, J. G. *J. Organomet. Chem.* **2003**, *669*, 32.